PROTON TRANSPORT IN PROTON EXCHANGE MEMBRANES

by

Jennifer Mary Schmeisser
Honours B.Sc., University of Waterloo, 1999

THESIS SUBMITTED IN PARTIAL FULFILLMENT OF
THE REQUIREMENTS FOR THE DEGREE OF

DOCTOR OF PHILOSOPHY

In the
Department of Chemistry

SIMON FRASER UNIVERSITY

2007

APPROVAL

Name: Jennifer Mary Schmeisser

Degree: Doctor of Philosophy

Title of Thesis: Proton Transport in Proton Exchange Membranes

Examining Committee:

Chair — Dr. Ross H. Hill
Professor, Department of Chemistry

Dr. Steven Holdcroft
Senior Supervisor
Professor, Department of Chemistry

Dr. George R. Agnes
Supervisor
Professor, Department of Chemistry

Dr. Zuo-Guang Ye
Supervisor
Professor, Department of Chemistry

Dr. Michael H. Eikerling
Internal Examiner
Assistant Professor, Department of Chemistry

Dr. Robert B. Moore
External Examiner
Professor, Department of Chemistry
Virginia Tech

Date Defended/Approved: August 27, 2007

Abstract

This work investigated several proton exchange membranes (PEMs): perfluorosulfonic acid-based polymers (**Nafion®**), sulfonated poly(ether ether ketone) (**S-PEEK**), radiation-grafted ethylenetetrafluoroethylene-grafted-poly(styrene sulfonic) acid (**ETFE-*g*-PSSA**), sulfonated α, β, β-trifluorostyrene-co-substituted α, β, β-trifluorostyrene (**BAM®**), sulfonated polystyrene-*b*-poly(ethylene-*r*-butylene)-*b*-polystyrene triblock copolymer (**S-SEBS**), and a series of novel photocurable polyelectrolytes. These polymer systems differ in their chemical structure, ion content, and morphology.

Proton conductivity and water sorption behaviour as a function of ion content for the S-PEEK, ETFE-*g*-PSSA, BAM, and S-SEBS series have been investigated at room temperature under fully hydrated conditions. A detailed analysis of the data has shown that strong links exist between conductivity and acid concentration, and that a deeper understanding of these effects can be gained by examining proton mobility. Results indicate that variations in mobility appear as a consequence of the different chemical structures.

The influence of water content was further investigated by evaluating the proton mobility of Nafion and each BAM membrane while equilibrated with water vapours of known relative humidities between 50 – 98% RH. The proton transport properties of BAM are highly susceptible to changes in relative humidity with the most dramatic effects being seen with the high ion content membranes. It is proposed that when these membranes lose water and shrink, they reorganize to form tortuous ion conductive pathways which retard proton movement.

A series of semi-interpenetrating network proton conducting membranes have been created by the photocuring of polymerizable polyelectrolyte liquids comprised of linear S-PEEK immersed in a solution of liquid monomers in a range of compositions. It has been shown that the relative composition of the components has a strong influence on mechanical properties, proton conductivity, and water sorption behaviour.

Dedication

To my Mother and Paul for their love, support,
and always believing in me.

To Mr. R. Roy for inspiring my love for Chemistry.

Acknowledgements

I would like to thank:

My senior supervisor Dr. Steven Holdcroft for allowing me to work under his supervision and for his guidance throughout the course of my studies.

My supervisory committee, Dr. George Agnes and Dr. Zuo-Guang Ye, and my examining committee, Dr. Michael Eikerling and Dr. Robert B. Moore, for their effective constructive criticisms of my thesis.

Past and current members of the Holdcroft group (the best group EVER!!!) for their friendship, support, and useful discussions.

Dr. Timothy Peckham and Dr. E. Johan Foster for proof-reading my thesis.

Dr. Bulent Mutus, Dr. James Green, Dr. James Gauld, and Dr. Zhuo Wang for their helpful ideas on how to improve my defence presentation.

Dr. Ana Siu for collecting differential scanning calorimetry data for the photocured materials.

The staff in the machine shop and the electronic shop for their never ending technical support and timely turnaround on my projects.

Dr. Steven Holdcroft, Simon Fraser University, Science Council of British Columbia, and Ballard Power Systems Inc. for financial support.

Table of Contents

List of Abbreviations

AC	alternating current
ACN	acrylonitrile
AFC	alkaline fuel cell
AFM	atomic force microscopy
BAM	Ballard Advanced Materials
DMA	dimethyl acetamide
DMSO	dimethyl sulfoxide
DS	degree of sulfonation
DSC	differential scanning calorimetry
DVS	dynamic vapour sorption
DVSS	dynamic vapour sorption system
ELC	Electrolite Corporation
ETFE	ethylene-alt-tetrafluoroethylene
ETFE-g-PSSA	ethylene-alt-tetrafluoroethylene-graft-poly(styrene sulfonic acid)
FEP	poly(tetrafluoroethylene-co-hexafluoropropylene)
FEP-g-PSSA	poly(tetrafluoroethylene-co-hexafluoropropylene)-graft-poly(styrene sulfonic acid)
FRA	frequency response analyzer
FTIR	fourier transform infrared
HAADF STEM	high angle annular dark-field scanning transmission electron microscopy
IEC	ion exchange capacity
IPN	interpenetrating network
IR	infrared
N117	Nafion® 117
NMR	nuclear magnetic resonance
PAFC	phosphoric acid fuel cell
PEM	proton exchange membrane

PEMFC	proton exchange membrane fuel cell
PI	photoinitiator
PSSA	poly(styrene sulfonic acid)
PVDF	poly(vinylidene difluoride)
PVP	poly(vinylpyrrolidone)
RH	relative humidity
RT	room temperature
SANS	small angle neutron scattering
SAXS	small angle x-ray scattering
semi-IPN	semi-interpenetrating network
SOFC	solid oxide fuel cell
S-PEEK	sulfonated poly(ether ether ketone)
S-PEEKK	sulfonated poly(ether ether ketone ketone)
S-SEBS	sulfonated polystyrene-b-poly(ethylene-r-butylene)-b-polystyrene
TEM	transmission electron microscopy
TGA	thermogravimetric analysis
UV	ultraviolet
UV-Vis	ultraviolet-visible
VPA	vinyl phosphonic acid
WAXS	wide angle x-ray scattering
XRD	x-ray diffraction

List of Symbols

α	degree of dissociation
A	area
a_i	activity
C_i	concentration
C_m	membrane capacitance
d	diameter
dm/dt	percentage change in mass as a function of time
F	Faraday's constant
f_i	activity coefficient
h	thickness
IEC^{eff}	effective ion exchange capacity
IEC^{exp}	experimental ion exchange capacity
IEC^{theo}	theoretical ion exchange capacity
λ	moles H_2O/moles acid
L	length
M_n	number average molecular weight
MW	molecular weight
μ	mobility
μ_e	mobility of an electron
μ'_{H+}	effective proton mobility
$\mu'_{H+(max)}$	maximum effective proton mobility
η	density of charge carriers
ρ_{dry}	dry density
ρ_{water}	density of water
R_c	contact resistance
R_m	membrane resistance
σ	conductivity

σ_e	electrical conductivity
σ_{H+}	proton conductivity
V_{dry}	dry volume
V_{hyd}	volume of partially hydrated membrane
V_{water}	volume of water
V_{wet}	volume of wet membrane
W	width
W%	weight percent
W_{dry}	dry weight
W_{wet}	wet weight
W_{hyd}	weight of partially hydrated membrane
X	inner radius of the outer electrode
X_v	water volume content
Y	radius of the inner electrode
Z'	real impedance
Z''	imaginary impedance
Z_i	ionic charge

List of Figures

List of Tables

Chapter 1: Introduction

1.1 Fuel Cells

Fuel cell technologies are currently under intense investigation because they are seen as efficient low emission alternatives to hydrocarbon combustion engines for the transportation industry. Their implementation will undoubtedly be an invaluable step towards continuing to meet our ever increasing energy demands. Sir William Robert Grove first introduced the fuel cell concept in 1839, but it was nearly 100 years later before a serious investigation was undertaken by Francis Thomas Bacon, who recognized the potential commercial applications.[1]

Fuel cells employ an electrochemical process that converts the chemical energy of a fuel directly into electrical energy. During operation, fuel is oxidized at the anode, while an oxidant is reduced at the cathode. An electrolyte situated between the anode and cathode serves to separate the fuels, balance the charge, and complete the electrochemical circuit. If a continuous supply of fuel is provided the fuel cell will operate uninterrupted. These devices have a significant advantage over conventional batteries, which must be discarded or recharged by an external power source. A selection of common fuel cell types are summarized in Table 1.1 according to their fuel and oxidant type, operation temperature, electrolyte type, and intended use.

Table 1.1 Comparison of common fuel cell technologies

Fuel Cell Type	Common Electrolyte	Fuel/Oxidant Type	Operating Temperature	Applications
Phosphoric Acid (PAFC)	Liquid phosphoric acid soaked in a matrix	H_2/O_2	150-200°C	• Distributed generation
Alkaline (AFC)	Aqueous solution of potassium hydroxide soaked in a matrix	H_2/O_2	90-100°C	• Military • Space
Solid Oxide (SOFC)	Solid zirconium oxide to which a small amount of yttria is added	H_2/O_2	650-1000°C	• Auxillary power • Electric utility • Large distributed power generation
Polymer Electrolyte Membrane (PEMFC)	Solid organic ion containing polymer	H_2/O_2 Methanol/O_2	50-100°C	• Back-up power • Portable power • Small distributed generation • Transportation

Adapted from the U.S. Department of Energy: Energy Efficiency and Renewable Energy Website (http://www1.eere.energy.gov)

1.2 Proton Exchange Membrane Fuel Cells

As a result of the anticipated worldwide oil crisis and the exponential growth of popular new portable electronic devices (laptops, cell phones, PDAs, etc), the current focus of fuel cell technology research is the proton exchange membrane fuel cell (PEMFC), Figure 1.1. In this system, a thin proton conducting film (a proton exchange membrane, PEM) separates the fuel (typically hydrogen or methanol) and oxidant (typically pure oxygen or air). During operation, the fuel of choice is reduced at the anode liberating protons and electrons. The protons are transported through the PEM to the cathode where they combine with oxygen and the electrons that travel through the external circuit. The overall product of the reaction is water.

Figure 1.1 Schematic of a Proton Exchange Membrane Fuel Cell

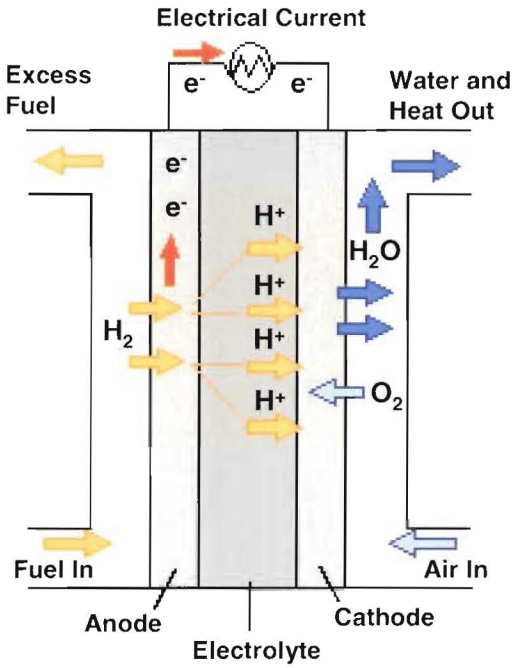

Reproduced from the U.S. Department of Energy: Energy Efficiency and Renewable Energy Website (http://www1.eere.energy.gov)

Proton exchange membrane fuel cells pose many practical advantages over other types of fuel cells. Incorporation of a solid electrolyte eliminates the electrolyte leakage issues and danger of handling the strong acids/bases that are present in phosphoric acid and alkaline fuel cells. Relatively low temperature operation makes them ideal candidates for portable power applications, and allows for the quick start-up that is key for successful implementation in automotive applications. Unfortunately, the requirement of expensive catalysts, the high sensitivity to fuel impurities, and a cost-effective PEM remain as obstacles that must be overcome before widespread commercialization of PEMFCs can occur.

1.3 Proton Exchange Membranes

PEMs are thin films of solid polymer electrolytes (SPEs) that consist of polymer networks with covalently bonded ion-containing functional groups capable of exchanging protons. Properties of PEMs are heavily influenced by the nature of the ionic group, the polymer backbone it's attached to, and the method and nature of attachment. Typically, the bound ion is a strong acid, such as sulfonic acid. Ion groups are incorporated into the SPE either by polymerization of monomers functionalized with ion groups, or introducing an ionic group to a base polymer, using a post-polymerization reaction.

Requirements of PEMs for practical use in fuel cells:

- chemical stability
- mechanical robustness
- impermeable to gases
- resistance to dehydration
- high proton conductivity (not lower than 0.1 S/cm)[2]
- low cost

Ion content within a PEM is expressed as the number of millimoles of ion exchange sites per gram of dry polymer, referred to as the ion exchange capacity (IEC). By definition, materials with high IECs contain a high concentration of acid groups, and a large number of protons. Therefore, it might be expected that to maximize proton conductivity, and hence fuel cell efficiency, the highest IEC material should be chosen. Unfortunately, the incorporation of large amounts of sulfonic acid generally leads to high water contents, due to its hydrophilic nature. This can have a severe impact on fuel cell performance because of the possibility of flooding at the cathode, as well as mechanical instability during cycling. For this reason, a balance must be struck between high sulfonic acid content and relatively low water content. The most efficient conductors will therefore be ones that conduct protons, while maintaining low water contents (i.e., use their water effectively).

The use of solid polymer electrolytes in fuel cells was first proposed by W.T. Grubb in 1959 with their application as power sources as early as the 1960's space missions.[1] The membranes employed in these early applications were the linear and cross-linked versions of polystyrene sulfonic acid PSSA (Figure 1.2). Unfortunately, chemical stability proved poor, and fuel cell operating lifetimes were only 200 hours at 60°C. Several studies investigating the degradation mechanism have been performed, and all conclude that the hydrocarbon backbone of PSSA is easily attacked by highly oxidative chemical species that are formed during fuel cell operation.[3-5] These attacks cause the loss of styrene groups and chain scission, resulting in mechanical breakdown. The fluorinated analogues of PSSA, poly(trifluorostyrene) sulfonic acid (Figure 1.2),

were found to be resistive to similar oxidative modes of degradation, due to the increased strength of the C-F bond as compared to the C-H bond.[6]

Figure 1.2 Chemical structures of (a) polystyrene sulfonic acid and (b) poly(trifluorostyrene) sulfonic acid

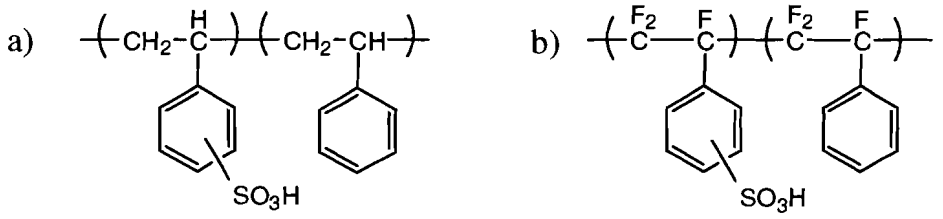

polystyrene sulfonic acid poly(trifluorostyrene) sulfonic acid

1.3.1 Perfluorinated Polymer Membranes

Although hydrocarbon-based membranes were the first materials employed in PEM fuel cells, their use was abandoned in favour of more chemically and morphologically stable perfluorinated membranes (Figure 1.3).

Figure 1.3 Chemical structure of commercially available perfluorinated polymer membranes (a) Nafion® (b) Dow® Membrane and (c) 3M

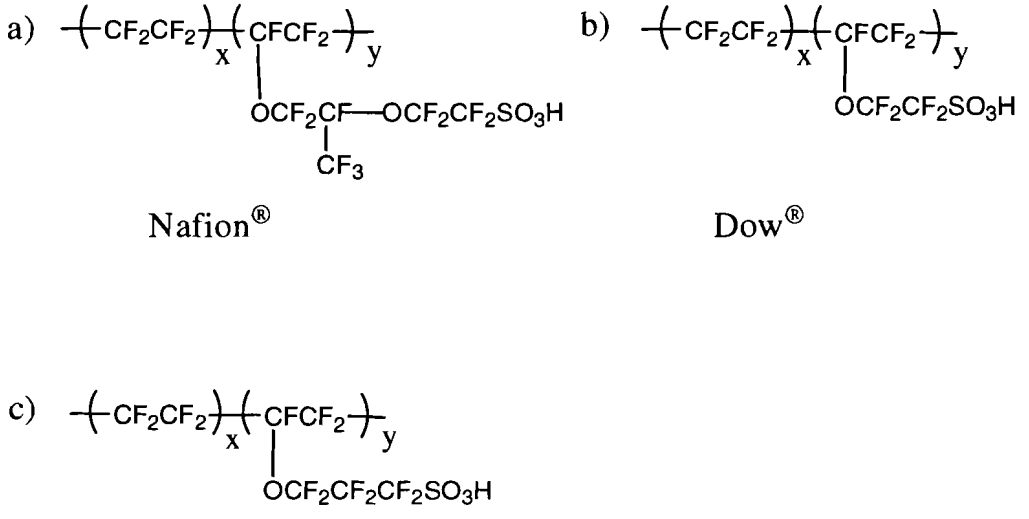

Nafion® Dow®

3M

The first family of commercially available perfluorinated proton exchange membranes was developed in the 1960s by DuPont, under the trademark Nafion® (Figure 1.3a).[1] Nafion consists of an extremely hydrophobic perfluorinated backbone, which provides morphological stability, with pendent vinyl ether side chains, each of which is terminated by a sulfonic acid group. It is widely commercially available, and is the most extensively studied PEM with regards to both conductivity behaviour and microstructure.[7] Due to its availability and superior properties (in terms of stability and performance), Nafion is considered to be the industry standard to which all other membranes are compared.

Twenty years after Nafions discovery, the Dow Chemical Company prepared its own perfluorinated polymer (Dow® Membrane) which has a similar chemical structure to Nafion except with shorter side chains (Figure 1.3b). Whereas Nafion is typically available in several low IEC forms (0.83, 0.91, 1.0 mmol/g), the Dow Membrane, because of its shorter side chains, can be prepared with comparatively higher IECs (1.18, 1.25 mmol/g). While both membranes exhibit similar structural and morphological properties, the Dow Membrane is able to achieve higher proton conductivity due to its higher ion content.[8] Unfortunately, due to the difficulty and expense of preparation, the Dow Membrane did not reach large scale production. Recently, new and cheaper routes have been developed for the synthesis of the DOW® monomer by Solvay Solexsis.[9] This will likely lead to a resurgence in investigating the use of this membrane for PEMFC applications; however, currently little information is available. Newer materials derived from the basic DOW® Membrane structure have also been developed by 3M in which the CF_2 side chain has been extended to three carbons (Figure 1.3c).[10]

Although several detailed structural models have been proposed for Nafion, there is general agreement that the sulfonated ether side chains phase separate from the fluoropolymer backbone to form ionic domains, due to the incompatibility of the hydrophilic side chains and the hydrophobic backbone. Upon hydration, the membrane absorbs water and the hydrophilic regions swell. It is believed that it is through these hydrated regions that water and protons are transported, while the hydrophobic domain provides morphological stability, and prevents dissolution of the polymer in water.[11] It should follow that the nature of these channels is key to the rate of proton transport.

The phase separated morphology was first proposed by Eisenberg and later refined by Gierke, using results from small angle x-ray scattering (SAXS) and small angle neutron scattering (SANS) experiments.[12,13] Gierke suggested a "cluster network model" that consists of small channels separating approximately spherical inverted micellar domains (Figure 1.4). The model indicates that the ion exchange sites reside near the water-polymer interface, and are imbedded in the water phase. Furthermore, Gierke suggests that upon dehydration the clusters do not simply decrease in diameter but in fact, the ion exchange sites reorganize to produce an increased number of clusters that contain less ion exchange sites per cluster. This is illustrated in Figure 1.4, where it can be seen that as the two hydrated clusters become dehydrated, they collapse into three smaller clusters, with the ion exchange sites per cluster decreasing from 7 to 5. The authors have calculated that for fully hydrated acidified Nafion 1200 (IEC = 0.83 mmol/g), the cluster has a diameter of 4 - 5 nm diameter, and contains ~ 70 ion exchange sites per cluster. It is important to note that the dry polymer also contains ionic clusters of ~ 1.8 nm, with 26 ion exchange sites per cluster.

Figure 1.4 Cluster network model illustrating the ionic cluster reorganization that occurs upon hydration/dehydration in Nafion

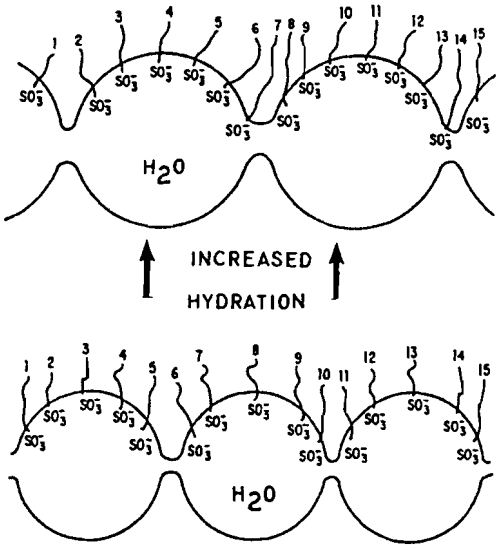

Reproduced with permission from *Perfluorinated Ionomer Membranes: The Cluster-Network Model of Ion Clustering in Perfluorosulfonated Membranes*; ACS Symposium Series 180; Eisenberg, A.; Yeager, H.L. Eds., Gierke, T. D.; Hsu, W. Y.; pg 293. © 1982 American Chemical Society.

Yeager and Steck proposed a three-region structural model (Figure 1.5) that consists of: ionic clusters (c); in which the majority of sulfonate exchange sites, counterions, and absorbed water exist; a fluorocarbon region (a), containing the fluorocarbon backbone; and an interfacial zone (b) that separates region (a) and (c).[14] Contained in region (b) would be pendant side chain material; a smaller amount of water; some sulfonate exchange sites, which have not been incorporated into clusters; and a fraction of the counterions.

Figure 1.5 Three-region structural model for Nafion (a) fluorocarbon, (b) interfacial zone (c) ionic clusters

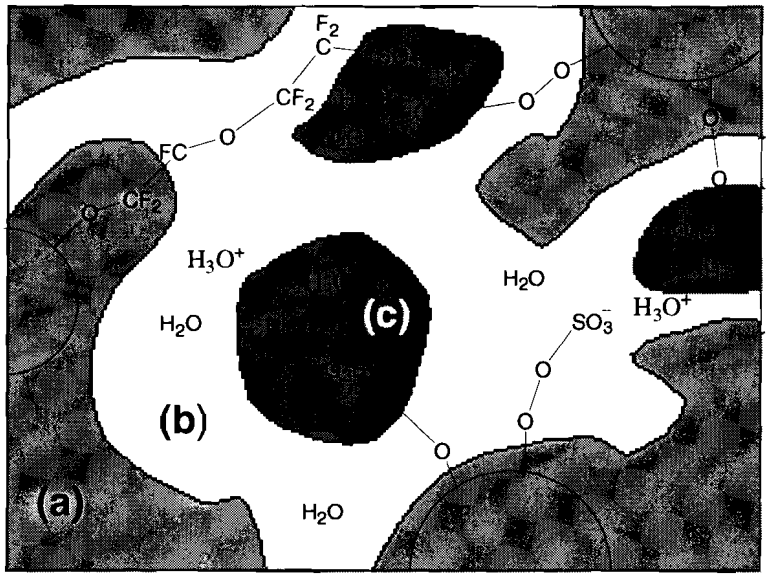

Reproduced with permission from *Perfluorinated Ionomer Membranes: Cation Exchange Selectivity of a Perfluorsulfonate Polymer*; ACS Symposium Series 180; Eisenberg, A.; Yeager, H.L. Eds., Yeager, H. L.; pg 49. © 1982, American Chemical Society

More recently, Gebel and coworkers have further refined the microphase separated model, using a series of results from small angle scattering techniques.[15-17] The model is very similar to Gierke's model at low water contents. They both describe the structure of Nafion as connected spherical domains of water embedded in the polymer matrix. However, Gebel has suggested that at high water contents, above 50 vol%, the structure inverts from a reverse micellar structure to a connected network of polymer rod-like particles (Figure 1.6).

Figure 1.6 Structure inversion model showing the progression of ionic domains with the incorporation of water (a) swollen membrane (b) percolation (c) structure inversion (d) connected network of polymer rods

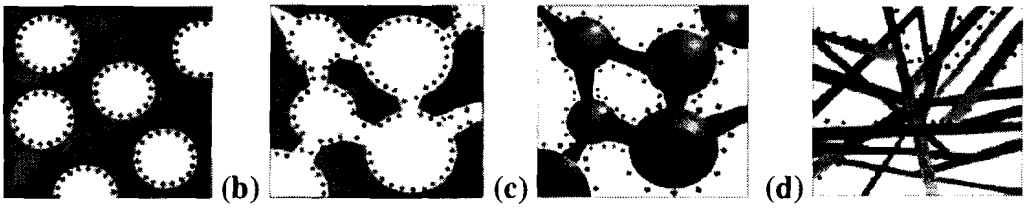

Reproduced with permission from *Polymer* Gebel, G., *41*, 5829, © 2000, Elsevier.

Gebel and coworkers have proposed that the polymer rods seen in the inverted structure also exist in the dry state forming a fibrillar structure that is made up of elongated polymeric aggregates surrounded with ionic charges. A simplified schematic representation of this bundled structure is shown in Figure 2.1a.[18]

Recently, microscopy techniques have become popular to investigate polymer morphology, as they allow for a direct observation of ionic clusters. Using transmission electron microscopy (TEM) and atomic force microscopy (AFM), several groups claim to have captured images of membrane morphologies, and used them to measure nanometre sized features that are attributed to ionic cluster size. [19-22]

1.3.2 Alternative Membranes

Nafion has been shown to be robust and have sufficient properties for use in hydrogen/oxygen fuel cells operating under ambient conditions.[23] However, it displays significant limitations for fuel cells that operate in low humidity (< 50% RH) and/or high temperature (> 120°C) environments. Furthermore, due to excessive swelling in methanol, Nafion is not an ideal candidate for direct methanol fuel cells, as the permeation of methanol from anode to cathode through the PEM reduces power density. For these reasons, there has been a renewed interest in developing novel materials that can satisfy these new technological requirements.

To aid in the design of new PEMs, a tremendous amount of effort has been invested into elucidating structure-property relationships to determine which physicochemical properties make one membrane perform better under a specific set of conditions. Several reviews comparing the plethora of new PEM candidates and their

respective advantages are available in the literature.[8,24,25] In terms of alternative polymeric membranes, there are two main classes: partially fluorinated and hydrocarbon-based.[25]

1.3.3 Partially Fluorinated Membranes

Partially fluorinated materials present a good compromise between cost and reliability. In most cases, they provide the morphological stability, but are easier to prepare than fully fluorinated materials. Two classes of partially fluorinated materials were used in this work and are discussed below.

Poly(trifluorostyrene) Membranes

The first type of polymer studied was prepared by Ballard Advanced Materials Corporation, and is based on a class of novel copolymers incorporating α,β,β-trifluorostyrene and substituted α,β,β-trifluorostyrene comonomers.[26,27] They were produced in the early 1990s, and are commonly known by their trademark name, BAM® (previously referred to in the literature as BAM3G). The general chemical structure and a schematic representation of the preparation of the simplest of these copolymers is shown in Figure 1.7. Briefly, the synthesis involves emulsion copolymerization of the substituted and un-substituted monomers, followed by subsequent sulfonation. Although the exact synthetic procedure is a trade secret, it is evident from the general scheme that IEC can be controlled by varying the ratios of monomers and/or controlling the post-sulfonation conditions.

Figure 1.7 Chemical structure and schematic for the preparation of BAM® copolymer

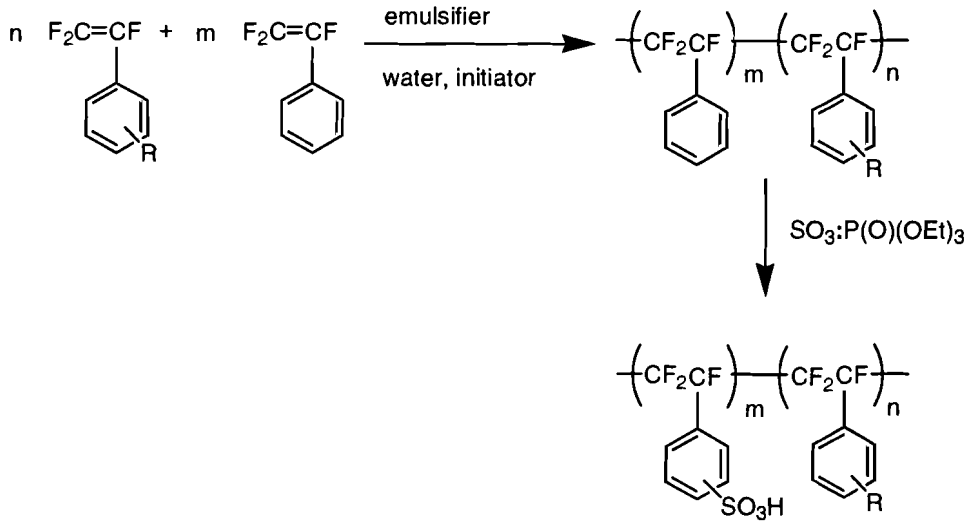

α, β, β-trifluorostyrene-co-substituted
α, β, β-trifluorostyrene (BAM)®

In general, BAM membranes are substituted analogues of linear poly(trifluorostyrene), discussed in Section 1.3. The unsubstituted version was first prepared in the early 1950s, but they were not deemed appropriate for fuel cell use because of extremely poor mechanical properties in the dry state.[6,28] As a means to resolve this concern, BAM membranes contain a substituent (R) on the non-ionic styrene species, which serves to internally plasticize the polymer and reduce brittleness.[29]

One of the most advantageous properties of these materials is that they can be prepared with a wide range of controlled sulfonic acid and water uptake values (1.1 - 2.7 mmol/g, 20 – 300 wt% water uptake).[30] Whereas most sulfonated linear hydrocarbon materials dissolve at such high IECs, BAM membranes maintain sufficient mechanical properties to be handled and tested, even after taking up as much as 300 wt% water.

Due to the proprietary nature of BAM, many of its intrinsic properties have not been well studied. Holdcroft and coworkers have reported the presence of minimal phase

separation in BAM using results of SAXS and TEM analysis, however they conclude that overall the large majority of sulfonic acid sites are dispersed homogenously throughout the membrane.[31]

More recently, Gebel and coworkers proposed a microstructure for BAM based on results of SANS experiments.[32] Experiments were performed on high IEC materials (2.10 and 2.40 mmol/g) in the swollen state (42 and 25 H_2O molecules per sulfonic acid respectively). The results have been interpreted as being indicative of a connected network of relatively small rod-like particles. Shown in Figure 1.8 is the fitting model that was used to elucidate the microstructure. Each particle contains a perfluorinated core of 4 Å diameter surrounded by a shell of phenyl rings of 2.5 Å diameter. Surrounding the particle is the outer shell, 4.5 Å thick, which consists of counterions and water. They suggest that as water content increases, connectivity between the rod-like particles decreases.

Figure 1.8 Schematic representation of rod-like particles present in swollen BAM

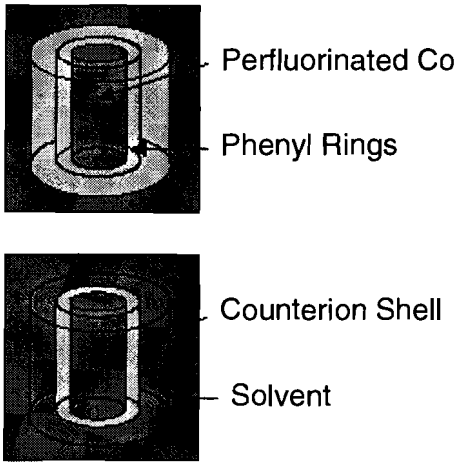

Reproduced with permission from *Journal of New Materials for Electrochemical Systems* Gebel, G.; Diat, O.; Stone, C., *6*, 17, © 2003, Journal of New Materials for Electrochemical Systems.

The authors do not claim to have found a definitive model but indicate that further SAXS and SANS studies are needed to confirm this structure. To date, the results of further studies have not been published.

Radiation Grafted Membranes

The second class of partially fluorinated materials used in this work were prepared by the radiation grafting technique.[4] These membranes consist of a base material (consisting of a polymer sheet) to which ion containing polymeric chains have been grafted. They are prepared via a three step process: 1) irradiation of a pre-formed base polymer film with γ-irradiation to form free radicals 2) grafting of monomers onto the radical centres and 3) sulfonation of the grafted chains. A range of materials with different IECs can be prepared by altering the grafting parameters. The key advantage of this technique is that ionic conductivity can be introduced into a pre-formed cost effective commercially available material, which is inherently stable.

Shown in Figure 1.9 are some of the most commonly studied radiation grafted membranes. Included are materials that consist of sulfonated polystyrene chains grafted onto base films, such as poly(tetrafluoroethylene-*co*-hexafluoropropylene) (FEP), ethylene-*alt*-tetrafluoroethylene (ETFE), and poly(vinylidene difluoride) (PVDF).

Due to the inherent stability of fully fluorinated materials, initial research focused on using FEP as the base material. Scherer and coworkers developed and fully characterized the physicochemical properties of polystyrene sulfonic acid membranes based on FEP films (FEP-*g*-PSSA).[33] Through in-situ fuel cell testing they found that under practical operating conditions, these materials can be optimized to give

performances comparable or superior to Nafion.[4,34] As a method to further reduce cost, partially fluorinated polymers can also be used as base materials.

Figure 1.9 Chemical structure of radiation grafted materials (a) ETFE-*g*-PSSA (b) PVDF-*g*-PSSA and (c) FEP-*g*-PSSA

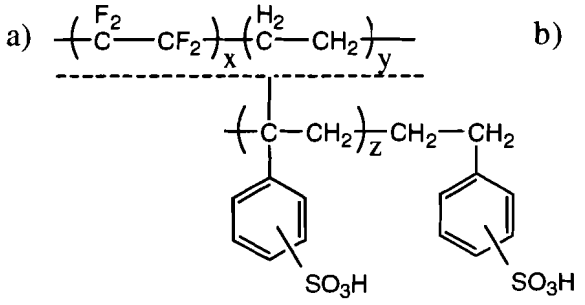

ETFE-*g*-PSSA

ethylene-alt-tetrafluoroethylene-graft-poly(styrene sulfonic acid)

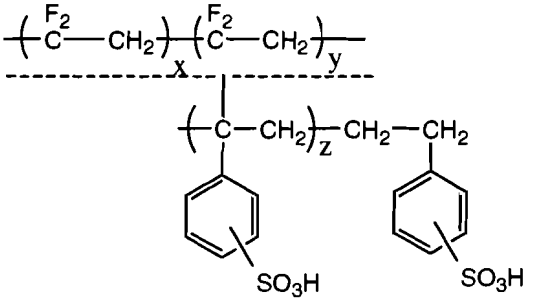

PVDF-*g*-PSSA

poly(vinylidene fluoride)-graft-poly(styrene sulfonic acid)

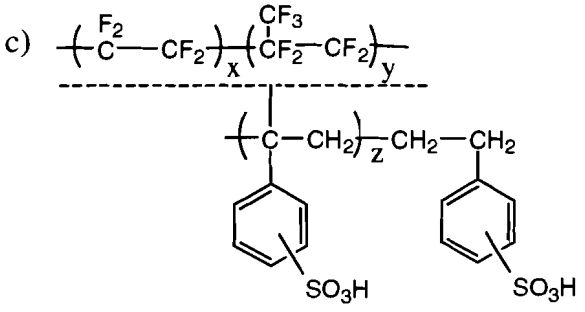

FEP-*g*-PSSA

poly(tetrafluoroethylene-co-hexafluoropropylene)-graft-poly(styrene sulfonic acid)

Horsfall and coworkers developed polystyrene sulfonic acid membranes based on ETFE and PVDF, and compared them to FEP materials and found that they have comparable fuel cell performance in both hydrogen and methanol fuel cells.[35-37] In fact, they conclude that the precise composition of the backbone is not as important to the

overall fuel cell performance, but more important are the grafting conditions and the overall sulfonic acid content (provided there are some fluorine atoms present on the base material).[37]

In comparison to Nafion, few microstructural studies have been performed on radiation grafted materials. For PVDF-*g*-PSSA, Jokela and coworkers have observed the presence of ionic aggregates of polystyrene chains embedded in the matrix polymer using WAXS and SAXS.[38] More recently, a direct observation of PVDF-*g*-PSSA morphology was made by Huang and coworkers using HAADF STEM (high angle annular dark-field scanning transmission electron microscopy), and compared to that of Nafion.[20] Using Ag^+ stained samples, they observed three phases in the PVDF-*g*-PSSA sample: dark regions corresponding to PVDF; grey regions due to aggregated sulfonated polystyrene, and bright dots indicating cluster-like sulfonated aggregates dispersed in the aggregated polystyrene regions (Figure 1.10). Nafion exhibited comparatively ordered and uniform arrays of ionic aggregates.

Figure 1.10 HAADF image of (a) Ag^+ stained Nafion and (b) Ag^+ stained PVDF-*g*-PSSA

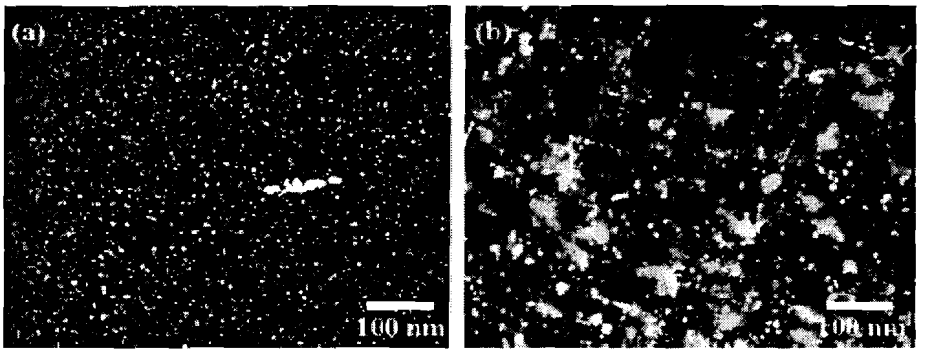

Reproduced with permission from *Applied Surface Science* Huang, H. S.; Chen, C. Y.; Lo, S. C.; Lin, C. J.; Chen, S. J.; Lin, L. J., *253*, 2685, © 2006, Elsevier.

HAADF images were captured once again after the samples had been equilibrated in a 50% methanol solution, and they observed that while the ionic clusters in Nafion swell to more than double their size, PVDF-g-PSSA changed only slightly.

1.3.4 Hydrocarbon Based Membranes

Proton exchange membranes made from hydrocarbon-based polymers have significant advantages that make them particularly attractive as possible alternatives to fluorine containing materials. They are typically cheaper to prepare, using materials that are often commercially available. Furthermore, with proper molecular design, materials possessing high decomposition temperatures can be prepared.[24] Two classes of hydrocarbon materials were used in this work and are discussed below.

Poly(ether ketone) Membranes

The first class of hydrocarbon materials used in this work was a series of sulfonated poly(ether ether ketone) membranes (Figure 1.11). Included in the figure is the structure of poly(ether ether ketone ketone), which is another membrane that has been referred to in the PEM literature, and very similar in structure to the polymer used here.[39] This class of materials has several advantages, which make it a particularly attractive alternate to fluorinated materials. The polymers are easily prepared via a post-sulfonation reaction of commercially available PEEK with concentrated sulfuric acid.[24] A series of membranes with well defined sulfonic acid contents can be prepared by simply controlling the time and temperature of the sulfonation reaction. They have been shown to possess good proton conductivity, have good thermal and chemical stability, are

generally soluble in organic solvents, and exhibit good performance in hydrogen and methanol/air fuel cells.[40,41]

Figure 1.11 Chemical structure of (a) sulfonated poly(ether ether ketone) S-PEEK and (b) sulfonated poly(ether ether ketone ketone) S-PEEKK

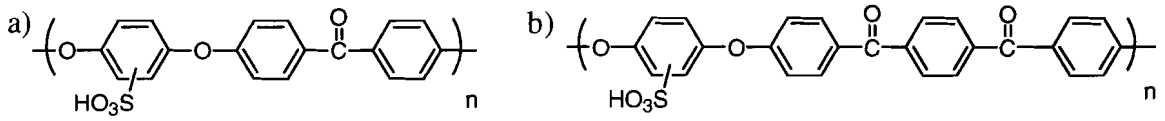

S-PEEK
sulfonated poly(ether ether ketone)

S-PEEKK
sulfonated poly(ether ether ketone ketone)

The morphology of sulfonated poly(ether ether ketone ketone) S-PEEKK was investigated by Kreuer using SAXS, and compared to that of Nafion.[11] He observed that while both Nafion and S-PEEKK exhibited phase-separated, water-filled channels, the channels in S-PEEKK were narrower, with a higher degree of branching, and possessed more "dead ends" (Figure 1.12). He attributed these structural differences to both the less pronounced hydrophobic/hydrophilic separation and comparatively inflexible backbone of S-PEEKK.

Figure 1.12 Proposed microstructure of (a) Nafion (b) S-PEEKK hydrocarbon membrane based on SAXS experiments

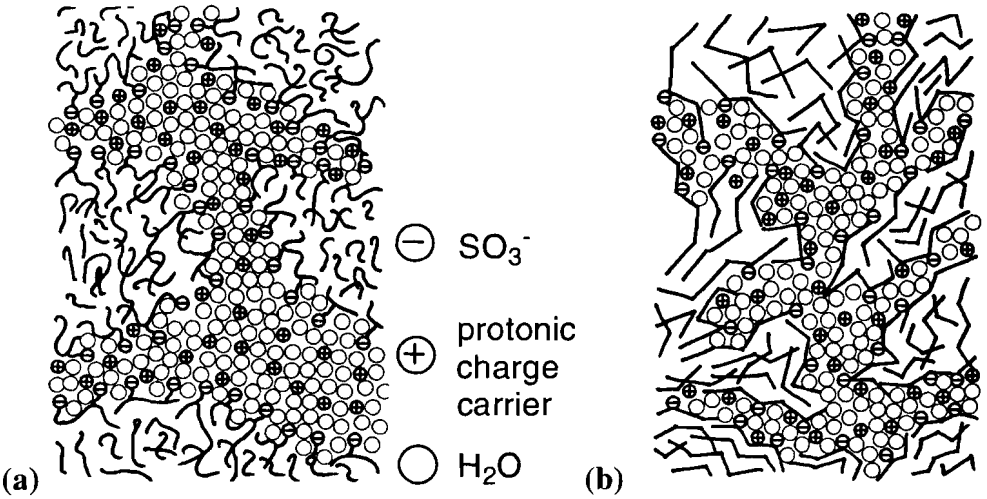

Reproduced with permission from *Journal of Membrane Science* Kreuer, K. D, *185*, 29, © 2001, Elsevier.

Sulfonated SEBS

Block copolymers consist of different blocks of polymerized monomers. For example, the block copolymer used in this work, sulfonated polystyrene-*b*-poly(ethylene-*r*-butylene)-*b*-polystyrene triblock copolymer (S-SEBS), also referred to the literature as DAIS, is composed of two sulfonated polystyrene blocks with a polyalkyl block between them (Figure 1.13). They are of particular interest because phase separation is promoted by the immiscibility of the constituent blocks.[42] Due to the vast number of possible block combinations, coupled with the ability to vary block length and sulfonation level, the block copolymerization synthetic strategy allows for infinite possibilities to tailor molecular structures and hence membrane morphology.

Figure 1.13 Sulfonated polystyrene-*b*-poly(ethylene-*r*-butylene)-*b*-polystyrene triblock copolymer (S-SEBS)

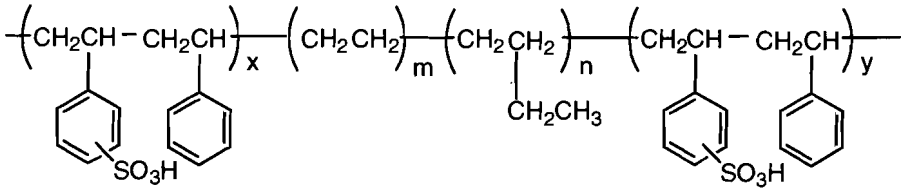

S-SEBS
sulfonated polystyrene-*b*-poly(ethylene-*r*-butylene)-*b*-polystyrene

S-SEBS has been employed as a low cost proton conductor by Dais-Analytic Corporation for use in hydrogen fuel cells at ambient temperatures and low current densities.[43] Using the samples from the data included in this work, Holdcroft and coworkers found that proton conductivities of S-SEBS membranes were very low, and appeared to be independent of IEC, as evidenced by the mere 0.02 S/cm increase over the IEC = 0.94 – 1.71 mmol/g range.[31] The authors also noted that efforts to elucidate morphological information for their S-SEBS samples were unsuccessful as the SAXS

spectra were featureless. However, water content was shown to be highly dependent on IEC, increasing by 100 H_2O/SO_3H between 1.13 – 1.71 mmol/g. Unfortunately, the extreme rise in water content causes a high degree of swelling, resulting in poor mechanical properties.[44]

1.4 Proton Transport in Proton Exchange Membranes

One key aspect that dictates fuel cell performance is the rate of proton transport from anode to cathode through the PEM. Insufficient proton transport has a negative impact on fuel cell performance through resistive losses.[1,45] All of the proposed structural models for Nafion are similar at low water contents, and the description of proton transport through the aqueous phase is supported by percolation theory.[46-48] With very low water contents, the conductive aqueous phase separates into ion containing clusters, which are randomly dispersed in an insulating fluorocarbon matrix. The clusters are well separated such that long range ion flow is impossible. With an increase in water content, the ionic clusters swell and interconnect to form pathways. As water content continues to increase, eventually a "percolation threshold" is reached where the pathways connect to form aqueous conductive channels through which long range ion content is possible. The definition of percolation threshold, as it relates to PEMs, is the water volume content (X_v) that is necessary for long range proton conduction to occur. This value has been calculated by Edmondson and Fontanella, assuming a power law relationship between proton conductivity and water volume content, and was found to be ~ 5 vol% for Nafion, Dow Membrane, and S-SEBS.[49] However, Hsu and coworkers suggest that the percolation threshold of Nafion is closer to 11 vol%.[46,48]

Protons in water do not exist as bare ions, but are strongly associated with surrounding water molecules to form dynamic aggregates, i.e., H_3O^+ (Hydronium ion); $H_5O_2^+$ (Zundel ion); and $H_9O_4^+$, (Eigen ion). When an electric field is applied, protons migrate due to electromotive forces, according to a combination of two competing mechanisms: the "vehicle mechanism" and the "Grotthuss mechanism".[50] An illustration of the differences between these mechanisms is shown in Figure 1.14. The vehicle mechanism describes a molecular diffusion process in which a hydrated proton aggregate moves through the aqueous environment as a single entity. The Grotthuss mechanism describes a structure diffusion process in which protons are transferred down a chain of hydrogen bonds followed by reorientation of the water dipoles.

Figure 1.14 Schematic of mechanisms for proton transport in water: (top) vehicle mechanism (bottom) Grotthuss mechanism

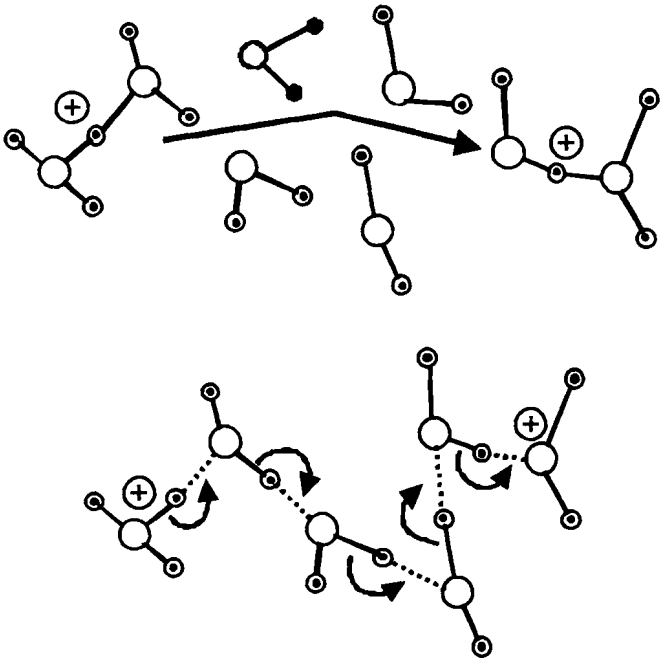

Reproduced with permission from *Polymer* Pivovar, B. S., *47*, 4194. © 2006, Elsevier.

A more thorough description of the Grotthuss mechanism, based on ab-initio MD simulations, suggests that transport of a single proton defect in water involves a periodic series of isomerizations between Zundel and Eigen ions (Figure 1.15).[51-55] As the Grotthuss mechanism relies on the rate of breaking and reforming of hydrogen bonds, any factor that either increases the average hydrogen bond energy, or disrupts the extent of hydrogen bonding in the network will be detrimental to this process. In an extensive hydrogen bonded network, the activation enthalpy for this process is low since the formation of a hydrogen bond in one part of the network, promotes the breaking of a hydrogen bond in another part of the network.[54]

Figure 1.15 Schematic of proton transport according to the Grotthuss mechanism

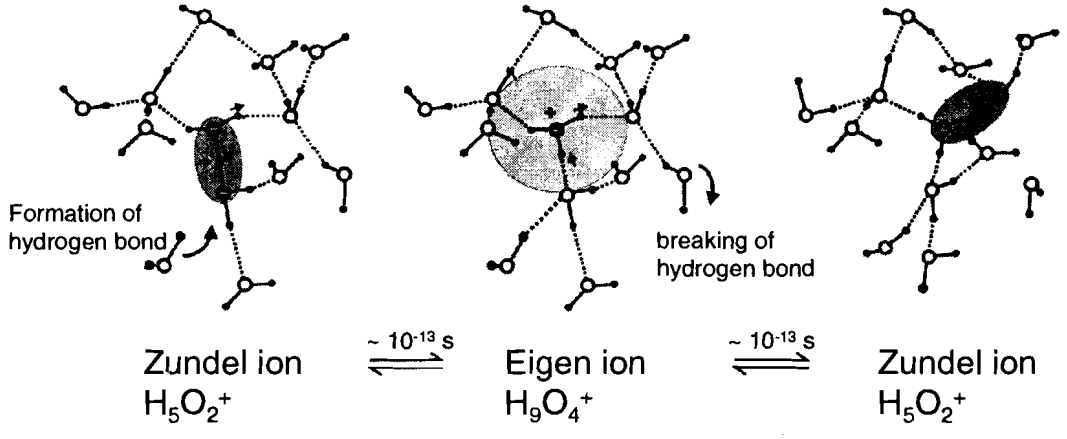

Reproduced with permission from *Solid State Ionics* Kreuer, K. D, *136-137*, 149 © 2000, Elsevier.

When sulfonic acid groups become hydrated, they donate their protons to the water contained in the aqueous phase of the PEM. Using the small molecule analogue of Nafion, triflic acid CF_3SO_3H, Paddison and coworkers have calculated that dissociation of the proton occurs when the ratio of water molecules to fixed sulfonic acid groups (λ) is equal to 3 H_2O/SO_3H, however, full shielding of the proton from the sulfonate

group does not to occur until $\lambda = 6$ H_2O/SO_3H.[56] Further investigation by Eikerling and Paddison has shown that this value can be as low as $\lambda = 2$ H_2O/SO_3H, depending on the strength of the acid, with more acidic small molecule analogues requiring less water molecules for dissociation.[57]

Applying an electric field across a hydrated PEM causes the protons to move within the aqueous phase of the membrane. Although several studies have been directed at elucidating the mechanism of proton transport in PEMs, it is a complex problem that does not have a single solution. However, it has been suggested that there are contributions from three transport mechanisms. In addition to the two discussed above, the Grotthuss and vehicle mechanisms, there exists a third "surface" transport mechanism where protons "hop" between the sulfonic acid groups that line the pore wall.[58] Shown in Figure 1.16 is a simplified schematic of the mechanisms of proton transport in Nafion.[59]

Two different types of water have been identified in Nafion membranes. "Bound" or surface water, is water that is strongly associated with, and highly ordered around the sulfonate groups along the pore wall through electrostatic attraction. "Bulk-like" water, is situated in the central region of the pore and exhibits properties similar to that of pure water (Figure 1.16).[60]

Figure 1.16 Simplified schematic of the proton transport in Nafion. A comparison of the surface mechanism, Grotthuss mechanism, and vehicle mechanism

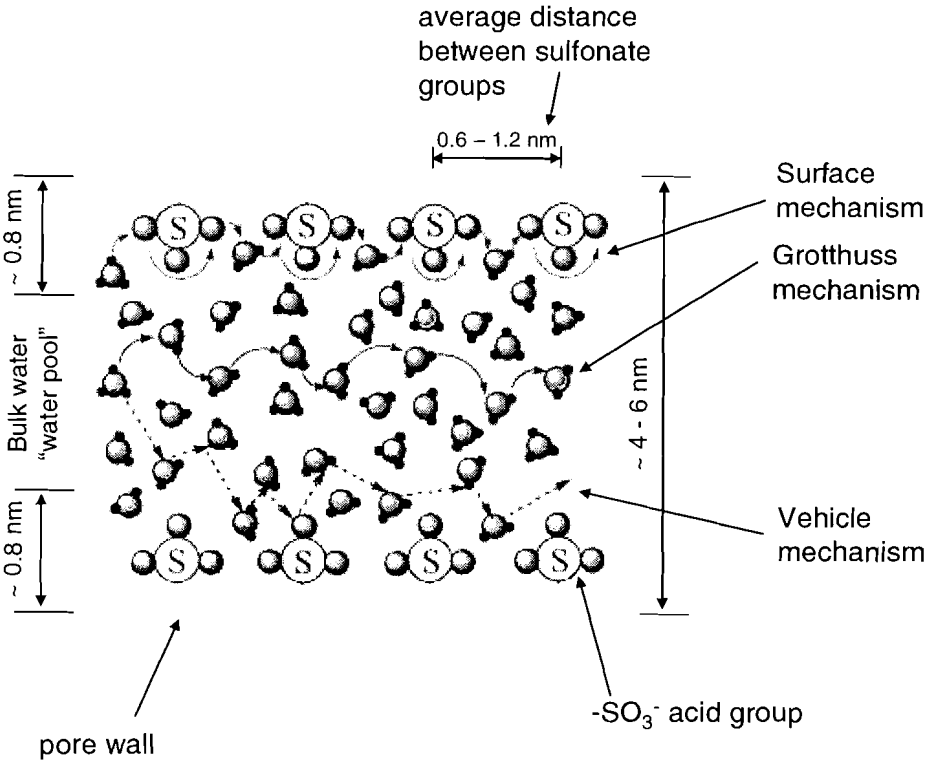

Reproduced with permission of John Wiley and Sons, Inc. from *Journal of Polymer Science Part B-Polymer Physics,* Choi, P.; Jalani, N. H.; Thampan, T. M.; Datta, R, *44,* 2183. Copyright © 2006, John Wiley and Sons Inc.

The mobility within the membrane will be influenced by at least four interrelated factors: which proton transport mechanism is dominant, the attraction of the protons to the negatively charged pore wall, the nature of the confined water, and the connectivity of the aqueous channels.[54] All of the above factors are either directly or indirectly affected by the water content in the membrane, λ.

Using a comparison between the H_2O diffusion coefficient, obtained from ^1H NMR, and the H^+ diffusion coefficient, obtained from conductivity measurements, Zawodzinski and coworkers have suggested that at high water contents both the vehicle

is dominant. They have shown that as water content decreases, the contribution of the vehicle mechanism increases, and the Grotthuss mechanism decreases.[61] At low water contents, the number of hydrogen bonding interactions is small which causes the remaining hydrogen bonds to be shortened and tightened. The result is an increased average hydrogen bond energy, which leads to a reduced rate of the bond breaking and forming processes. Since bond breaking and forming is necessary for structural diffusion, the Grotthuss mechanism is depressed.[54]

Eikerling and Kornyshev have calculated that under conditions of minimal hydration, $\lambda = 1 - 2$ H_2O/SO_3H, proton transport occurs along the surface of the pore wall via a proton hopping mechanism between sulfonic acid groups, mediated by intermediate water molecules. The authors have shown that the activation enthalpy of the surface mechanism increases considerably with the average distance of sulfonic acid head groups.[58] Other factors that affect the rate of proton transport along the pore surface include the conformation of the fluorocarbon backbone, flexibility of the side chains, degree of aggregation and associations of sulfonic acid groups.[62]

Historically, proton transport properties have been linked primarily to ionic conductivity, measured by AC impedance spectroscopy, either in an operating fuel cell (in-situ) or under conditions that mimic a particular fuel cell system of interest (ex-situ).[63] As proton conductivity has been observed to be dependant on sulfonic acid content, systematic studies are performed by varying sulfonic acid content and measuring proton conductivity. Resulting conductivity trends are then correlated to the connectivity and size of the water-saturated channels, the latter of which is measured using supplementary

analytical techniques, such as transmission electron microscopy (TEM) and x-ray diffraction (XRD).[25]

1.5 Research Outline

To date, Nafion remains the preferred candidate for hydrogen/oxygen proton exchange membrane fuel cells operating under ambient conditions. However, a shift towards the development of novel materials is occurring, in order to satisfy technological requirements for fuel cells that operate at high temperatures, under low humidity conditions, and for specialized applications. Typically, a series of independent PEMs is developed based on a common polymer backbone with varying sulfonic acid contents. The backbone and target sulfonic acid contents are generally chosen by a random "hit or miss" approach. The objective of this research was to provide systematic insight into the relationship between polymer structure and proton transport properties that could potentially be used to improve the efficiency of PEM development. To achieve this goal, a variety of structurally different PEM polymer systems were chosen and systematically investigated.

Chapter 2 is based on published work and presents an in-depth analysis of the relationship between proton conductivity and water content in fully hydrated PEMs.[64] In this chapter, a systematic method was developed and employed to investigate the proton transport properties of four independent main chain sulfonated polymer systems. Each series comprised a minimum of three independent membranes varying by sulfonic acid content (IEC). As IEC has a significant impact on water content, adjusting the IEC presented an *indirect* method to control water content within the polymer systems, while keeping the polymer backbones of the membranes fixed. The combination of proton

conductivity and water content data allowed for a description of the mobility of protons in the PEM.

The method developed in chapter 2 was also used in chapter 3 to gain insight into the proton transport properties of one of the previously investigated main chain sulfonated PEMs under conditions of controlled relative humidity (RH). Varying the RH of the environment provided a *direct* method to control water content inside the membrane. This permitted a systematic study of individual membranes rather than averaging properties over an entire series. Proton conductivities and water contents were measured on samples subjected to a series of relative humidity environments between 50 – 98% RH. From this data, proton mobilities were calculated and used to evaluate individual membranes, as well as to draw comparisons between them.

Chapter 4 is based on published work that describes the synthesis and characterization of a series of conformable proton-conducting thin films prepared from photocurable liquid polyelectrolytes.[65] The resultant photocured films are semi-interpenetrating networks comprising a linear proton-conducting guest polymer, sulfonated poly(ether ether ketone), in the presence of a statistically cross-linked host polymer matrix comprising divinylsulfone, vinylphosphophonic acid, and acrylonitrile. A systematic investigation was performed to determine the effect of host/guest composition on physicochemical properties. Photocuring of the host cross-linked polymer structure was monitored using UV and IR spectroscopy. Thermogravimetric analysis and differential scanning calorimetry were used to determine the decomposition and glass transition temperatures, respectively.

Chapter 2: Preparation and Proton Transport in Main-Chain, Statistically Sulfonated Proton Exchange Membranes

2.1 Introduction

The development and fundamental understanding of new proton exchange membranes (PEMs) have been of particular interest in proton exchange membrane fuel cell (PEMFC) research for some time.[6,25,63,66] Although there are differing opinions as to the exact organizational microstructure of PEMs, it is widely accepted that in general for most PEMs, water-saturated channels form upon membrane hydration. This is due to the phase separation of the normally hydrophobic polymer backbone from the bound sulfonic acid groups. Proton conduction is thought to occur through these water-saturated channels, mediated by the sulfonic acid groups and in conjunction with water that is either closely related, associated with the acid groups, or present as bulk water in the channels.[7,15,17]

Nafion® membranes have been at the forefront of PEM development, offering the best combination of performance, durability, and reliability to date. Nevertheless, as the technological requirements for automotive and stationary applications are becoming

---

* Sections of this work have been reproduced by permission of the Royal Society of Chemistry: *Journal of Materials Chemistry*, Peckham, T. P.; Schmeisser, J.; Rodgers, M.; and Holdcroft, S., 17, 3255, © 2007, RSC Publishing
Conductivity and water content data for the S-SEBS polymers used in this work were measured by Dr. Vesna Basura.

increasingly rigorous, there is a growing need for PEMs that have improved properties over those offered by Nafion membranes.[11,67]

One of the methods most commonly used to develop new PEMs with tailored functionality is to start with a common polymer backbone and create a series of independent membranes by varying the sulfonic acid content. A systematic study is then performed to examine the effect of polymer backbone and degree of sulfonation on fuel cell pertinent properties. As this is normally an iterative or random "hit or miss" approach, it is generally not a very effective method for creating membranes with desirable properties. A more efficient approach would be to first obtain a fundamental understanding of the structure-property relationships for these materials before attempting to design a new PEM.

The goal of this work has been to perform an-depth analysis of proton conductivity data in hopes of garnering additional insight into proton transport properties that can potentially be used in the design of new materials with improved levels of proton conductivity. The approach used to attain this goal was to perform a systematic study of the transport properties of four sulfonated model PEM series (Figure 2.1b-e): a five membrane series of sulfonated poly(ether ether ketone) **S-PEEK**; a three membrane series of radiation-grafted ethylenetetrafluoroethylene-grafted-poly(styrene sulfonic) acid **ETFE-*g*-PSSA**; a five membrane series of sulfonated α, β, β-trifluorostyrene-co-substituted α, β, β-trifluorostyrene **BAM®**; and a three membrane series of sulfonated polystyrene-*b*-poly(ethylene-*r*-butylene)-*b*-polystyrene triblock copolymer **S-SEBS**. The industry standard **Nafion** was used for comparative purposes (Figure 2.1a). Where each series varies in polymer backbone chemical structure, the membranes within each series

have a common polymer backbone, but vary with respect to the extent of sulfonic acid incorporated into the polymer.

Included in Figure 2.1, beside each chemical structure, is a simplified cartoon of the polymer morphology. All of the polymers fall into one of two categories: side chain sulfonated or main chain sulfonated. Nafion is a side chain sulfonated membrane, as there is a "spacer" (vinyl ether group) that separates the sulfonic acid group from the backbone. Comparatively, S-PEEK; ETFE-*g*-PSSA; BAM; and S-SEBS are all main chain sulfonated, as the ionic sites are directly attached to the polymer backbone.

Figure 2.1 Chemical structure and cartoon representation of PEM series used in this study a) Nafion b) S-PEEK c) BAM d) ETFE-*g*-PSSA and e) S-SEBS

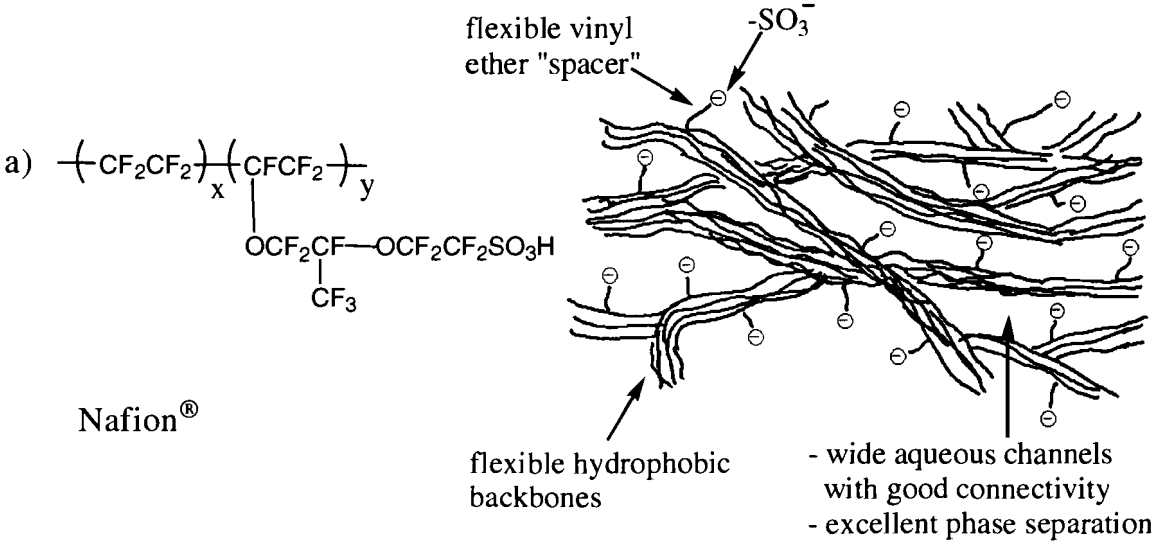

b)

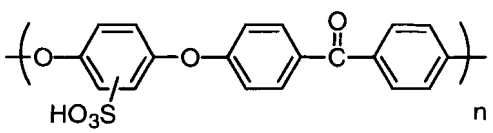

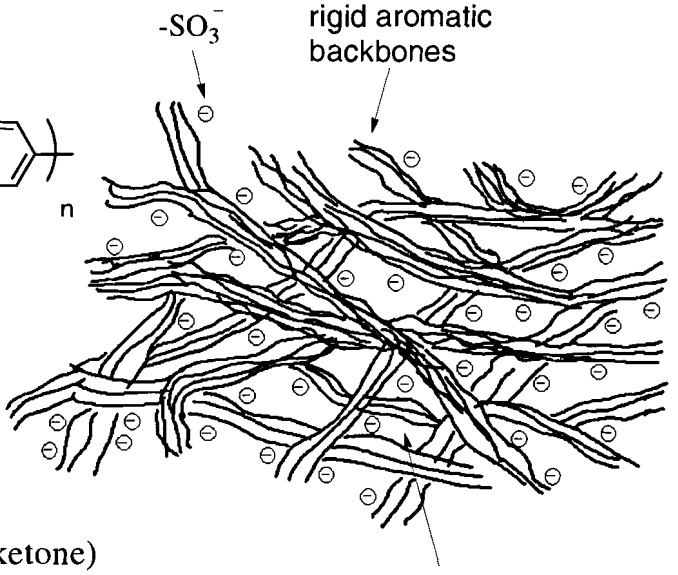

S-PEEK
sulfonated poly(ether ether ketone)

- narrow, highly branched aqueous channels with many "dead ends"
- good phase separation

c)

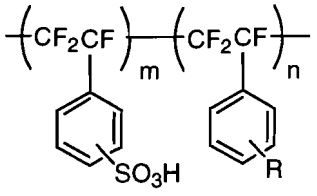

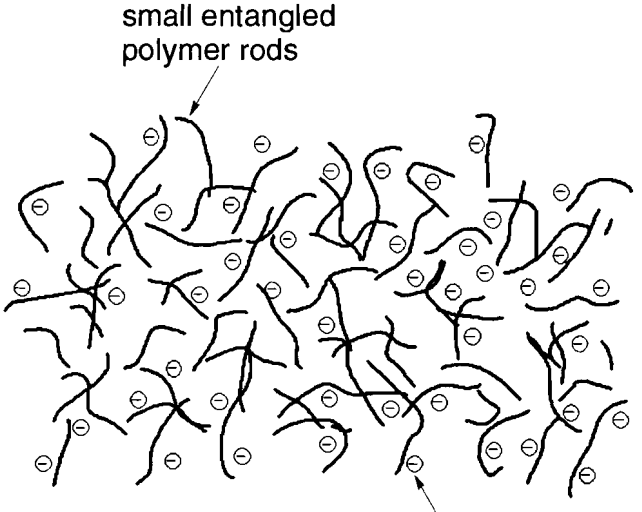

α, β, β-trifluorostyrene-co-substituted
α, β, β-trifluorostyrene (BAM)®

- homogenously distributed sulfonate groups
- poor phase separation

BAM morphology proposed based on SAXS and SANS data of high IEC samples (IEC 2.10 and 2.40 mmol/g)

d)

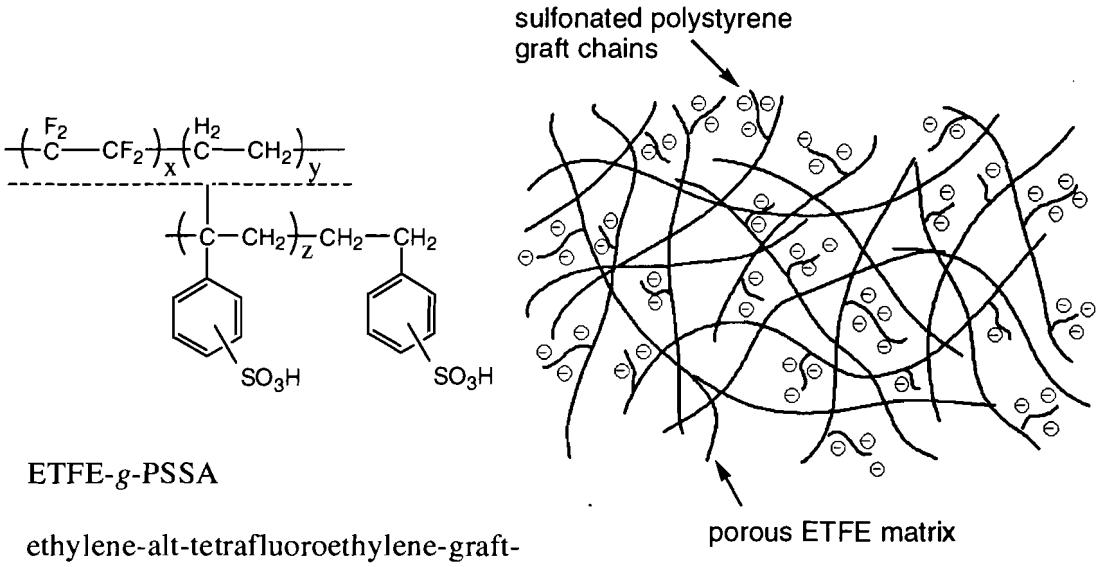

ETFE-*g*-PSSA

ethylene-alt-tetrafluoroethylene-graft-poly(styrene sulfonic acid)

e)

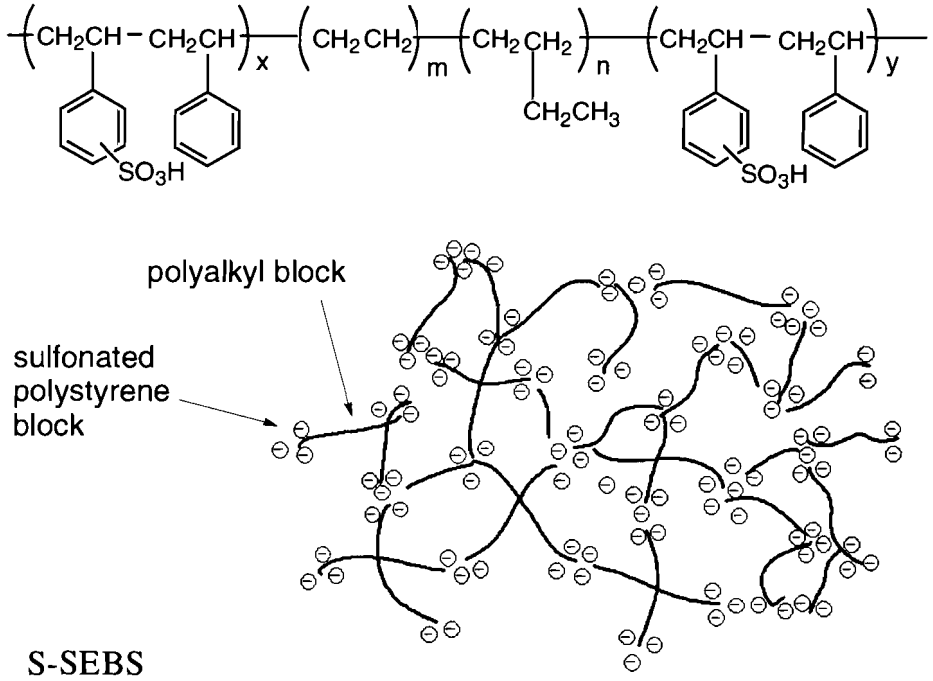

S-SEBS

sulfonated polystyrene-*b*-poly(ethylene-*r*-butylene)-*b*-polystyrene

Figure 2.2 Strategy for the analysis of proton conductivity data as a function of IEC

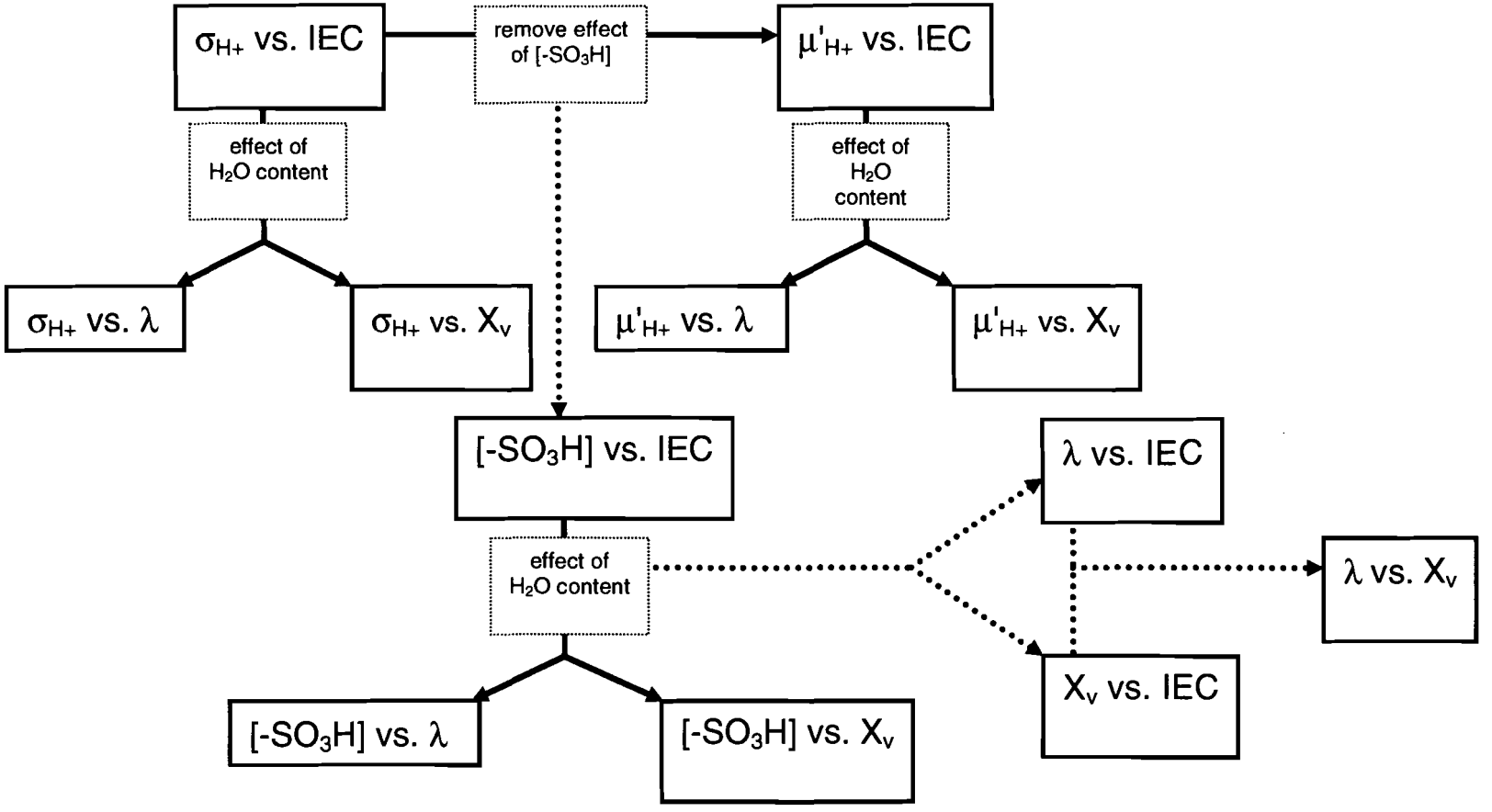

2.1.1 Approach to Data Analysis

An in-depth analysis was performed, that examined the relationships between proton conductivity and water content. Measurements were performed on samples in the fully hydrated state under ambient conditions (1 atm, room temperature). The analysis itself was divided into four sections: proton conductivity; water content analysis; proton concentration; and effective proton mobility. Figure 2.2 illustrates the various component plots for each section.

Proton Conductivity

Although both water content and the density of acid groups have an influence on the conduction of protons in the PEM, only the density of acid groups remains consistent within a membrane, irrespective of the membrane environment. Thus, the relationship between proton conductivity (σ_{H+}) and the density of acid groups (i.e., IEC) at a fixed temperature and humidity is an effective starting point for an analysis.

Water Content Analysis

IEC can have a significant impact on the amount of water absorbed by the membrane. As the number of sulfonic acid groups increases, the overall hydrophilicity of the material increases, and consequently more water is absorbed. As proton conductivity is also related to water content, however, determining the relationship between water content and proton conductivity is required. Water content of a PEM is commonly described in terms of water uptake (weight % increase for PEM from dry to wet state).

Water uptake as a volume percentage, also described as the water volume fraction (X_v), is used as a replacement here for water uptake as a weight percentage:

$$Water\ Content\ (vol\%) = X_v = \frac{V_{water}}{V_{wet}} \qquad [2.1]$$

where V_{water} is the volume of water contained in the membrane and V_{wet} is the total volume of the wet membrane.

Figure 2.3 Schematic representation of X_v

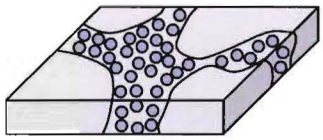

For the purpose of this work, X_v is a more useful measure as it represents the actual percentage of the volume of the membrane that is occupied by water (Figure 2.3). This is particularly useful for membranes with very high water uptakes, as will be seen in the discussion on the BAM and S-SEBS membranes. In the case of Equation 2.1, the volume of water was calculated by considering all of the water in the membrane as bulk water (rather than a combination of bulk-like and bound water), and assuming a water density of 1 g/mL.

Proton Concentration

As increasing IEC for PEMs generally leads to an increase in water content, it is also convenient to standardize water content for acid concentration, thereby permitting comparisons between PEMs with different IEC values. Acid concentration is determined according to the following equation:

$$[-SO_3H] = \frac{\text{moles of } -SO_3H}{V_{wet}} \qquad [2.2]$$

where $-SO_3H$ refers to bound sulfonic acid moieties in the PEM, moles of $-SO_3H$ is given by (IEC)*(dry mass of polymer), and V_{wet} is the wet volume of the membrane.

The titration technique, used to determine IEC, measures the concentration of $-SO_3H$ groups in the membrane, rather than an actual free proton concentration. Therefore, $[-SO_3H]$ represents the overall concentration of protons in the membrane, without distinguishing between those protons that are mostly associated with the sulfonic acid groups and those that are fully dissociated and thus mainly present in the bulk water.

Another key relationship is the ratio of the moles of water to the moles of acid, λ. Essentially, this value provides a measure of the number of water molecules that are contained in the membrane for each $-SO_3H$ group (also commonly used as a representation of water content).

$$\lambda = \frac{moles\ H_2O}{moles\ SO_3H} \qquad [2.3]$$

Where λ suggests more of a "microscopic" representation of water molecules per sulfonic acid content, $[-SO_3H]$ offers a more "macroscopic" representation of moles of acid in a fixed volume of wet membrane. Shown in Figure 2.4 is a schematic of the difference between the two measures of acid content.

Figure 2.4 Schematic representation of (a) λ (shown $\lambda = 5\ H_2O/SO_3H$) and (b) $[-SO_3H]$

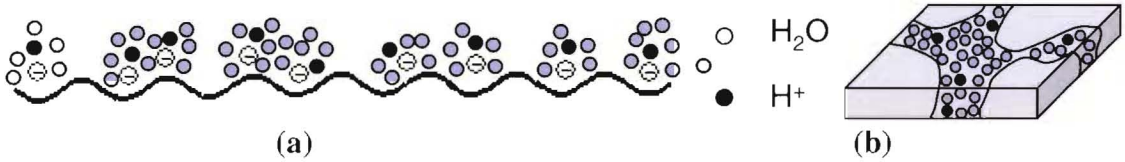

Plotting both X_v and λ as a function of IEC, allows for a determination of whether water content increases steadily as a function of acid content, or whether there are any sudden, sharp increases. In the latter case, this is a sign of increased swelling, and is an important point to note due to the strong effect it will have upon [$-SO_3H$] and, hence, upon proton conductivity.

Another important plot is to see how λ varies as a function of X_v. In common with determining how water content varies as a function of acid content, this plot also will show if swelling occurs at a consistent rate (λ increases steadily as a function of X_v), or if there are sudden increases (λ increases suddenly as a function of X_v). There is also a third case where swelling is very limited (i.e. λ remains the same over a wide range of X_v). Finally, a plot of λ as a function of X_v also permits relative comparisons between different PEMs, and will show whether certain membranes are able to achieve a given λ value at lower X_v values than for other membranes.

Proton Mobility

Mobility, μ, is defined as the rate of transport of a species under an applied electric field ($cm^2s^{-1}V^{-1}$). Upon examination of the general definition of electrical conductivity, σ_e, we see that it is simply a function of the quantity of charge carriers in a given volume, η, and the mobility of those charge carriers, μ_e:[68]

$$\sigma_e = \eta e \mu_e \qquad [2.4]$$

This general relationship is easily extended to conductivity of ionic systems when only one of the charged species is mobile (i.e., the transference number of that species is equal to one):

$$\sigma = Fa_i|Z_i|\mu; \qquad [2.5]$$

where σ is the specific conductivity of the ion, F is Faradays constant, a_i is the activity of the ion, and Z_i is the charge on the ion. The activity, a_i, can be defined by the following equation:

$$a_i = f_i C_i \qquad [2.6]$$

where f_i describes the degree of dissociation of the ion and C_i is the analytical concentration of the ion.

This relationship is applicable for an estimation of proton mobility from proton conductivity in PEMs as the negatively charged $-SO_3^-$ counter-ions are tethered to the backbone, rendering them immobile, resulting in a transference number of one for the positively charged protons.

$$\sigma_{H^+} = F[H^+]\mu_{H^+} \qquad [2.7]$$

In fact, a more correct description of the above equation is to replace $[H^+]$ with the activity value for H^+. This requires accurate knowledge of the activity coefficient, which is concentration dependent, and an unattainable value in these systems. The activity, as previously shown in Equation 2.6, is related to *f*, the degree of dissociation (dependent upon both the pKa of the acid group as well as the water content of the PEM), and is thus a factor in the mobility of the proton. In fact, proton mobility in the aqueous phase of a PEM does not fall into the classical view of mobility of free ions in solution. For example, strong binding of a proton to the tethered anion (or anions) as it traverses the membrane should be considered as an impediment to its mobility. Hence, the calculated proton mobility is an "effective" mobility that includes the uncertainties of the

activity coefficient for H^+. In the extreme, if all the acid groups in the membrane remain undissociated, the effective mobility value is zero.

Given that the analytical acid concentration [$-SO_3H$], rather than proton concentration [H^+], is the quantity measured by titration, [$-SO_3H$] has been substituted for [H^+] in Equation 2.7 as seen in Equation 2.8. Therefore, calculation of proton mobility allows a "normalized" proton conductivity to be determined; i.e., acid concentration effects are removed. By doing this, it is possible to view the relative contributions of both proton mobility and acid concentration (itself consisting of contributions from both acid and water contents) to the experimentally measured proton conductivity.

In addition to the effect dissociation and tethered anionic groups have on mobility, there are additional effects that further distinguish the mobility of protons in a PEM from the classical picture. One of these relates to the connectivity and long range transport path for protons. This is schematically illustrated in Figure 2.5 in which a) is characterized as having a more tortuous conduction pathway, with a series of dead-ends, compared to the conduction pathway in b), which is more linear. The supposition, therefore, is that proton mobility will be effectively greater in b) relative to a). In fact, Kreuer has previously invoked these concepts of smaller conduction channels and dead ends in order to explain the lower proton mobility in S-PEEKK compared to Nafion.[11]

Figure 2.5 **Connectivity of aqueous domains in PEMs (white = aqueous domains) where the degree of tortuosity of proton conduction pathway is greater in (a) than (b)**

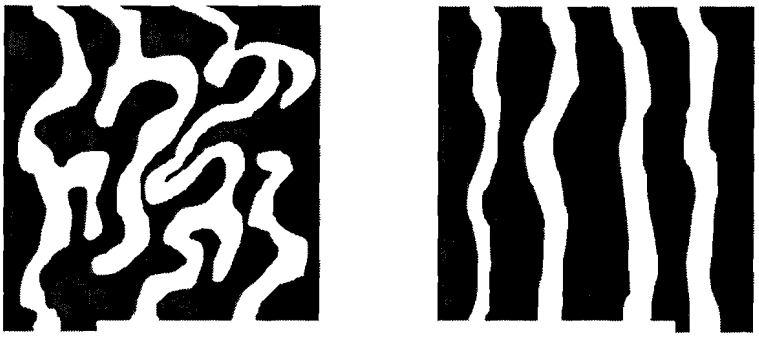

a) b)

The distance between acid groups may also play a role in the mobility of protons. Pores having different distances between acidic groups are shown schematically in Figure 2.6. As the proton-bearing, positively charged species (e.g., H_3O^+, $H_2O_5^+$ and/or $H_4O_9^+$ ions) are transported between the negatively charged, tethered $-SO_3^-$ groups, it may be expected that it will be more difficult for a proton to be transported over the larger distances between $-SO_3^-$ in a) in comparison to the shorter distances between $-SO_3^-$ groups in b). Therefore, this could lead to a lower proton mobility in a) in comparison to b).[58,69,70]

Figure 2.6 **Spatial proximity of neighbouring acid groups within an aqueous channel where the distance between acid groups is greater in (a) than (b)**

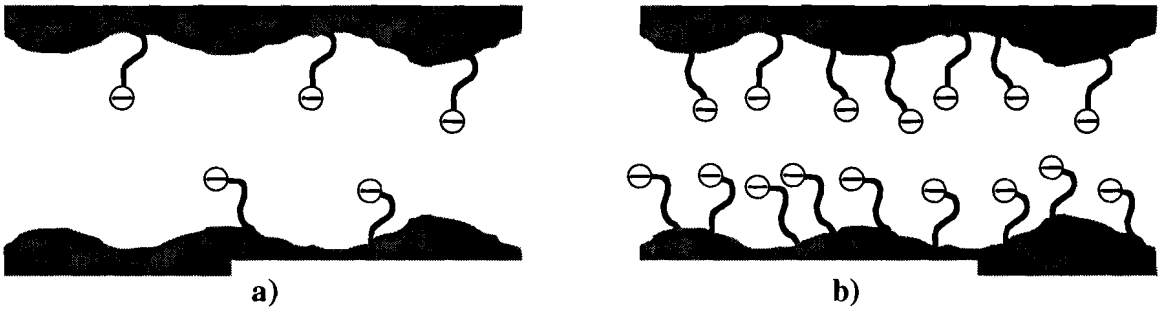

The "effective" proton mobility, μ'_{H+}, as derived from the proton conductivity data (Equation 2.12), therefore, incorporates terms that relate to acid dissociation (or pKa), tortuosity (Figure 2.5), and spatial proximity of neighbouring acid groups (Figure 2.6).

$$\sigma_{H^+} = F[-SO_3H]\mu'_{H^+} \qquad [2.8]$$

2.2 Experimental

2.2.1 Membranes

As received BAM® membranes (provided courtesy of Ballard Advanced Materials), as received ETFE-*g*-PSSA membranes (provided courtesy of Cranfield University, UK), as received S-SEBS membranes (Dais-Analytic Corporation), in-house synthesized S-PEEK membranes, and treated Nafion 117® (DuPont) were used in this work.

BAM and ETFE-*g*-PSSA membranes were received in the dry acidified form. To ensure complete protonation, the membranes were soaked in 0.5 M H_2SO_4 for 48 hours. The membranes were cut into ~ 5 x 5 cm sheets, and hydrated in Milli-Q ultra pure H_2O (18 MΩ) for a minimum of 24 hours prior to use.

Nafion was received in the dry form. Impurities in Nafion were removed according to a literature procedure.[61] Strips of Nafion were boiled in a 3 vol% H_2O_2 solution for two hours, boiled in Milli-Q (18MΩ) H_2O for 2 hours, boiled in 0.5 M H_2SO_4 for two hours, and finally rinsed in boiling Milli-Q H_2O for two hours. Treated Nafion samples were hydrated in Milli-Q H_2O for a minimum of 24 hours prior to use.

S-PEEK membranes were prepared according to the synthetic procedure outlined in Section 2.3.1 The cast membranes were stored in the dry form. No treatment procedure was performed. The membranes were cut into ~ 5 x 5 cm sheets and hydrated in Milli-Q H_2O for a minimum of 24 hours prior to use.

2.2.2 Water Content Analysis

Circular samples (8.48 mm diameter) were cut from fully hydrated sheets and soaked in Milli-Q water for a minimum of 12 hours. Wet weights, W_{wet} (+/- 0.0001 g), were obtained after blotting with a Kimwipe to remove surface water. This was carried out on as short a time scale as possible (< 30 s) to avoid water loss to the atmosphere. Dry weights, W_{dry} (+/- 0.0001 g), were obtained after membranes were vacuum (1 mmHg) dried to a constant weight (+/- 0.0005 g) at 80°C for two hours and cooled in a desiccator. For all samples, constant weight was achieved after drying for 2 hours.

Membrane volumes were obtained for both wet, V_{wet}, and dry, V_{dry}, samples by measuring diameter, d, with a calliper (+/ 0.1 mm), thickness, h, with a micrometer (+/ 0.001 mm), and applying the following relationship:

$$Volume = \frac{1}{4}\pi d^2 h\,; \qquad [2.9]$$

2.2.3 Ion Exchange Capacity

Ion exchange capacity, IEC, determined using a direct titration method, represents the number of millimoles (mmol) of ion exchange sites per dry gram of polymer, and was used to quantify sulfonic acid content in this work. Circular samples (8.48 mm diameter and ~ 70-200 μm thickness) were cut and placed in 2M HCl, and stirred for 12 hours. The membranes were then transferred to a new beaker containing Milli-Q water and

stirred for 30 minutes, after which the water was decanted and replaced with fresh water and stirred for another 30 minutes. This process was repeated two more times. The acidified membranes were then immersed in 50 mL of 2M NaCl solution for 2 hours, with occasional agitation, and titrated with standardized NaOH to the phenolphthalein endpoint. Before obtaining a dry weight, the membranes were reprotonated with HCl, rinsed with Milli-Q water, vacuum (1mmHg) dried at 80°C to a constant weight, and cooled in a desiccator. Ion exchange capacity was calculated as follows:

$$IEC(mmol\ SO_3H/g) = \frac{(vol.\ \mathrm{NaOH}, mL) \times (conc.\ \mathrm{NaOH}, M)}{(dry\ wt.\ of\ membrane, g)} \qquad [2.10]$$

Since the density of acid groups remains consistent within a membrane, irrespective of the environment, IEC was used in conjunction with the acronym for the polymer to differentiate between the samples in each series (i.e., the BAM 2.46 sample is composed of a BAM membrane that has been sulfonated to an average IEC of 2.46 mmol/g).

2.2.4 Ionic Resistance

Ionic Resistance was measured using AC impedance spectroscopy with a Solartron 1260 frequency response analyzer (FRA), employing a transverse two-electrode configuration. Rectangular samples of hydrated membranes were cut to the required dimensions (length, L, and width, W, measured using a calliper, +/- 0.1 mm, and thickness, h, using a micrometer, +/- 0.001 mm), Figure 2.7a. To ensure complete protonation, i.e., no contamination from the knife or cutting surface, samples were soaked in 0.5 M H_2SO_4 for 24 hours, followed by soaking in Milli-Q water for a minimum of 12 hours prior to use.

Figure 2.7 (a) Rectangular PEM sample dimensions. (b) Pt/Teflon® conductivity probe

a)

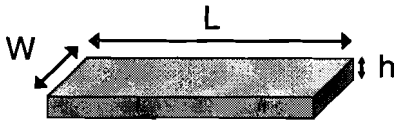

b)

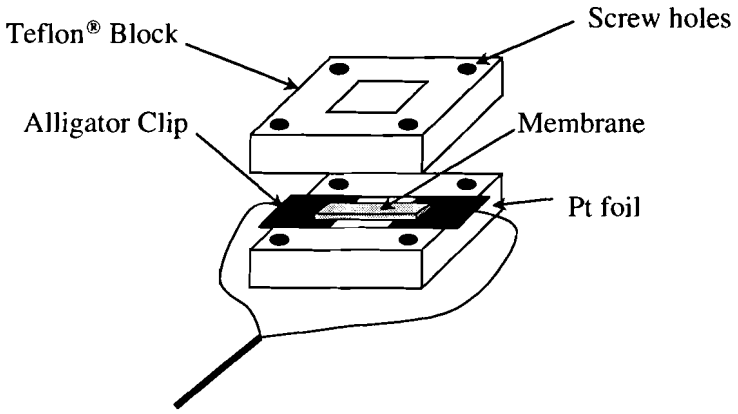

Samples were removed from water, blotted with a Kimwipe to remove surface water, and laid across two platinum electrodes (0.5 x 1 cm) 1 cm apart and fixed in place by attaching them to an inert Teflon block (2 x 2 cm). Another Teflon block was placed on top, and four nylon screws were used to immobilize the membrane inside the probe during measurement.[71] Probe assembly was carried out on as short a time scale as possible (< 1 min) to keep the samples from losing water to the atmosphere before completion of the measurement. All measurements were carried out on fully hydrated samples at room temperature, under ambient atmosphere.

Two wires fitted with alligator clips connected the probe to the FRA, and ionic resistance was measured by applying a 100 mV sinusoidal AC voltage between the two platinum electrodes over 10 MHz – 100 Hz frequency range, and measuring the AC resistance (i.e., impedance). Data was analyzed using commercial software (Zplot,

Scribner Associates), and a detailed explanation of the analysis is included in Section 2.3.2.

2.3 Results

2.3.1 Synthesis of Sulfonated Poly(ether ether ketone)

S-PEEK polymers were synthesized by electrophilic sulfonation of poly(ether ether ketone), PEEK, with sulfuric acid similar to the method described by Huang et.al.[72] A solution composed of 18 g of PEEK (supplied by Victrex® Mn ~ 110,000 g/mol), dissolved in 300 mL concentrated sulfuric, acid was heated to 50-55°C. Portions were removed at random time intervals, Table 2.1, to obtain a series of polymers of varying sulfonic acid content. Each S-PEEK polymer was precipitated in deionized water, until a neutral pH of the water was obtained, followed by vacuum drying (1mmHg) at 90°C overnight.

Table 2.1 Sulfonation reaction times for the synthesis of S-PEEK

Sample	Reaction Time (hrs)
S-PEEK 1.99	4
S-PEEK 2.14	6.5
S-PEEK 2.30	8
S-PEEK 2.45	10
S-PEEK 2.56	15

S-PEEK ionomer films were prepared by solution casting from dimethyl sulfoxide (DMSO). The corresponding S-PEEK polymer was dissolved (~25 wt %) in DMSO, with stirring, at room temperature until a clear solution formed, which was then cast onto glass plates, and heated under ambient atmosphere at 90°C overnight. Films of 70-150 μm were released from the casting plate by immersing in deionized water for 2-10

minutes. Cast membranes were subsequently washed in deionized water to remove residual solvent.

2.3.2 Proton Conductivity

Proton conductivities can be extracted from ionic resistance measurements. Included in Figure 2.8 is a series of typical complex-plane plots of the imaginary impedance (Z'') verses real impedance (Z') for representative samples of PEMs used in this study. Figure 2.8a shows five fully hydrated BAM membranes of various IECs; BAM 1.36, BAM 1.86, BAM 1.96, BAM 2.20, and BAM 2.46. Nafion has been included for comparison. A series of semi-circles was observed, in which the size of the semi-circle varies with both IEC and membrane dimensions. Similarly, both of the S-PEEK and ETFE-*g*-PSSA series yielded semi-circles whose size varied with IEC and dimensions. Representative data for one membrane in each series, ETFE-*g*-PSSA 3.28 and S-PEEK 2.12, is included in Figure 2.8b.

Figure 2.8 **Complex-plane impedance plots for (a) the BAM PEM series with various IECs and Nafion 117(b) S-PEEK 2.12 and ETFE-*g*-PSSA 3.28 at 25°C**

a)

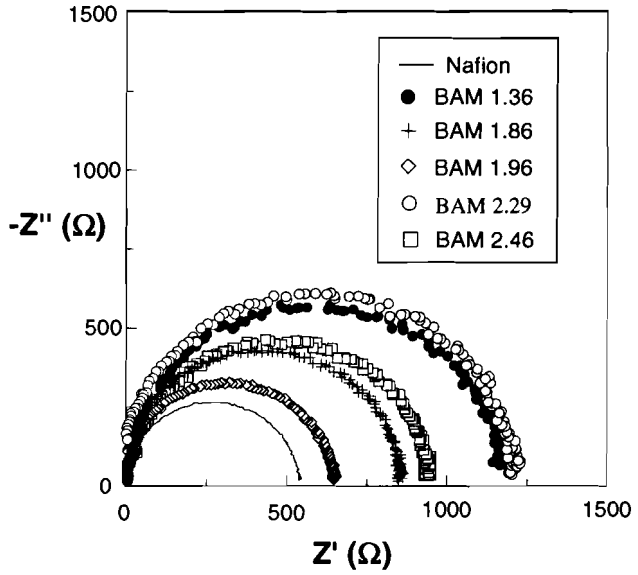

b)

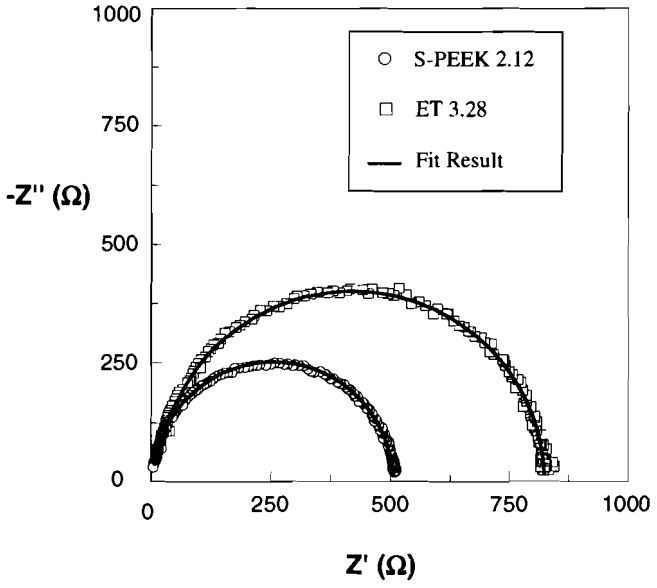

Figure 2.9 Fitted result for BAM 2.46

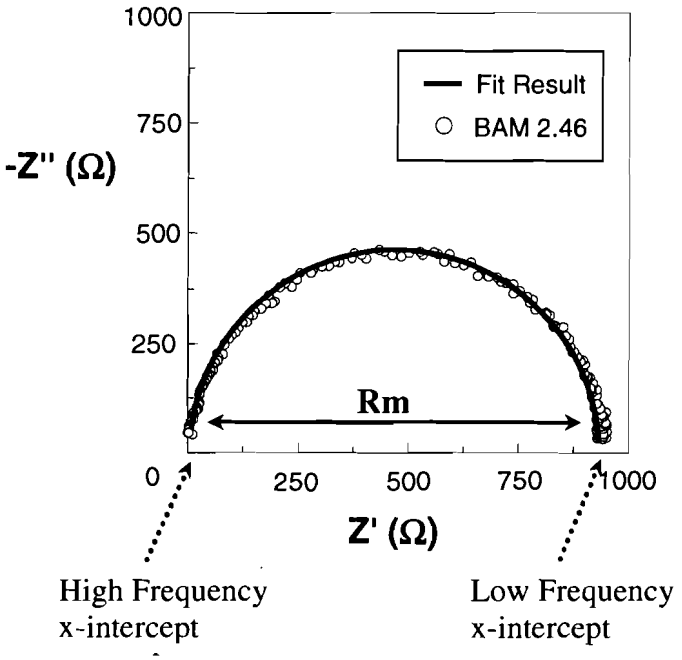

The complex-plane plot for BAM 2.46 has been highlighted as an example of how ionic resistance was abstracted from impedance data (Figure 2.9). Fitting was performed by non-linear least squares regression to a Randles equivalent circuit model (Figure 2.10).[73] The model consists of membrane capacitance, C_m, acting in parallel with membrane ionic resistance, R_m. A contact resistance, R_c, arising from the membrane/electrode interface, acts in series with the above. In essence, an approximation of the data can be made by taking the difference between the high frequency and low frequency x-intercepts, i.e., the diameter of the semi-circle.

Complex-plane plots of membranes in all three PEM series, BAM, ETFE-*g*-PSSA, and S-PEEK, fit near perfect semi-circles. The low values of contact resistance

measured, R_c, compared to that of membrane resistance, < 1%, indicate that there is sufficient contact between the Pt electrodes and membrane surface.

Figure 2.10 Randles equivalent circuit model used to fit PEM impedance data

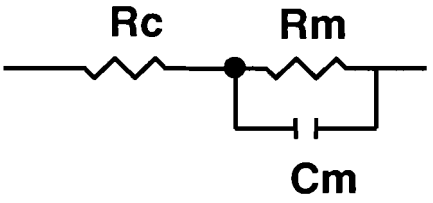

Ionic resistance in of itself does not provide a meaningful method to compare the proton transport of different materials because it does not take into account the dimensions of the membranes, which are impossible to keep consistent between membrane samples. To normalize the samples with respect to dimension, ionic resistance, R_m, was used to calculate proton conductivity, σ_{H+}, according to the following relationship:

$$\sigma_{H^+} = \frac{L}{R_m A}; \qquad [2.11]$$

where L is the spacing between the Pt electrodes (1.0 cm) and A is the cross sectional area of the membrane (W×h).

A summary of the data necessary to perform the data analysis is shown in Table 2.2. Proton conductivity values reported here for S-PEEK are consistent with those reported in the literature across a similar IEC range.[74]

Table 2.2 Summary of data for fully hydrated Nafion, BAM, S-PEEK, ETFE-*g*-PSSA, S-SEBS PEMs

Membrane	IEC (mmol/g)	X_v	λ mol H_2O/ mol SO_3H	[-SO_3H] (M) ± 10%	σ_{H+} (S/cm) ± 5%	$\mu'_{H+}*10^3$ ($cm^2s^{-1}V^{-1}$) ±11%
Nafion	0.97	0.41	20	1.11	0.09	0.87
BAM 1.36	1.36	0.33	14	1.34	0.06	0.45
BAM 1.86	1.85	0.55	24	1.27	0.12	0.97
BAM 1.96	1.96	0.62	31	1.12	0.14	1.30
BAM 2.20	2.20	0.82	76	0.60	0.10	1.74
BAM 2.46	2.46	0.85	84	0.56	0.09	1.74
ETFE-*g*-PSSA 2.12	2.13	0.58	22	1.78	0.15	0.85
ETFE-*g*-PSSA 2.56	2.56	0.63	24	1.46	0.17	1.19
ETFE-*g*-PSSA 3.28	3.27	0.73	29	1.28	0.20	1.59
S-PEEK 1.99	1.99	0.35	13	1.52	0.04	0.26
S-PEEK 2.14	2.14	0.40	15	1.52	0.07	0.45
S-PEEK 2.30	2.30	0.49	19	1.40	0.10	0.73
S-PEEK 2.45	2.45	0.53	24	1.22	0.12	1.02
S-PEEK 2.56	2.56	0.66	42	0.88	0.14	1.67
S-SEBS 0.94	0.94	0.25	24	0.69	0.03	0.45
S-SEBS 1.13	1.13	0.38	46	0.69	0.05	0.75
S-SEBS 1.71	1.71	0.84	147	0.56	0.05	0.93

2.4 Discussion

2.4.1 Proton Conductivity as a Function of Acid and Water Content

An investigation of the effect of sulfonic acid content (i.e. IEC) on proton conductivity is the most frequently used initial approach to explore the potential usefulness of a novel series of membranes for fuel cell applications (Figure 2.11).

Figure 2.11 Proton conductivity of fully hydrated Nafion, S-PEEK, ETFE-*g*-PSSA, BAM, and S-SEBS as a function of IEC.

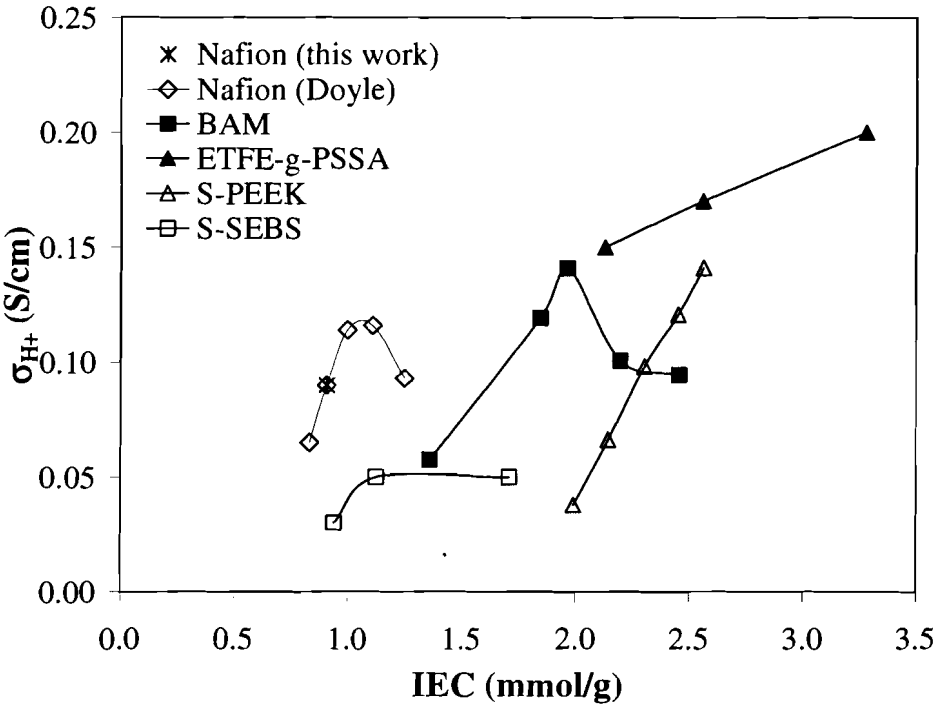

Conductivity data for Nafion (◇) taken from reference 75

An examination of Figure 2.11 reveals that within the range of available IECs, the acid content in all five membrane systems studied in this work, S-PEEK; ETFE-*g*-PSSA; BAM; S-SEBS; and Nafion, is sufficient to have reached the percolation threshold; i.e., the point at which there is an adequate degree of connectivity between ionic domains for the transport of protons and water through the membrane. Beyond the percolation

threshold, the trend generally observed for the majority of PEMs is an improvement in conductivity with increasing IEC. This is normally assumed to be a result of an increased density of sulfonic acid groups and increased water content, water being necessary to ensure the protons are sufficiently dissociated for mobility.

It is clear from Figure 2.11, that an increase in IEC content results in large variations of proton conductivity in S-PEEK and BAM. In contrast, both ETFE-*g*-PSSA and S-SEBS exhibit a more modest variation in conductivity. A comparison of S-PEEK with the baseline, Nafion, suggests that the percolation threshold is reached at a considerably lower IEC value for Nafion, as evidenced by the comparatively higher conductivity value of Nafion at low IEC. As the sulfonic acid groups in Nafion are separated from the polymer backbones via a flexible spacer unit, microphase separation of the hydrophilic portion of the polymer from its hydrophobic portion is more readily achieved than in the case of the main chain sulfonated S-PEEK. Therefore, this enables Nafion to form broad, continuous channels for proton transport through the membrane. In the case of S-PEEK, the channels are narrower with a greater number of "dead ends", thereby leading to decreased proton transport, as previously reported by Kreuer.[11]

Of all the PEMs examined here, ETFE-*g*-PSSA displays the largest average IEC value (3.27 mmol/g), and exhibits the best overall conductivity (0.20 S/cm). Relative to S-PEEK, ETFE-*g*-PSSA has higher conductivity values over the IEC range 2.0 – 2.6 mmol/g (e.g. more than double the σ_{H+} than S-PEEK at IEC ~ 2.1 mmol/g). Since BAM is the closest in chemical structure to ETFE-*g*-PSSA (i.e., they both possess sulfonated aromatic groups and are partially fluorinated), it might be anticipated to display some similarities in conductivity behaviour. However, in contrast to both S-PEEK and ETFE-

g-PSSA, where conductivity was always seen to be increasing as a function of IEC, Figure 2.11 clearly shows that conductivity of BAM reaches a maximum around IEC = 2.0 mmol/g, and then decreases rapidly, such that at IEC = 2.2 mmol/g, the observed value is 30% lower than seen at IEC = 2.0 mmol/g. Similar behaviour has also been reported by Doyle and coworkers, for samples of Nafion of variable IEC (data from reference 75 and included in Figure 2.11 for comparison).[75] They observed an increase in conductivity for Nafion between IEC = 0.83 – 1.11 mmol/g followed by a drastic decrease at 1.25 mmol/g. Gebel and coworkers have also reported this phenomenon during an investigation of the conductivity of Nafion membranes swollen to various water contents (X_v). S-SEBS membranes also appear to be reaching a maximum conductivity, however the conductivity values are far lower than any of the other membranes and show very little dependency on IEC, evidenced by a mere 0.02 S/cm increase over the available IEC range.

Since protons travel through the aqueous phase, it is important to investigate the relationship between proton conductivity and water content. BAM, S-PEEK, and S-SEBS all seem to be reaching a maximum conductivity as water content increases. This can be seen in Figure 2.12a (σ_{H+} vs. λ), and more clearly in Figure 2.12b (σ_{H+} vs. X_v). Similar conductivity values are observed for S-PEEK and BAM over the range X_v = 0.5 - 0.6 and λ = 10 – 30 H_2O/SO_3H, however, beyond these water contents the conductivity of BAM significantly decreases. S-SEBS maintains a low conductivity, despite achieving a very high water content, λ = 147 H_2O/SO_3H and X_v = 0.84, and shows very little dependency on water content. ETFE-*g*-PSSA on the other hand, does not appear to be reaching a maximum and possesses much higher conductivity values than any of the

other membranes for similar λ and X_v. However, given the more limited data set available for ETFE-*g*-PSSA and S-SEBS, it is unclear whether these are reflective of definite trends. Interestingly, whereas Nafion exhibited relatively high conductivity at low IEC, it exhibits a similar degree of conductivity to S-PEEK for the same water content (virtually identical values in Figure 2.12a and slightly higher for Nafion in Figure 2.12b). An explanation for this observation can be found in Section 2.4.2.

Due to the hydrophilic nature of the $-SO_3H$ group, IEC can have a strong influence on water content, both λ and X_v (Figure 2.13). The relationship between these two measures of water content allows for a comparison of differences in swelling behaviour (Figure 2.14). Assuming linear behaviour of ETFE-*g*-PSSA, over the IEC range of ~ 2.1 - 2.4 mmol/g, ETFE-*g*-PSSA possesses similar λ and greater X_v values as compared to that of S-PEEK (Figure 2.13). However, a comparison at IEC ~ 2.5 mmol/g shows that whereas the λ values for S-PEEK are significantly higher in comparison to ETFE-*g*-PSSA (42 and 24, respectively), both S-PEEK and ETFE-*g*-PSSA have almost the same X_v value (0.66 and 0.63, respectively). It appears that S-PEEK is going through a transition, in which the polymer begins to swell at a much faster rate than at lower IECs, as evidenced by the large change in X_v, for a small change in λ (Figure 2.14). However, a linear extrapolation of the data for ETFE-*g*-PSSA suggests that λ values similar to S-PEEK would be found over the X_v range of 0.3 – 0.5. Given the differences in the chemical structures of S-PEEK and ETFE-*g*-PSSA, the presence of a preformed matrix in ETFE-*g*-PSSA (wherein there are crystalline regions that do not swell, thereby acting as physical cross-links) and the chemical cross-linking that may occur during the irradiation grafting process, used to obtain ETFE-*g*-PSSA, it is not surprising that ETFE-

g-PSSA is unable to swell as easily as S-PEEK. It is also important to note that where ETFE-*g*-PSSA is produced from an extruded matrix, S-PEEK is cast and therefore, ETFE-*g*-PSSA may be naturally more porous than S-PEEK.

On the other hand, BAM and S-SEBS are able to attain much higher water contents and exhibit much more drastic swelling than S-PEEK or ETFE-*g*-PSSA (Figure 2.13 and Figure 2.14 respectively). Even at IEC = 2.2 mmol/g, BAM has already achieved $X_v = 0.82$ and $\lambda = 76$ H_2O/SO_3H, which are 12 – 25% higher X_v and a 2 – 3 times higher λ than either S-PEEK or ETFE-*g*-PSSA are able to attain at their maximum IECs. S-SEBS exhibits even more extreme swelling behaviour incorporating nearly twice the H_2O/SO_3H as compared to BAM. The higher degree of swelling in BAM and S-SEBS is likely related to the presence of a more flexible backbone in comparison to S-PEEK, as well as the absence of a matrix polymer and/or cross-linking that is present in ETFE-*g*-PSSA (Figure 2.14). S-SEBS swells to an even higher degree than BAM at least partially due to the purely hydrocarbon nature of S-SEBS, whereas BAM is partially fluorinated, giving it more hydrophobic character. Surprisingly, both BAM and S-SEBS are able to hold a high water content ($X_v = 0.85$ at IEC = 2.5 mmol/g) without completely losing mechanical integrity (i.e., the sample will return to its original dimensions upon drying) or dissolving.

Figure 2.12 **Proton conductivity of fully hydrated Nafion, S-PEEK, ETFE-*g*-PSSA, BAM, and S-SEBS membranes as a function of a) λ and b) X_v**

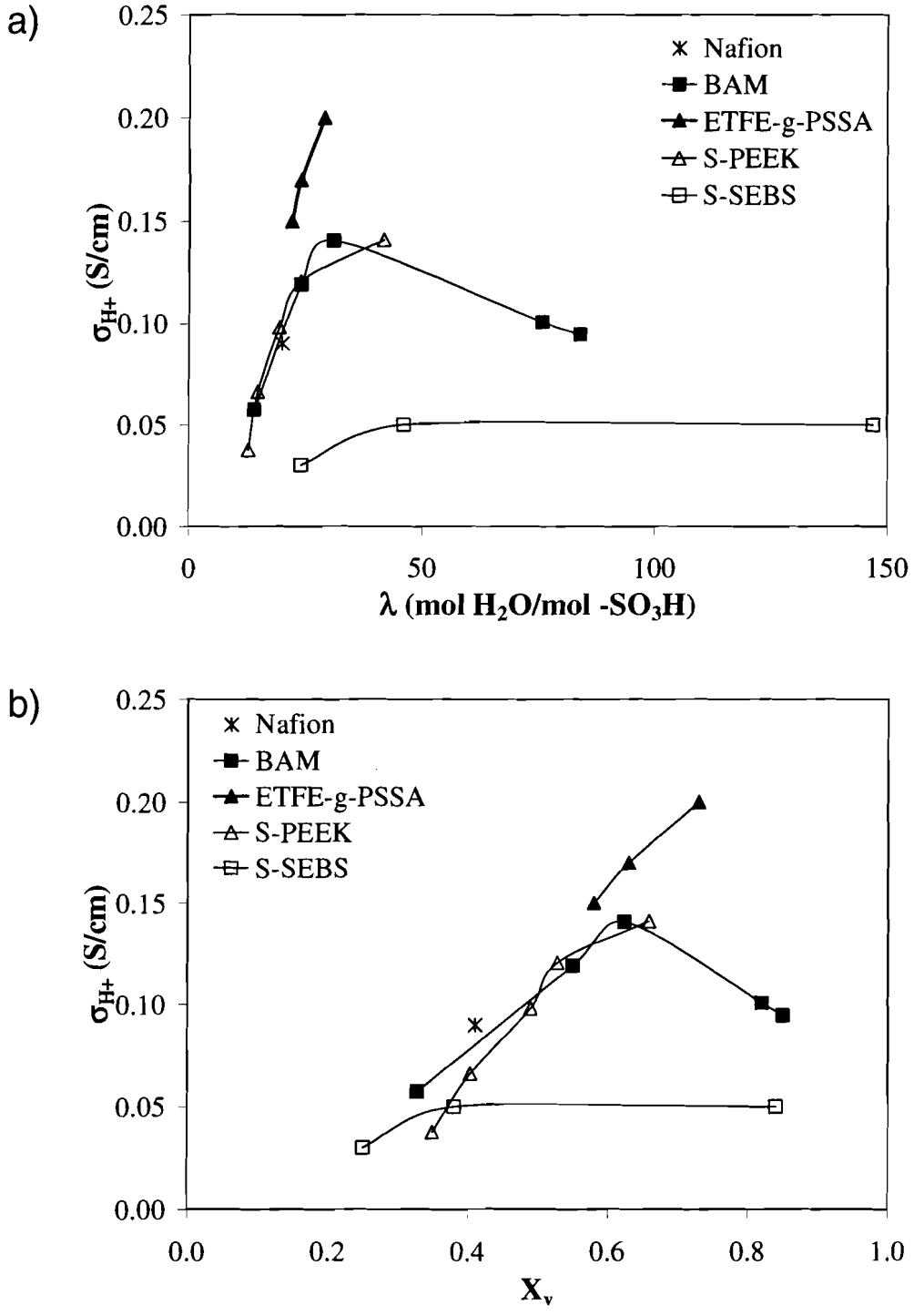

Figure 2.13 (a) λ as a function of IEC and (b) X_v as a function of IEC; for fully hydrated Nafion, S-PEEK, ETFE-*g*-PSSA, BAM, and S-SEBS membranes

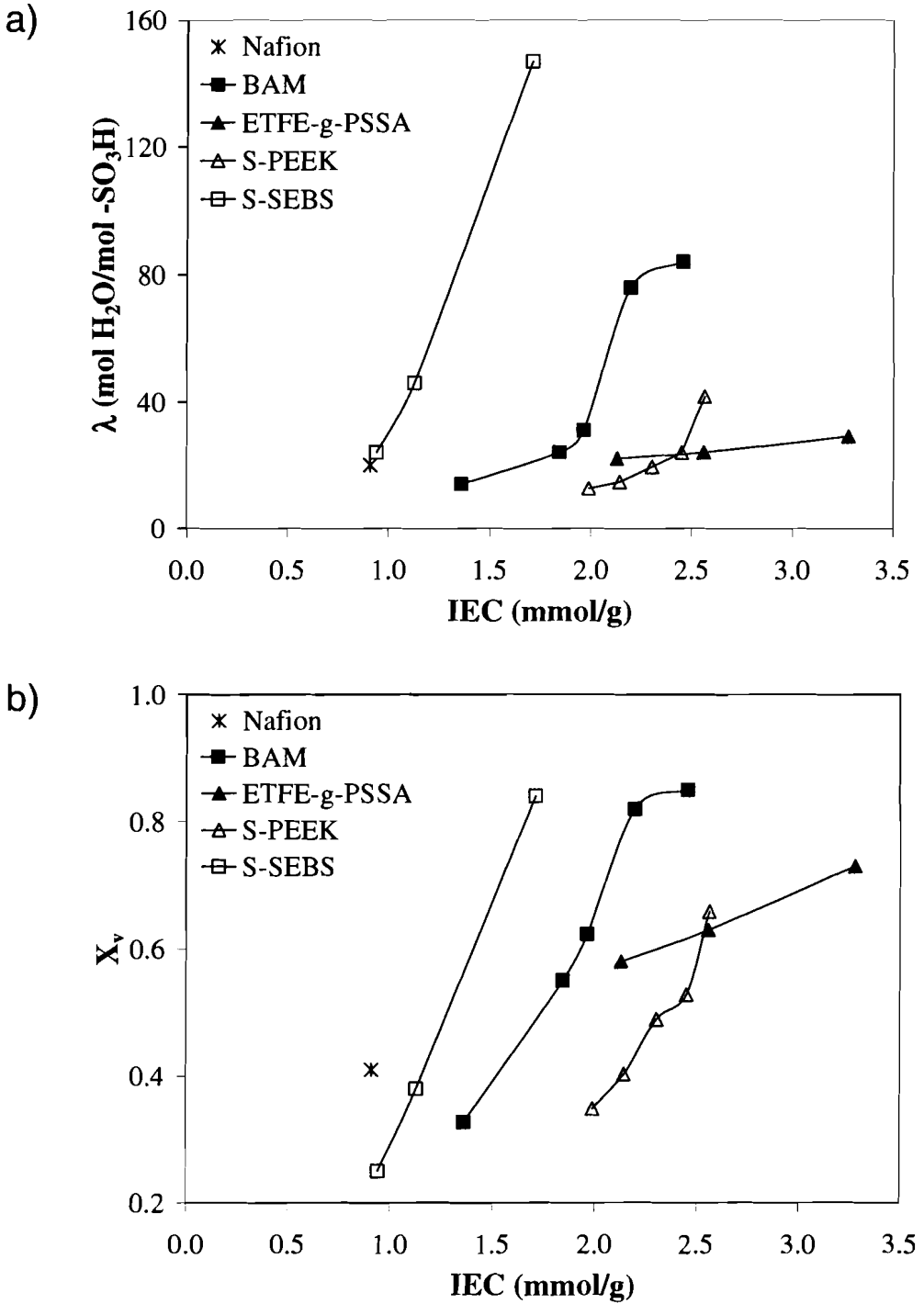

Figure 2.14 **λ as a function of X_v for fully hydrated Nafion, S-PEEK, ETFE-*g*-PSSA, BAM, and S-SEBS**

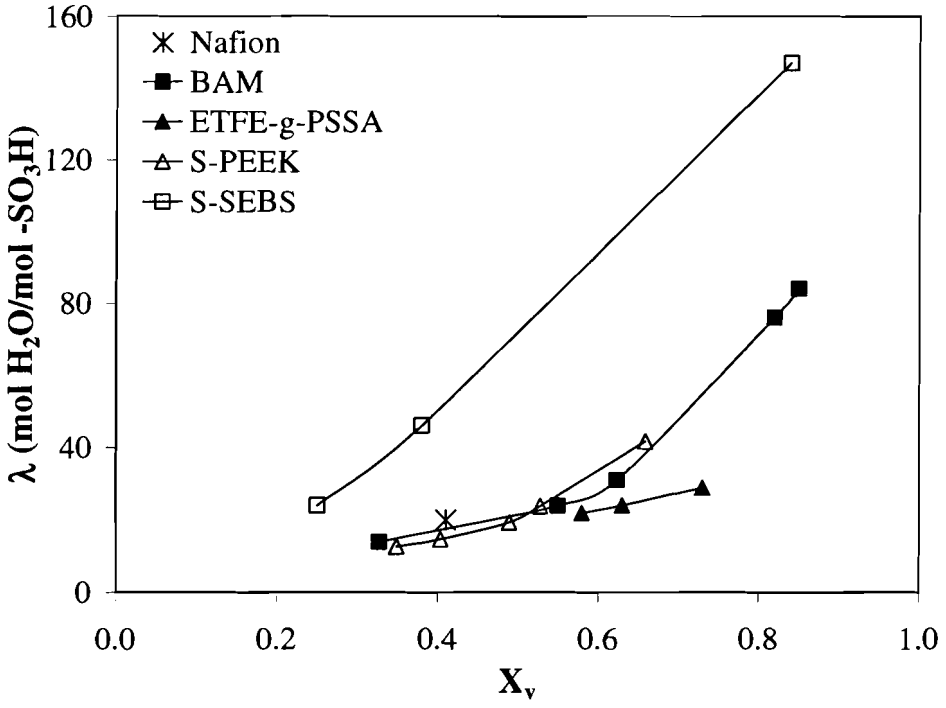

2.4.2 Effective Proton Mobility and Acid Concentration as a Function of Acid and Water Content

Additional information can be obtained from examining the effective proton mobility, μ'_{H+}, of the studied polymer systems. For all membranes, an increase in IEC also leads to an improvement in μ'_{H+} (Figure 2.15a). As it has been shown that an increase in IEC leads to an increase in water content (Figure 2.13), the trend for mobility is not surprising. This improvement is due to at least three factors: 1) larger water contents lead to greater dissociation of the protons from the SO_3^- groups; 2) increasing water content changes the shape and enlarges the size of the aqueous channels; 3) larger water contents lead to better network connectivity of aqueous pathways.

At a first approximation, [$-SO_3H$] might also be expected to increase at higher IECs, since this implies that there are a greater number of sulfonic acid groups available.

However, as can be seen in Figure 2.15b, [-SO_3H] actually decreases due to the disproportionate increase in water content with increasing IEC. Although higher water contents enable greater dissociation of protons, and hence higher μ'_{H+}, a significant increase in water content results in a dilution of the available sulfonic acid groups and thus a decrease in the observed values of [-SO_3H].

It has been previously observed that as λ increases, σ_{H+} is approaching a maximum in the case of S-PEEK, and has reached a maximum in the case of S-SEBS. However, for the data that were available for these series, there is no definite indication that higher water content would lead to lower proton conductivity, unlike the trend observed for BAM. As μ'_{H+} is increasing (Figure 2.16a) while [-SO_3H] is decreasing (Figure 2.16b) it appears that a balance is achieved for σ_{H+} as a function of water content. In other words, water content must achieve a level at which proton dissociation is sufficiently high enough for good mobility, yet there must not be too much water because this leads to dilution of the available acid sites.

Figure 2.15 **a) Effective proton mobility and b) acid concentration of fully hydrated Nafion, S-PEEK, ETFE-*g*-PSSA, BAM, and S-SEBS as a function of IEC**

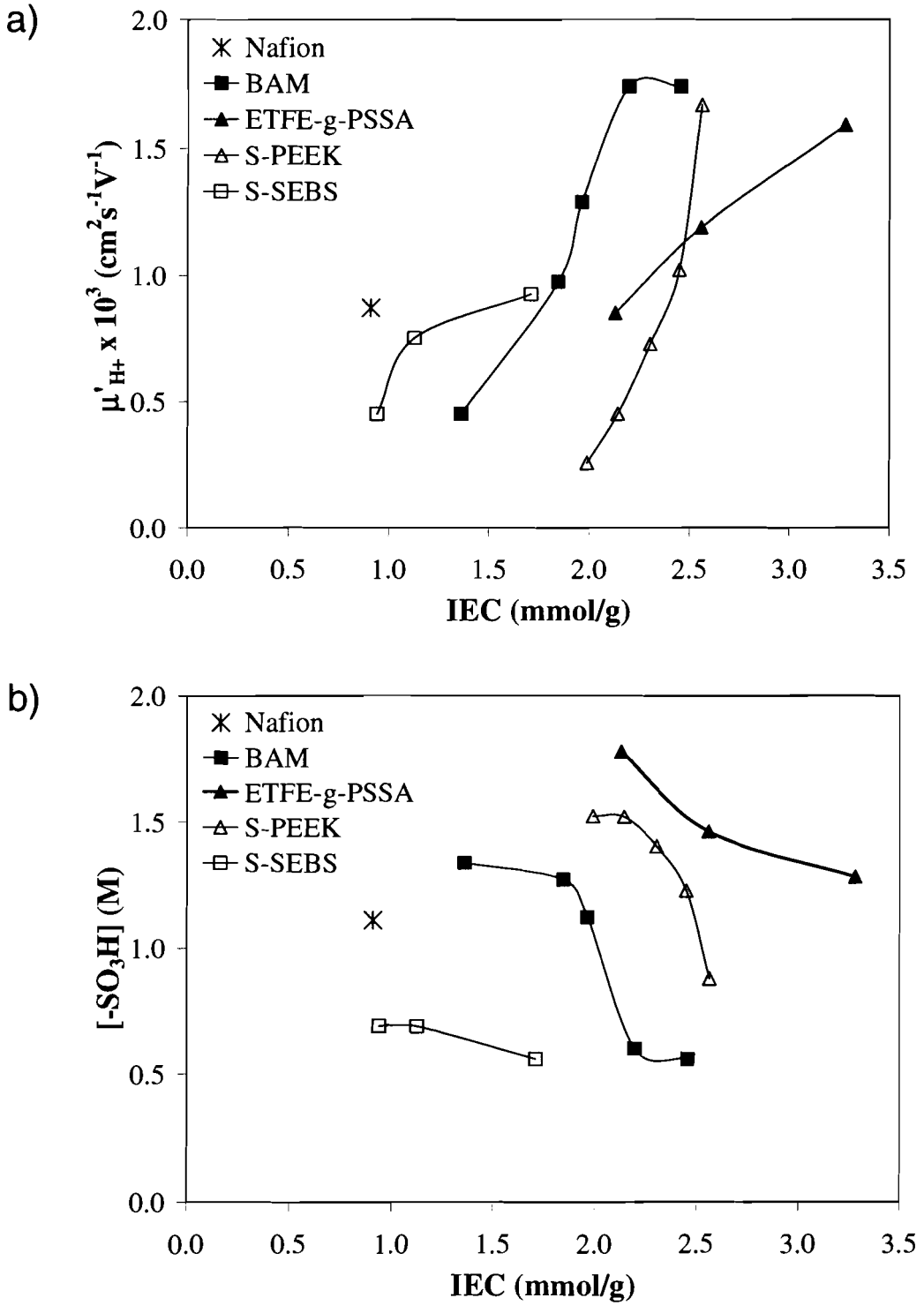

Figure 2.16 a) Effective proton mobility and b) acid concentration of fully hydrated Nafion, S-PEEK, ETFE-*g*-PSSA, BAM, and S-SEBS as a function of λ

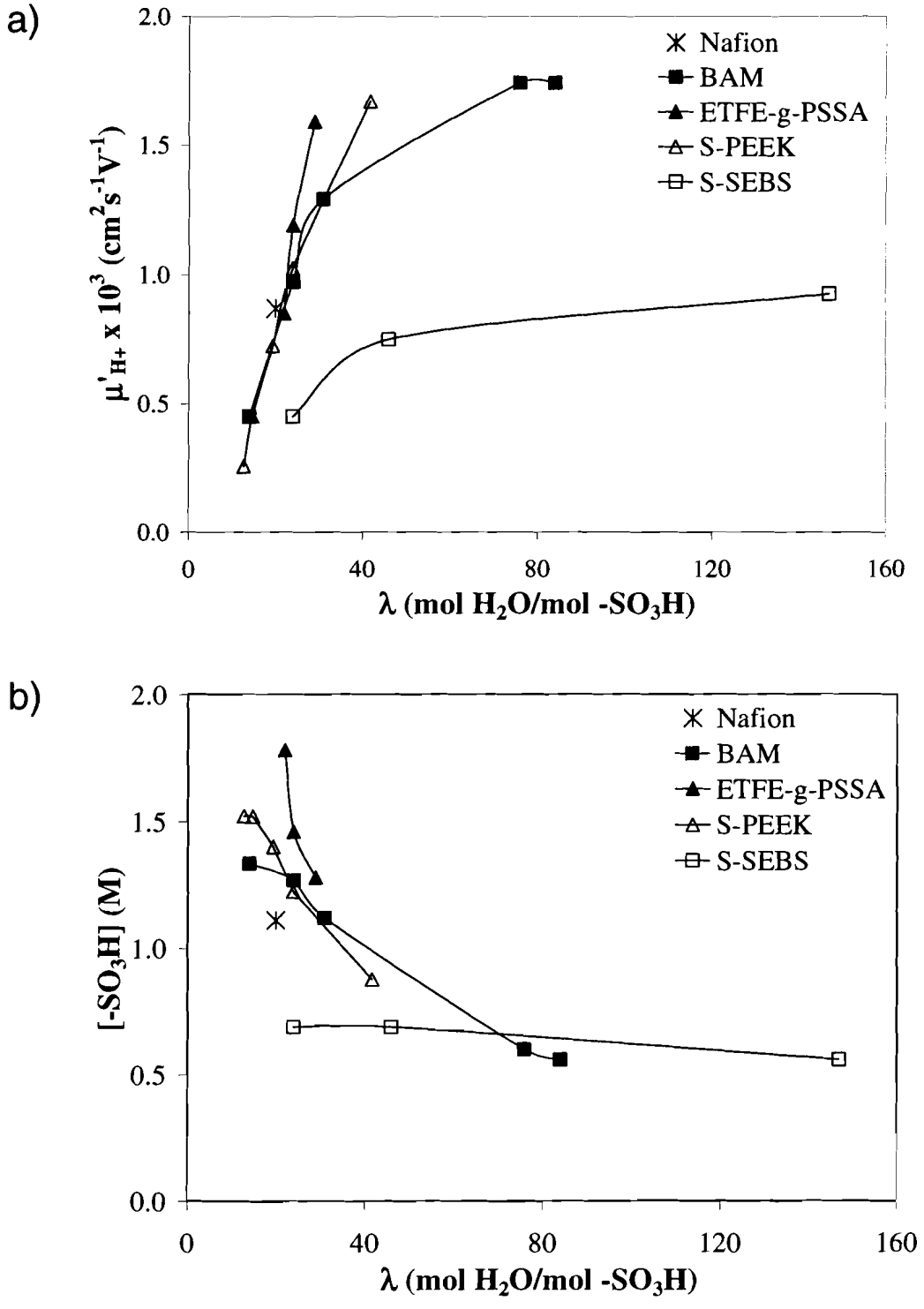

The effect of X_v on μ'_{H+} and $[SO_3H]$ reveals additional information (Figure 2.17). To make a meaningful comparison between S-PEEK, ETFE-*g*-PSSA, and BAM, data at IEC ~ 2.5 mmol/g was compared. Table 2.3 provides a summary that will be used as a reference.

Table 2.3 Summary of X_v, λ, $[-SO_3H]$, μ'_{H+}, and σ_{H+} for fully hydrated S-PEEK, ETFE-*g*-PSSA, and BAM at IEC ~ 2.5 mmol/g

Membrane	IEC (mmol/g)	X_v	λ mol H_2O/ mol SO_3H	$[-SO_3H]$ (M)	σ_{H+} (S/cm)	$\mu'_{H+}*10^3$ ($cm^2s^{-1}V^{-1}$)
BAM	2.46	0.85	84	0.56	0.09	1.74
ETFE-*g*-PSSA	2.56	0.63	24	1.46	0.17	1.19
S-PEEK	2.56	0.66	42	0.88	0.14	1.67

At IEC ~ 2.5 mmol/g, S-PEEK has ~ 40% higher μ'_{H+} than ETFE-*g*-PSSA, even though both membranes have similar X_v, yet S-PEEK exhibits a lower value for σ_{H+}. This situation arises due to dilution of the protons, as evidenced by the higher λ value of S-PEEK, and also its considerably lower $[-SO_3H]$. The higher effective acid concentration of ETFE-*g*-PSSA is likely due to its restricted increase in λ, which limits the amount of water that the membrane can absorb, and thus helps mitigate against dilution of protons allowing for higher σ_{H+}. On the other hand, ETFE-*g*-PSSA also benefits from an uptake of water that is sufficient to maintain a high enough proton mobility and, therefore, leads to a higher level of conductivity for ETFE-*g*-PSSA relative to S-PEEK.

Figure 2.17 a) Effective proton mobility and b) acid concentration of fully hydrated Nafion, S-PEEK, ETFE-*g*-PSSA, BAM, and S-SEBS as a function of X_v

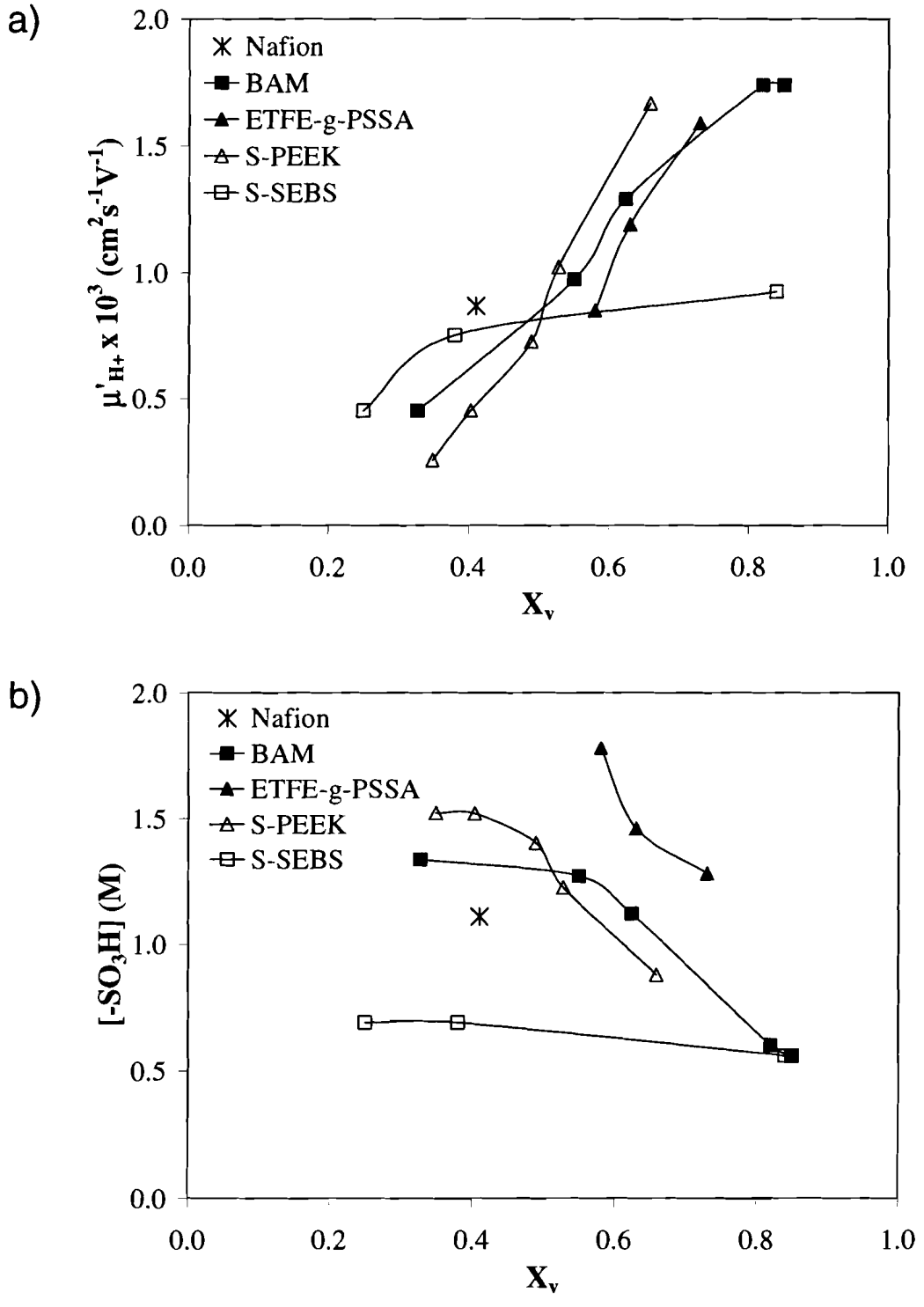

As was shown earlier, BAM is capable of absorbing enormous amounts of water without dissolving. However, this does not appear to be an advantage as the σ_{H+} of BAM actually starts to decrease beyond IEC = 2.0 mmol/g. At IEC ~ 2.5 mmol/g, μ'_{H+} values for BAM are ~ 5% higher than S-PEEK, and ~ 50% higher than ETFE-*g*-PSSA. However, the σ_{H+} is lower than anticipated due to the fact that the proton concentration of BAM is considerably lower than either S-PEEK or ETFE-*g*-PSSA

2.4.3 Maximum Effective Mobility

Further examination of Figure 2.17a reveals that for at least two of the membranes, BAM and S-SEBS, a maximum mobility, $\mu'_{H+(max)}$, is being reached with increasing X_v. Beyond this point the addition of more water no longer improves the efficiency of ion transport but serves only to dilute the protons. Gebel and coworkers have also reported similar behaviour for Nafion membranes swollen to various degrees in water via treatment at elevated temperatures and pressures. They measured the conductivity as a function of water content and observed an increase until X_v ~ 0.5 after which the conductivity decreased sharply. Using concurrent results from SAXS and SANS studies, they proposed this behaviour was the result of a structure inversion from a reverse micellar structure to a connected network of polymer rods at $X_v = 0.5$.[15] Beyond this water content, the system changed from being water in polymer to polymer in water.

More recently, they conducted a similar investigation of BAM membranes using the same methodology. They conclude that similar to Nafion, a structural evolution is occurring but continuously over the range of water contents rather than at one fixed water content. Based on results of SANS studies, they propose that the morphology of their

high IEC BAM membranes (IEC 2.10 and 2.40 mmol/g) resembles small entangled polymer rods that become further apart when hydration levels increase.[32] However, they do not propose a morphology for the low IEC membranes. The results of this work suggest that a similar structural evolution is occurring in these BAM membranes between 1.96 – 2.20 mmol/g where the structure begins to resemble more of a polymer in water and, hence the transport properties no longer improve with increasing IEC (or water content). However, this is not to say that the polymer no longer has an effect on proton transport or the same $\mu'_{H+(max)}$ should be observed for the S-SEBS series at high water content.

The $\mu'_{H+(max)}$ of S-SEBS is roughly half that of BAM. The $\mu'_{H+(max)}$ was anticipated to be much higher for both membranes, given that they contain ~85 vol% water. This information would suggest that even at such high water contents there still remains a significant interaction of the protons with the sulfonate groups. One possibility is that the protons in these systems are ineffectively shielded from the pore wall. As protons are certainly more effective than water molecules at shielding other protons from the pore wall, it may be the case that when water contents get very large and proton concentration drops, the proton/proton shielding becomes ineffective causing all protons to be more electrostatically attracted to the pore wall.

The fact that S-SEBS has an even lower $\mu'_{H+(max)}$ suggests that the proton/sulfonate interaction is even more pronounced in S-SEBS than in BAM. This is consistent with the fact that the pKa of the sulfonate group in S-SEBS should be slightly higher than that of BAM, due to the more electron withdrawing nature of the C-F group attached to the styrene, as compared to the C-H group on S-SEBS. However, this is

unlikely to be the only factor as the $\mu'_{H+(max)}$ values are much lower. The fact that S-SEBS is a block copolymer, with the sulfonate blocks separated by an alkyl block, suggests that the long range proximity of the acid groups is quite low. If the proton mobility is occurring near the pore wall, like is being suggested here, it is possible that the large, dense, regions of negative charge may act as proton "traps" retarding mobility. The presence of proton traps in hydrated Nafion has been suggested by Petersen and Voth to account for their observation that the Grotthuss-type shuttling actually reduces the net diffusion.[76] Furthermore, these results are consistent with the observation by Edmondson and Fontanella, using a comparison of the H_2O diffusion coefficients obtained from ^1H NMR, and the H^+ diffusion coefficients obtained from conductivity measurements, that the contribution of the vehicle mechanism in S-SEBS is more dominant than that of the Grotthuss mechanism.[43]

On the other hand it is impossible to predict what the $\mu'_{H+(max)}$ value would be for either ETFE-*g*-PSSA or S-PEEK as mobility has not begun to level off over the IEC range available for these membranes. However, if the above explanation is assumed to be correct, and given the fact that the proton concentration of S-PEEK is decreasing more rapidly, it is possible that S-PEEK will reach a $\mu'_{H+(max)}$ at a lower X_v than ETFE-*g*-PSSA.

2.5 Conclusions

An in-depth analysis of proton conductivity and water content data has been developed, and has provided additional information on the observed proton transport behaviour for a group of main-chain, statistically sulfonated PEMs. It is clear that proton

mobility is heavily influenced by IEC, and hence water content. It appears that within each series of membranes the best mobility is achieved for the materials with the highest water content. From the results it is predicted that PEM series which suffer from dilution effects at high IEC will exhibit a maximum achievable proton mobility and that the value is related to polymer structure and proton concentration. The estimated maximum mobility of BAM and S-SEBS are low and this has been attributed to the less pronounced phase separation and the ineffective shielding of protons from the pore wall. In the case of S-SEBS, the relatively lower maximum mobility is credited to the higher pKa of the sulfonic acid group, and the overall decreased proximity of the sulfonic acid sites, due to the separation of the sulfonic acid blocks by the alkyl block.

Chapter 3: Proton Transport in Sulfonated α, β, β-trifluorostyrene-co-substituted α, β, β-trifluorostyrene Proton Exchange Membranes Under Controlled Environmental Conditions

3.1 Introduction

The work in this chapter presents a similar proton mobility evaluation as that presented in chapter two, although instead of comparing membranes with different chemical structures, membranes within one PEM series have been compared. Here, the conductivity behaviour of the α, β, β-trifluorostyrene-co-substituted α, β, β-trifluorostyrene series is examined, Figure 3.1a, where water content was varied by alteration of the relative humidity (RH) of the membrane environment, rather than by varying ion content. Nafion is included for comparison, Figure 3.1b.

Figure 3.1 PEM series used in this study

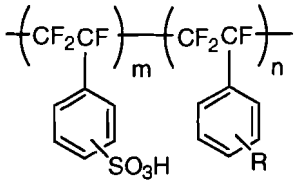

α, β, β-trifluorostyrene-co-substituted α, β, β-trifluorostyrene (BAM)®

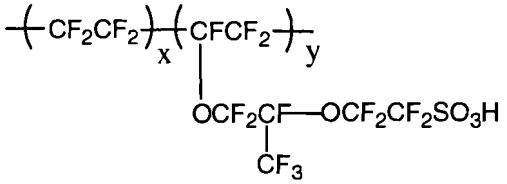

Nafion®

The rationale for this investigation is two-fold. Firstly, for the study in chapter 2, the proton mobility of membranes, which had been allowed to equilibrate in liquid water,

was evaluated. It is known, however, that PEMs take up more water when in contact with liquid water rather than water vapour, even when the RH of the membrane environment approaches 100%. This phenomenon is known as "Schroeder's paradox".[77] For example, in the case of Nafion membranes, the λ value (mol H_2O/mol $-SO_3H$) for a water saturated membrane can be as much as 6 H_2O molecules greater, as compared to a membrane equilibrated in an environment of ~ 100% relative humidty.[78] While it is certainly possible that there may be regions of the PEM being exposed to liquid water during fuel cell operation, it is also likely that the PEM will be exposed to water in the vapour state at some point in time. This is particularly true for fuel cells that are intended to operate at high temperatures (120 – 200°C) where evaporation of the weakly bound water has a detrimental effect on proton transport.[2] For this reason, it is crucial to know to what degree the proton transport changes when the membrane is exposed to the various levels of hydration that are possible during operation. The method used here allows for the possibility of examining the proton transport properties of PEMs over a range of "realistic" RH fuel cell conditions.

Secondly, while it was shown in chapter 2 to be useful to study the conductivity behaviour of a PEM series as a whole, it is also important to be able to independently study the conductivity characteristics of any particular membrane within a series. Focussing on one membrane allows for the possibility of determining structure-property relationships in greater detail, as well as evaluating membranes for which only one IEC is easily obtainable (e.g., Nafion).

In an effort to address these needs, the conductivity and water content of each α, β, β-trifluorostyrene-co-substituted α, β, β-trifluorostyrene membrane was measured on

samples that had been allowed to equilibrate with water vapours of known relative humidities between 50 – 98% RH. Water contents were measured at 25°C using a gravimetric dynamic vapour sorption system, which flows humidified vapour across a membrane sample and monitors the weight change as water is absorbed or desorbed by the material. This technique is a well established method for the determination of water sorption behaviour in the pharmaceutical and polymer packaging industry.[79,80] Furthermore, it has been shown to be useful for sorption behaviour in interpenetrating network polymer hydrogels.[81] Most recently, and following the completion of this work, a paper was published by Burnett and coworkers, establishing the technique for use in measuring water sorption isotherms of PEMs.[82] It has the distinct advantage that mg size samples can be accurately evaluated. Independently, proton conductivities of membranes equilibrated under the same relative humidity conditions were measured at 25°C using AC impedance spectroscopy.

The strategy for the analysis of proton conductivity and water content data in this chapter is similar to that discussed in Section 2.1.1, however, RH is being altered rather than ion content. To illustrate this change in the analysis, the flow chart from Chapter 2 Figure 2.2, is reconstructed with RH substituting for IEC, Figure 3.2. The work in this chapter applies the outlined analysis method to the five membrane α, β, β-trifluorostyrene-co-substituted α, β, β-trifluorostyrene polymer system (IEC 1.36 – 2.46 mmol/g), and Nafion to be used for comparison. The results of the RH analysis were then compared to the results obtained from the previous water-saturated membrane study, presented in chapter 2.

Figure 3.2 Strategy for the analysis of proton conductivity data as a function of RH

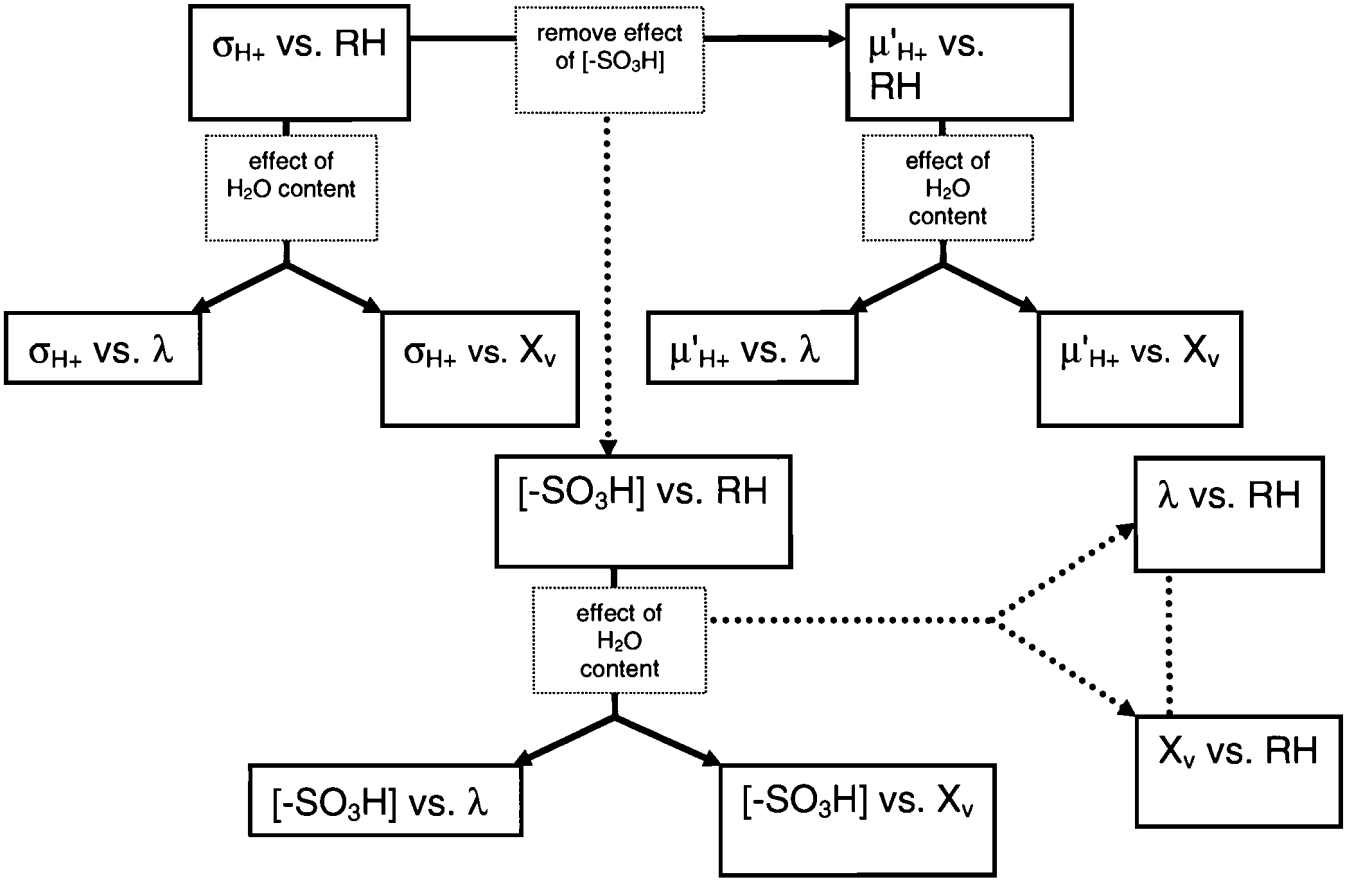

3.2 Experimental

3.2.1 Membranes

As received BAM® membranes (provided courtesy of Ballard Advanced Materials) and treated Nafion® 117 (Dupont) were used in this work.

BAM membranes were received in the dry acidified form. To ensure complete protonation, the membranes were soaked in 0.5 M H_2SO_4 for 48 hours. The membranes were cut into ≈ 5 x 5 cm sheets, and hydrated in Milli-Q ultra pure H_2O (18 MΩ) for a minimum of 24 hours prior to use.

Nafion was received in the dry form. Impurities in Nafion were removed according to a literature procedure.[61] Strips of Nafion were boiled in a 3 vol% H_2O_2 solution for two hours, boiled in Milli-Q (18MΩ) H_2O for 2 hours, boiled in 0.5 M H_2SO_4 for two hours, and finally, rinsed in boiling Milli-Q H_2O for two hours. Treated Nafion samples were hydrated in Milli-Q H_2O for a minimum of 24 hours prior to use.

3.2.2 Water Content Analysis

Isothermal water uptakes/losses of PEM membranes in equilibrium with water vapours of known relative humidities (50-98% RH, +/- 1.5%) were measured using an automated dynamic vapour sorption (DVSS) analyzer (DVS-1000, Surface Measurement Systems, UK). Both a schematic and interior photograph of the DVSS instrument are included in Figure 3.3. An explanation of the operation and data analysis follows.

Figure 3.3 **(a) Schematic of the DVSS* (b) Photograph of the interior of the DVSS, inset showing quartz sample pan**

a)

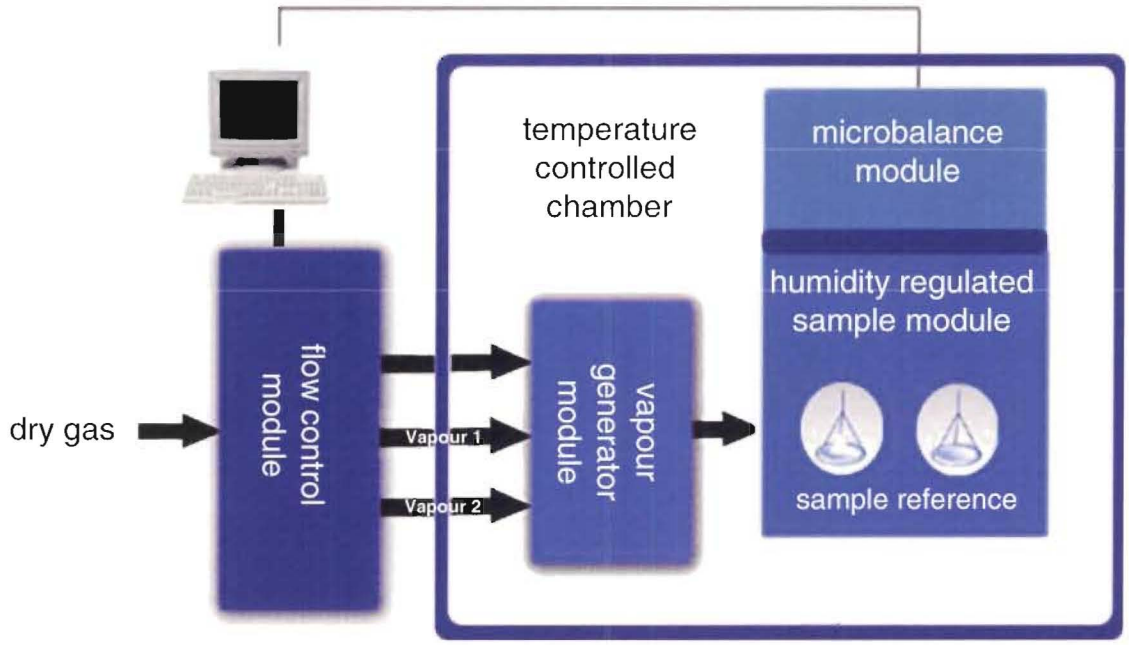

b)

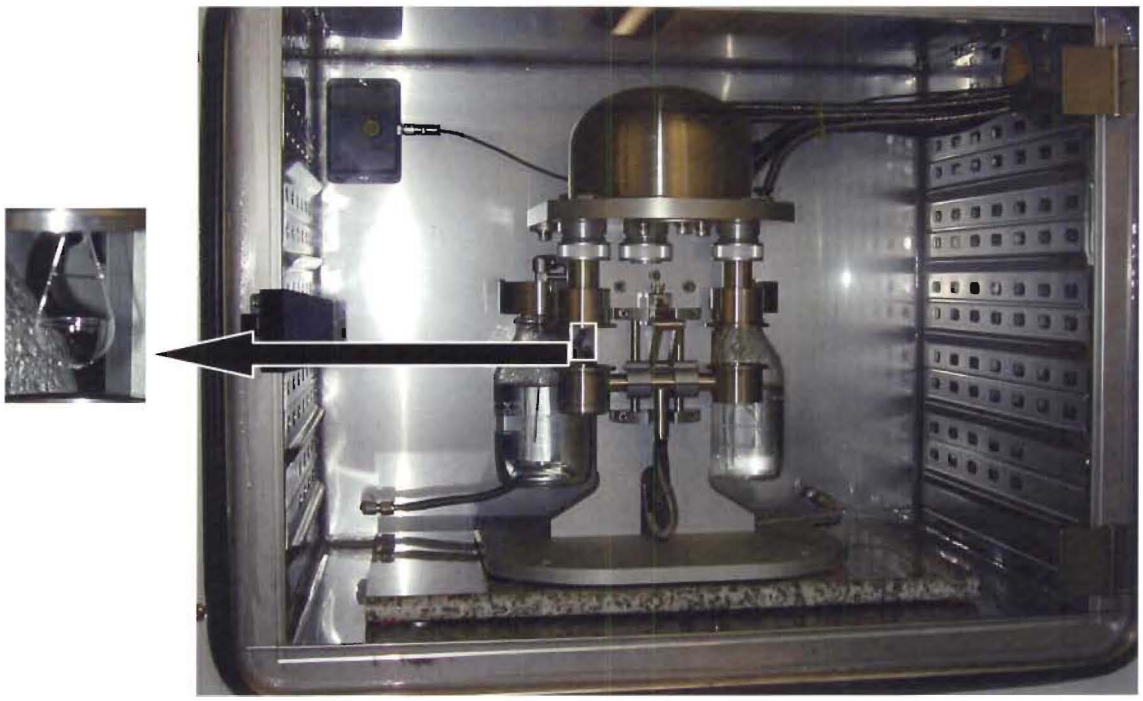

* Reproduced with permission from the Surface Measurement Systems website (http://www.smsuk.co.uk), © 2007

DVSS Operation

During operation, pre-set mixtures of water-saturated and dry nitrogen (pre-purified, Praxair Inc.) gases flow across the PEM sample, and the weight change resulting from the absorption/desorption of water is recorded. Water-saturated nitrogen vapour is created by bubbling dry nitrogen gas through a water-filled glass bottle. The gas mixtures are regulated with a mass flow controller that uses factory calibrated water vapour partial pressure tables to generate the desired relative humidity conditions.*

The system itself consists of two matched weight (217 mg) quartz round bottom pans hung from a recording microbalance (+/- 0.1 μg) via two platinum wire hooks. One of the pans holds the PEM sample of interest and the other remains empty as a reference. Using a reference pan is intended to account for any water condensation on the sample pan, as they are both subjected to identical temperature/RH conditions.

Isothermal conditions are maintained with a temperature controlled incubator (+/- 1°C), which houses the entire DVSS system, including the microbalance, both quartz pans, the water bottles, and the gas input lines. Before use, the entire system must be equilibrated at the temperature of interest (in this work 25°C). Equilibration takes between 1-2 hours.

Prior to sample loading, the microbalance is calibrated with a platinum calibration weight, and then tared with both quartz pans empty. Small strips of wet membrane (1-4 mg) are placed in the sample pan, and the system is closed to the atmosphere. Water

---

* Partial pressure tables were created by Surface Measurements Systems using salt solutions of known relative humidity.

83. Nyquvist, H. *International Journal of Pharmacy, Technology and Products Manufacturing* **1983**, *4*, 47.

vapours of known relative humidities flow across the sample at a rate of 100 mL/minute, and weights recorded every 10s. Experiments are fully automated according to user defined sequences, where each sequence consists of several methods. An example of a sequence used in this work would have the first method subjecting the sample to conditions of 0% RH until a constant weight was obtained, the second method increasing the relative humidity in intervals of 5 or 10% RH and obtaining a constant weight at each step, W_{hyd}, and the third method performing a post heating (100° C) of the sample to obtain a dry weight for reference, W_{dry}. The weight of water contained in the membrane at any particular level of hydration can then be calculated by taking the difference between $W_{hyd} - W_{dry}$.

Constant weight can be obtained using two methods. The first is referred to as a timed method. An RH is selected and an experiment length (time) is chosen manually. This type of method is particularly useful for samples that require long absorption times. On the other hand, the instrument can also be set to recognize when a constant weight has been obtained and step to the next humidity. This is called a dm/dt method, where dm/dt means the percentage of change of mass as a function of time. This value is set depending on the sample size, according to Equation 3.1. For samples that absorb large amounts of water, an average of the weight and dry sample weight is taken and used as the dm/dt value.

$$\frac{dm}{dt} = \frac{2.0\times10^{-5}}{\text{sample weight}\,(g)} \qquad [3.1]$$

Data Analysis

Since the volume of partially hydrated samples cannot be directly measured during the DVSS experiments, the volumes were estimated according to the procedure by Edmondson and Fontanella.[49] Volumes of dry membranes, V_{dry}, were calculated using the density of the dry material, ρ_{dry}, and the weight of the dry sample, W_{dry}.

$$V_{dry} = \frac{W_{dry}}{\rho_{dry}} \qquad [3.2]$$

Hydrated membrane volumes, V_{hyd}, at particular RHs were calculated by assuming that the volume change upon absorption/desorption was due solely to the volume of water incorporated, V_{water}. The volume of water incorporated was calculated by taking the difference between the hydrated membrane weight, W_{hyd}, and dry weight, W_{dry} and dividing the result by the density of water, ρ_{water} (taken as 1.0 g/mL).

$$V_{hyd} = V_{dry} + V_{water} \qquad [3.3]$$

$$V_{water} = \frac{W_{hyd} - W_{dry}}{\rho_{water}} \qquad [3.4]$$

Water content as a volume percentage, X_v, could then be measured according to the following relationship:

$$X_v = \frac{V_{water}}{V_{hyd}} \qquad [3.5]$$

Acid concentration was determined according to:

$$[-SO_3H] = \frac{\text{moles of } -SO_3H}{V_{hyd}} \qquad [3.6]$$

where $-SO_3H$ referred to bound sulfonic acid moieties in the PEM, moles of SO_3H was given by (IEC)*(dry mass of polymer), and V_{hyd} was the hydrated volume of the membrane.

The number of water molecules that were contained in the membrane for each $-SO_3H$ group was calculated using:

$$\lambda = \frac{moles\, H_2O}{moles\, SO_3H} \qquad [3.7]$$

3.2.3 Ion Exchange Capacity

Ion exchange capacities (mmol/g) were measured by the direct titration method described in Section 2.2.3.

3.2.4 Ionic Resistance

Ionic resistance was measured using AC impedance spectroscopy with a Solartron 1260 frequency response analyzer (FRA) employing a transverse two-electrode configuration. Rectangular samples of hydrated membranes were cut to the required dimensions (length, L, and width, W, measured using a calliper, +/- 0.1 mm, and thickness, h, using a micrometer, +/- 0.001 mm), Figure 3.4a. To ensure complete protonation (i.e. no contamination from the knife or cutting surface), samples were soaked in 0.5 M H_2SO_4 for 24 hours, followed by soaking in Milli-Q water for a minimum of 12 hours prior to use.

Samples were removed from water, blotted with a Kimwipe to remove surface water, laid across two platinum electrodes (0.5 x 1 cm) 1 cm apart and fixed in place by attaching them to an inert Teflon block (2 x 2 cm). Another Teflon block was placed on

top, and four nylon screws were used to immobilize the membrane inside the probe during measurement. Both blocks have identical 1 × 1 cm holes cut out of the centre to allow for membrane equilibration with the atmosphere, Figure 3.4b.[71]

Membrane equilibration with water vapours of known relative humidity (+/- 1.5% RH) were obtained at 25°C (+/- 0.1°C) by placing the entire Pt/Teflon probe assembly into a computer controlled environmental test chamber SH-241, ESPEC North America Inc.) through a 2" side port. A sponge-like cap with a 1 cm hole bored in it was used to plug the port to allow for quicker and more accurate equilibration, while allowing the FRA to connect directly to the Pt/Teflon probe at all times. Temperature and relative humidity conditions were confirmed using an independently operated humidity sensor and digital thermometer.

Two wires fitted with alligator clips connected the probe to the frequency response analyzer, and ionic resistance was measured by applying a 100 mV sinusoidal AC voltage between the two platinum electrodes over 10 MHz - 100Hz frequency range and measuring the AC resistance (*i.e.* impedance). Measurements were collected every half hour during equilibration until constant ionic resistance was obtained, which took 2-6 hours for most samples.

Data was analyzed using commercial software (Zplot, Scribner), and a detailed explanation of the analysis is included in Section 2.3.2.

Figure 3.4 **(a) Rectangular PEM sample dimensions. (b) Pt/Teflon® conductivity probe**

a)

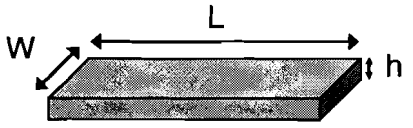

b)

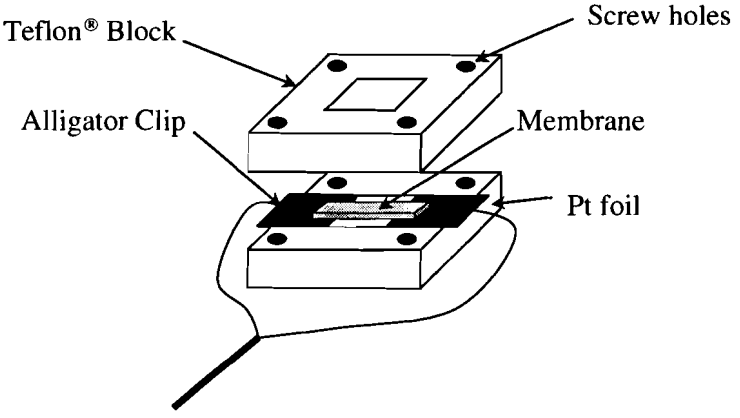

3.3 Results

3.3.1 Water Sorption Characteristics

Weights of each of the 5 BAM membranes, and Nafion membrane, were measured using dynamic vapour sorption according to an automated sequence similar to the one described in section 3.2.2. Sample weight was measured once membranes had reached equilibrium with water vapours of the following RH values; 0, 10, 20, 30, 40, 50, 60, 70, 80, 85, 90, 95, 98% RH. Most of the absorption profiles are a result of a combination of more than one experiment. Measuring the absorption characteristics of BAM 2.20, Figure 3.5a-c, is an example of one such situation in which the final results were the combination of two experiments.

Experiment #1

In the first method of the sequence, a dm/dt method, a constant weight was obtained between 0 – 80% RH in 10% increments and between 85 - 95% RH in 5% increments. The water sorption isotherm, weight as a function of time, is shown in Figure 3.5a. The measured relative humidity has been included as a reference. For example, at the beginning of the experiment, time zero, the relative humidity was set to 0% RH and measured to be ~ 1.5%, which resulted in a decreased sample weight as the water desorbed from the membrane. The humidity was held constant at 0% RH until the sample had reached a constant weight 0.924 +/- 0.001 mg (~ 380 minutes). At that time, the humidity was stepped up to the next increment, 10% RH, and held constant until a constant weight had been achieved, and so on. The last step of the method was meant to be the step to 98% RH, but the humidity could not be maintained. The instrument defaulted to the final method for post-heat drying, Figure 3.5b, where a heater that surrounds the sample is ramped to 100°C and held there for 2 hours. The sample is then cooled to 25°C, and the dry weight is recorded. The dry weight must be obtained once the sample has returned to 25°C because the instrument, including the microbalance, is calibrated at 25°C. An enlarged image of the final stage of the post-heat drying method is included in Figure 3.5c.

Figure 3.5 **Experiment #1, (a) BAM 2.20 water sorption isotherm between 0 – 98% RH (b) post-heat drying cycle, (c) enlarged picture of the final stages of the post-heat drying cycle**

a)

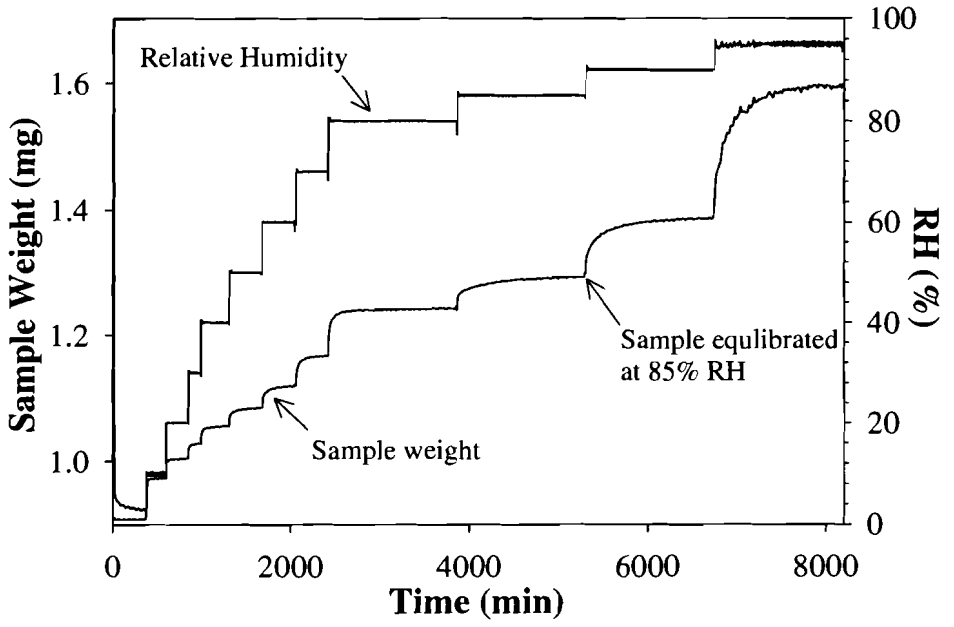

b)

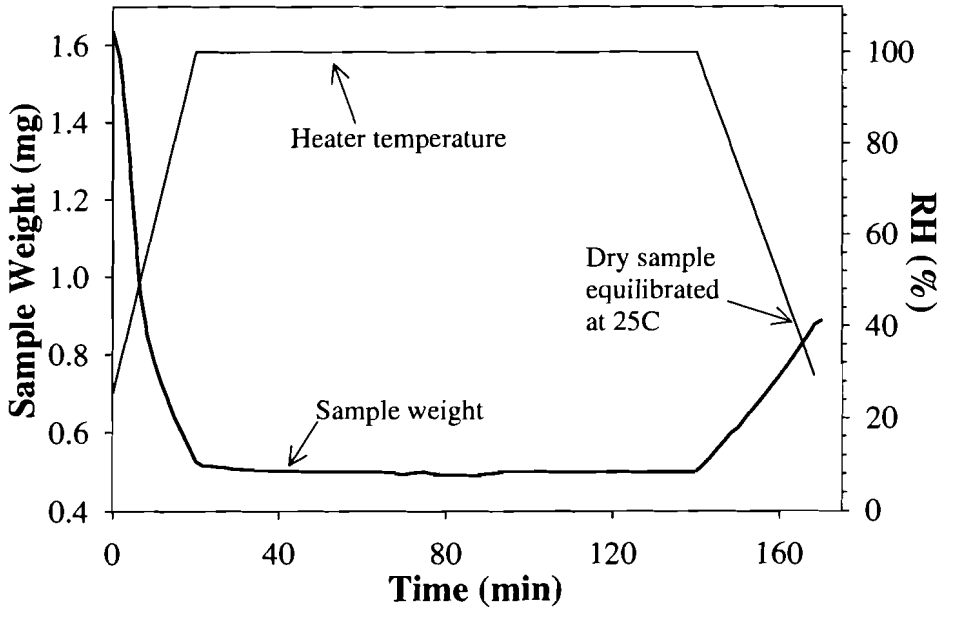

c)

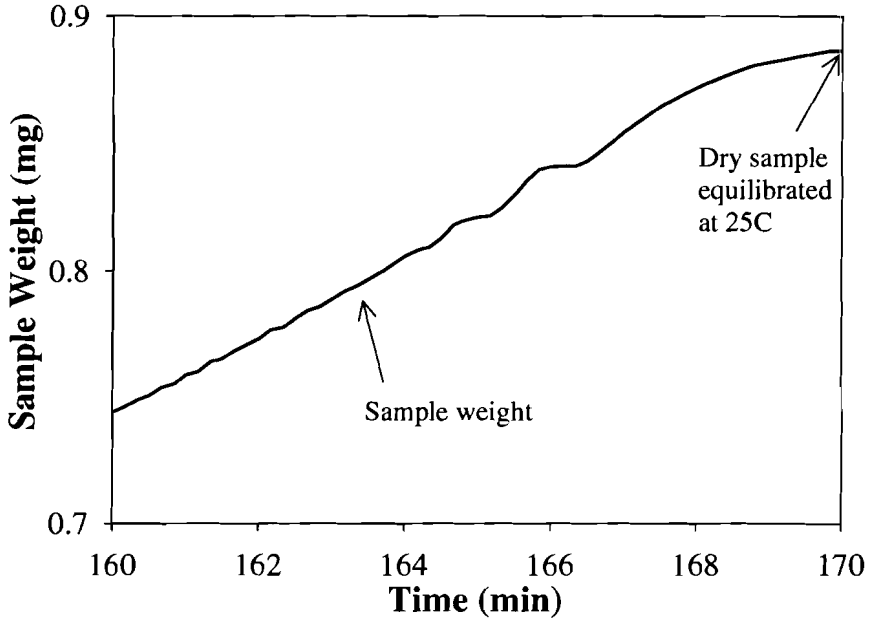

Experiment #2

A second experiment was performed on a fresh sample. The first method used was the dm/dt method, set to obtain a constant weight at 0% and between 80-95% RH in 5% increments (Figure 3.6a). A second method was a timed experiment, in which the humidity was set to 98% RH, and held constant for 8000 minutes (133 hours) to obtain a constant weight (Figure 3.6b).

Water absorption data obtained has been used to calculate water content as a volume percentage X_v, number of water molecules per acid group λ, and acid concentration [$-SO_3H$] for each relative humidity step. Complete data summary tables for each membrane are included at the end of this chapter in Table 3.4 to Table 3.9. See section 2.1.1 for a detailed description of the above parameters.

For any membrane in which more than one experiment was used, several overlapping RH values were studied to ensure the data were consistent. For example, in

the case of BAM 2.20, both experiments measured water uptake at 80, 85, 90, and 95% RH. The λ values calculated for both experiment #1 and #2 across the overlapping RH values are in good agreement, Table 3.1. Values reported in the overall data summary tables are an average of those overlapping humidity steps (where appropriate), and are highlighted in the table.

Table 3.1 **Comparison of λ values for BAM 2.20 obtained for both experiment #1 and #2 discussed in the text above, and the values reported in the data summary table (values in grey are the average of experiment #1 and #2)**

Relative Humidity (%)	**λ (mol H_2O/mol $-SO_3H$)**		
	Experiment #1	Experiment #2	Reported Values
0	1.0	----	1.0
10	2.4	----	2.4
20	3.3	----	3.3
30	3.9	----	3.9
40	4.7	----	4.7
50	5.5	----	5.5
60	6.6	----	6.6
70	7.9	----	7.9
80	10.1	10.3	10.2
85	11.5	11.7	11.6
90	13.6	14.4	14.0
95	20.1	20.6	20.4
98	----	46.3	46.3

Figure 3.6 **Experiment #2 –BAM 2.20 water sorption isotherm (a) 80 – 95% RH, (b) 98% RH**

a)

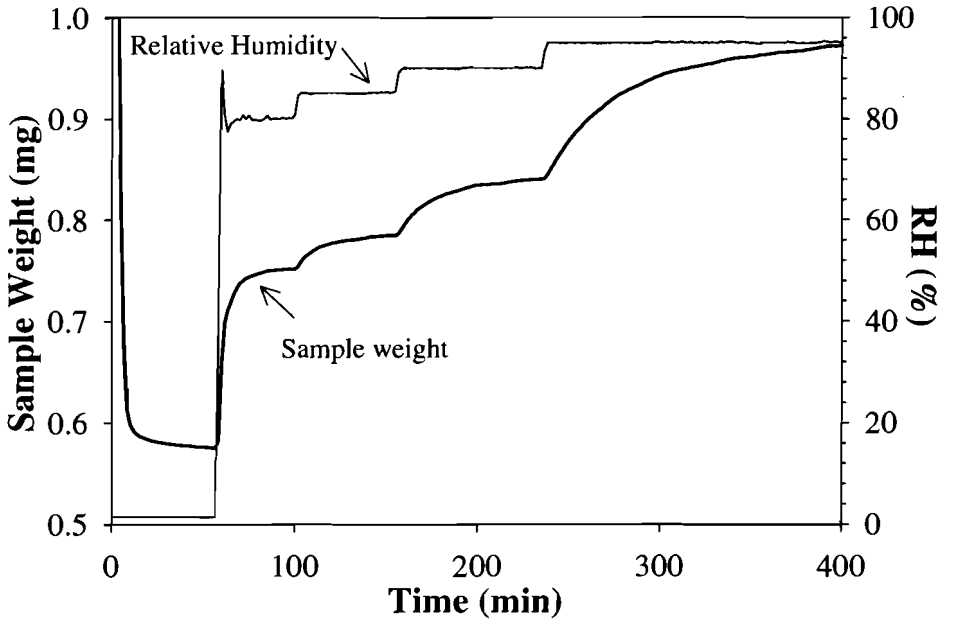

b)

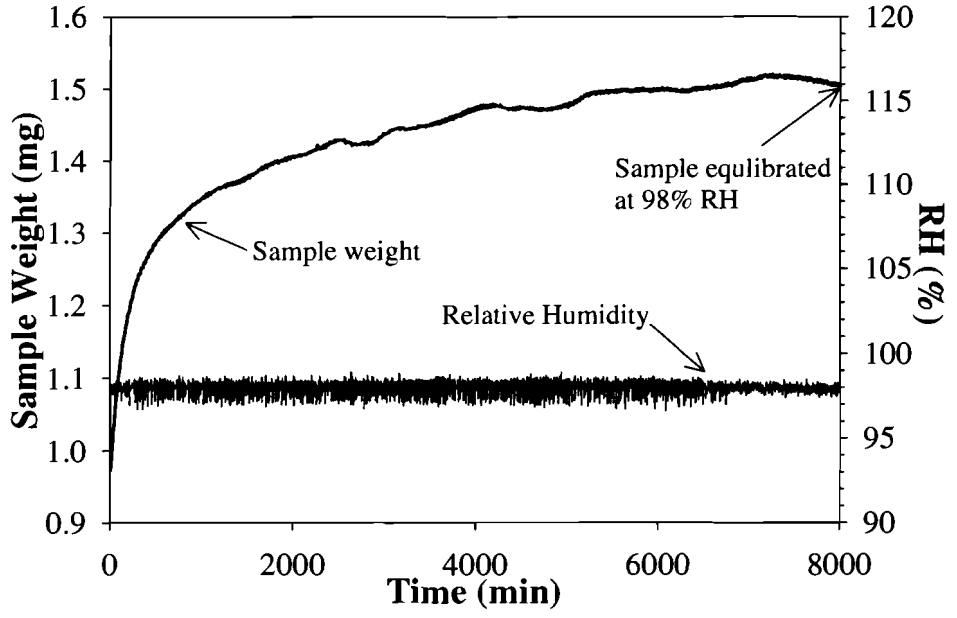

3.3.2 Proton Conductivity

Ionic resistances for each of the BAM membranes (IEC = 1.36, 1.86, 1.96, 2.29, and 2.46 mmol/g) were measured at 25 °C on samples that had reached equilibrium with water vapours of 50, 60, 70, 80, 85, 90, 95, or 98% RH. Nafion is also included for comparison. Included in Figure 3.7 is a series of typical complex-plane plots of the imaginary impedance (Z'') versus real impedance (Z') for BAM 2.20 in equilibrium with water vapours of 80, 90, and 98% RH. A series of semi-circles was obtained in which the size of the semi-circle decreases with an increase in RH.

Figure 3.7 Ionic resistance of BAM 2.20 in equilibrium with water vapours of 80, 90, and 98% RH

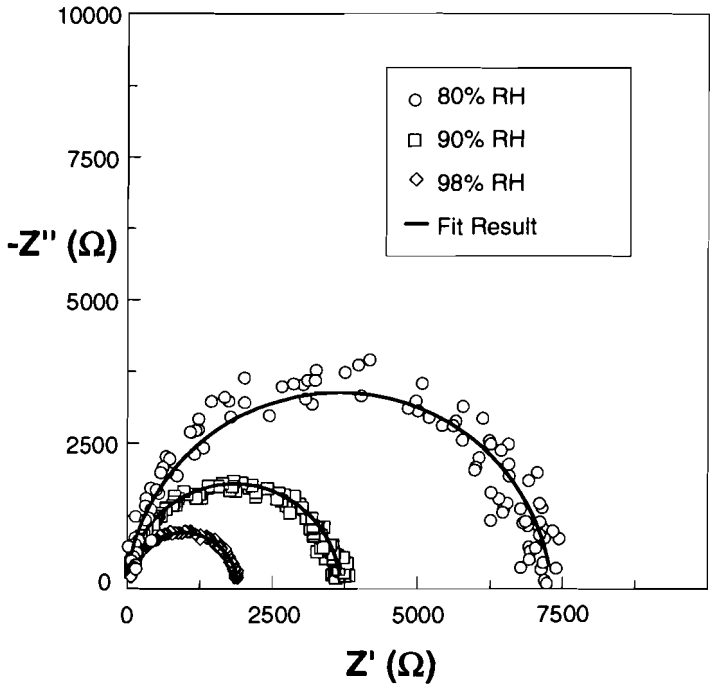

Each semi-circle was fitted by non-linear least squares regression to a Randles equivalent circuit model. A detailed description of the model and the method for

abstracting proton conductivity from the result is provided in section 2.3.2. Calculated proton conductivities, σ_{H+}, are included in Table 3.4 to Table 3.9.

3.4 Discussion

3.4.1 Water Sorption Behaviour of BAM membranes as a Function of Increasing Relative Humidity

The effect of increasing the relative humidity of the membrane environment on the water content of the BAM series and Nafion was studied between 50 - 98% RH at 25°C. The water sorption isotherms shown in Figure 3.8 reveal that for all membranes, an increase in RH leads to an increase in water content, due to the hydrophilic nature of the materials.

Although X_v increases at a similar rate for all membranes, the volume percent of water contained at any one particular RH varies according to the membrane IEC. With the exception of Nafion, between 95 – 98% RH, the membrane water content in the high RH regime appears to be roughly ordered by IEC, Nafion (IEC = 0.91 mmol/g) ≅ BAM 1.36 < BAM 1.86 < BAM 1.96 < BAM 2.20 ≅ BAM 2.46 (Figure 3.8a). If the number of waters per sulfonic acid, λ, are plotted in place of X_v the profiles of the membranes become easier to compare (Figure 3.8b). Between 50 – 70% RH all membranes have roughly the same λ (between 4 – 8 H_2O/SO_3H) regardless of IEC, whereas between 70 - 98% RH, λ increases as a function of IEC. It is suggested that the water molecules that are taken up in the low RH range act to solvate the sulfonate group and that any subsequent incorporation of water begins to add to the bulk water. This is supported by

the fact that after 70% RH the increase in water content becomes more pronounced and increases dramatically.

At 98%, the behaviour resembles the water-saturated trend with the three lowest IEC membranes, BAM 1.36, 1.85 and 1.96, having relatively low λ values (13 – 21 H_2O/SO_3H) and the two highest IEC values, BAM 2.20 and 2.46, having much larger λ values (46 and 56 H_2O/SO_3H, respectively). This suggests that the high IEC membranes take up a much higher percentage of bulk water than the low IEC membranes. The extreme water uptake by the high IEC membranes between 95 – 98% RH is responsible for the drastic decreases in proton concentration, by ~ 50% (Figure 3.9). Comparatively, the decrease in proton concentration of low IEC membranes is less than 10%.

Measuring water content of Nafion as a function of RH (or water activity) is something that has been reported in the literature by many groups.[84-86] Unfortunately, there is no standard literature procedure, making comparison of absolute values nearly impossible. A comparison of the Nafion isotherm, shown in Figure 3.8b, with a variety of those reported in the literature, has shown that the trend is consistent.[84-87] However, the absolute calculated λ values differ consistently by 1 – 2 H_2O/SO_3H at each water activity, likely due to a difference in drying protocol. It was reported by Bunce and coworkers that membrane samples dried at room temperature under vacuum still contain one H_2O/SO_3H.[88] Zawodzinski and coworkers report that the last water molecule can be removed by either drying at elevated temperatures under vacuum, or drying at room temperature over P_2O_5.[84] Unfortunately, the DVSS system does not have the functionality required to expose the samples to high temperatures, under vacuum.

However, all membranes were treated in a consistent manner in an effort to make the comparison within this work meaningful.

Based on the observation that all membranes take up less water when exposed to 98% RH, versus liquid water, it appears that both Nafion and BAM exhibit behaviour consistent with "Schroeder's paradox" (Figure 3.10).[77] Nafion exhibits a ~5 H_2O/SO_3H decrease in λ between fully hydrated and 98% RH. This value has been reported in the literature to be anywhere from a 5 – 6 decrease in H_2O/SO_3H.[61] The observation that the effect is greater in Nafion than in BAM 1.36, is consistent with the fact that Nafion is expected to have a comparatively more hydrophobic surface making condensation of water on the surface more difficult than in BAM 1.36. Condensation being necessary for the absorption of water into the pores. A comparison within the BAM series shows that the water content difference between the wet state and 98% RH is merely 1 H_2O/SO_3H for BAM 1.36, as opposed to 28 H_2O/SO_3H for BAM 2.46. BAM 2.46 exhibits a much more drastic difference in water uptake between the wet and 98% RH state because a larger percentage of its water is expected to be bulk-like and it is reasonable to assume that bulk water would be more easily lost than water that is strongly associated with the sulfonate groups. However, this does not hinder the membranes from achieving their maximum λ again once immersed in liquid water, suggesting that the changes are not permanent.

Figure 3.8 **Water sorption isotherms for Nafion and BAM measured at 25°C between 50-98% RH. Effect of increasing the relative humidity of the environment on (a) X_v (b) λ**

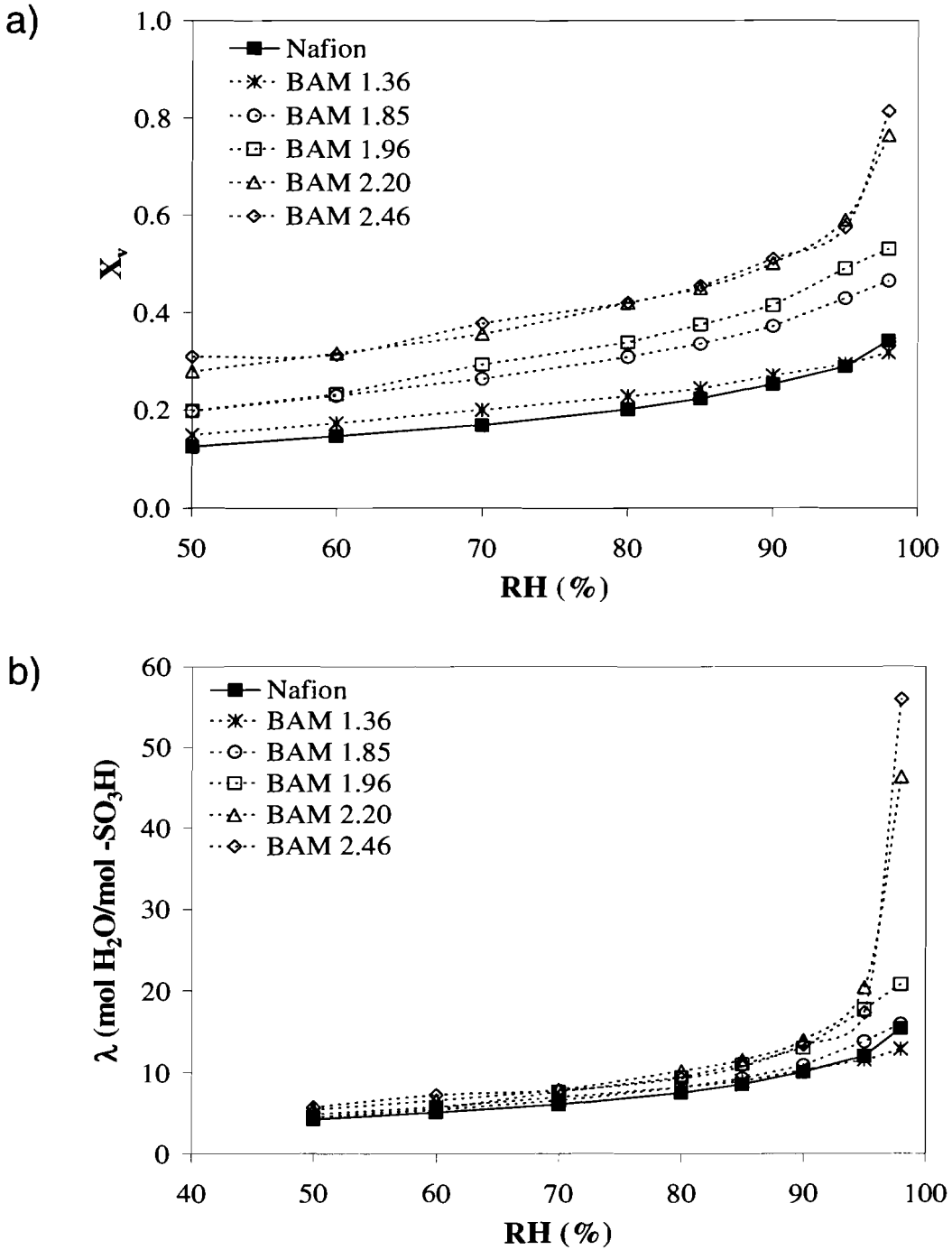

Figure 3.9 **Analytical proton concentration of Nafion and BAM membranes as a function of relative humidity between 50 - 98% RH at 25°C**

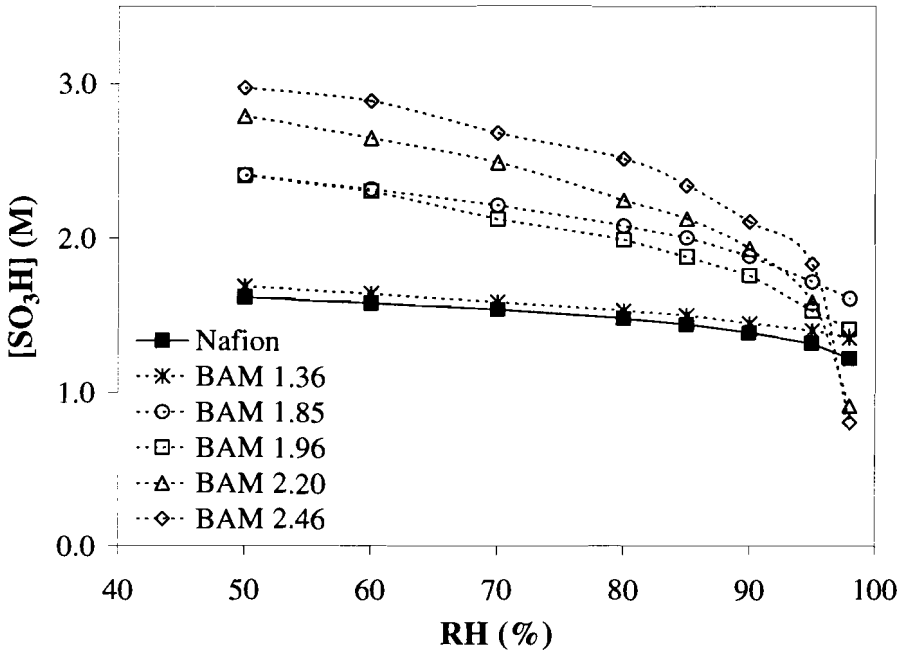

Figure 3.10 **Comparison of λ for Nafion and BAM membranes between the fully hydrated state and when exposed to 98% RH**

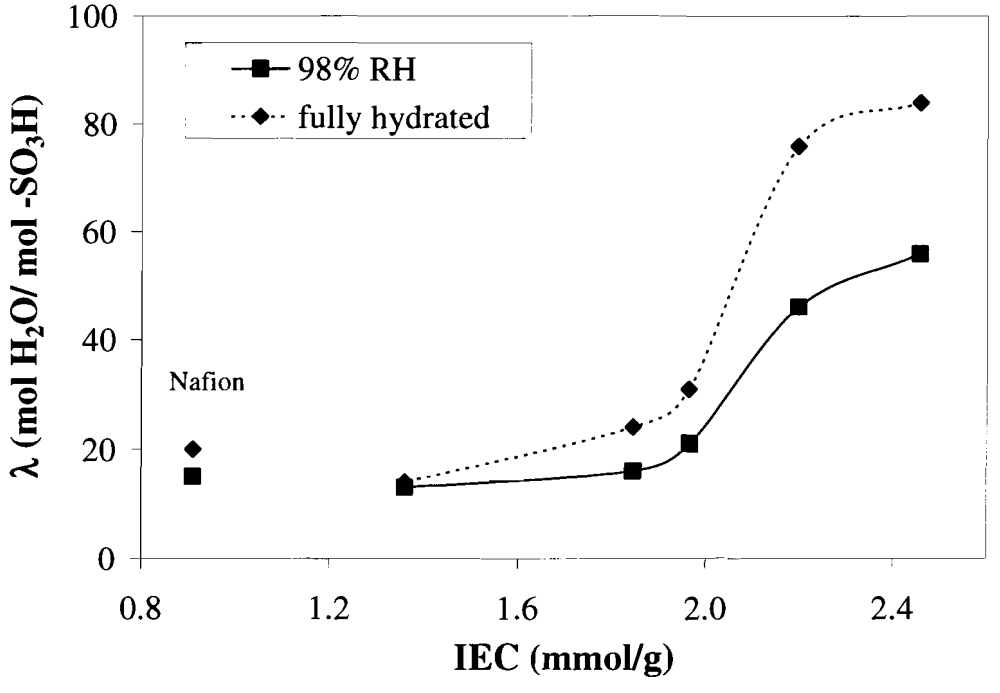

3.4.2 Proton Conductivity of BAM Membranes as a Function of Increasing Relative Humidity

Since proton conductivity and water content are intimately linked, it is not surprising that an increase in relative humidity has a dramatic effect on proton conductivity (Figure 3.11). For all membranes, the effect is an increase in conductivity over the entire relative humidity range. Again the trend is consistent with work in the literature but the exact values are off by a consistent factor due to differences in drying protocol.[84] Further examination of Figure 3.11 also reveals information regarding the extent of dependence of conductivity on RH. The BAM membranes show a marked improvement in conductivity (10 - 25 times higher) with an increase from 50 – 98% RH. Comparatively, while Nafion has the highest conductivity in the lower humidity regime (50 – 85% RH), it exhibits only a small improvement with increasing RH (5 times higher). In fact, it has a maximum conductivity at 98% RH which is similar to the BAM membranes that have more than double the acid content (0.91 vs. 2.20 and 2.46 mmol/g).

Shown in Figure 3.12 is the conductivity behaviour as a function of water content. Nafion exhibits a higher proton conductivity than any of the BAM membranes across almost the entire λ range (Figure 3.12a). A comparison within the BAM series shows that for low λ values all membranes have similar conductivities, yet as λ increases, the membrane profiles diverge. It might have been expected that membranes with similar λ would exhibit the same conductivity, however, at high λ they are quite different. This can be explained by the fact that changes in λ are accompanied by changes in X_v (Figure 3.12b), resulting in differences in proton concentration. This effect can be removed by considering proton mobility in place of proton conductivity (discussed later).

Figure 3.11 Proton conductivity of Nafion and BAM membranes as a function of relative humidity between 50 – 98% RH at 25°C

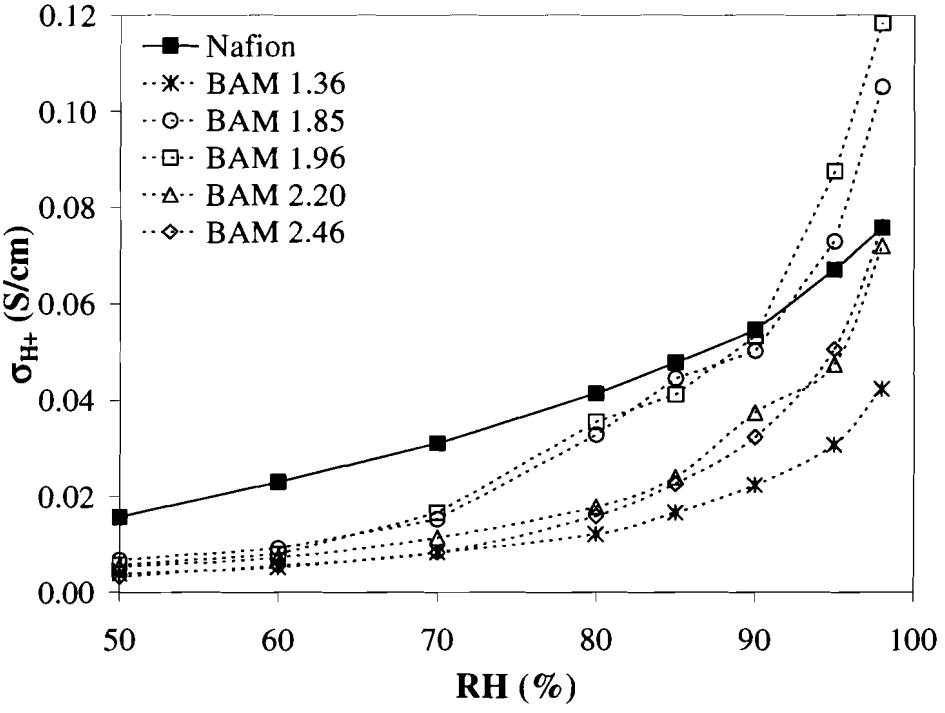

It has been reported in the literature that the percolation threshold of PEMs can be calculated by examining the exponential relationship between conductivity and X_v, and that the value lies somewhere in the 5 - 11 vol% range.[46,48,49] As can be seen in Figure 3.12a, the BAM membranes clearly exhibit a power law increase in conductivity with increasing X_v. It would appear that Nafion has a lower percolation threshold than any of the BAM membranes, since at the lowest X_v available, it has not even begun to exhibit a power law decline in conductivity that BAM has.

Figure 3.12 Proton conductivity of BAM as a function of water content (a) λ (b) X_v

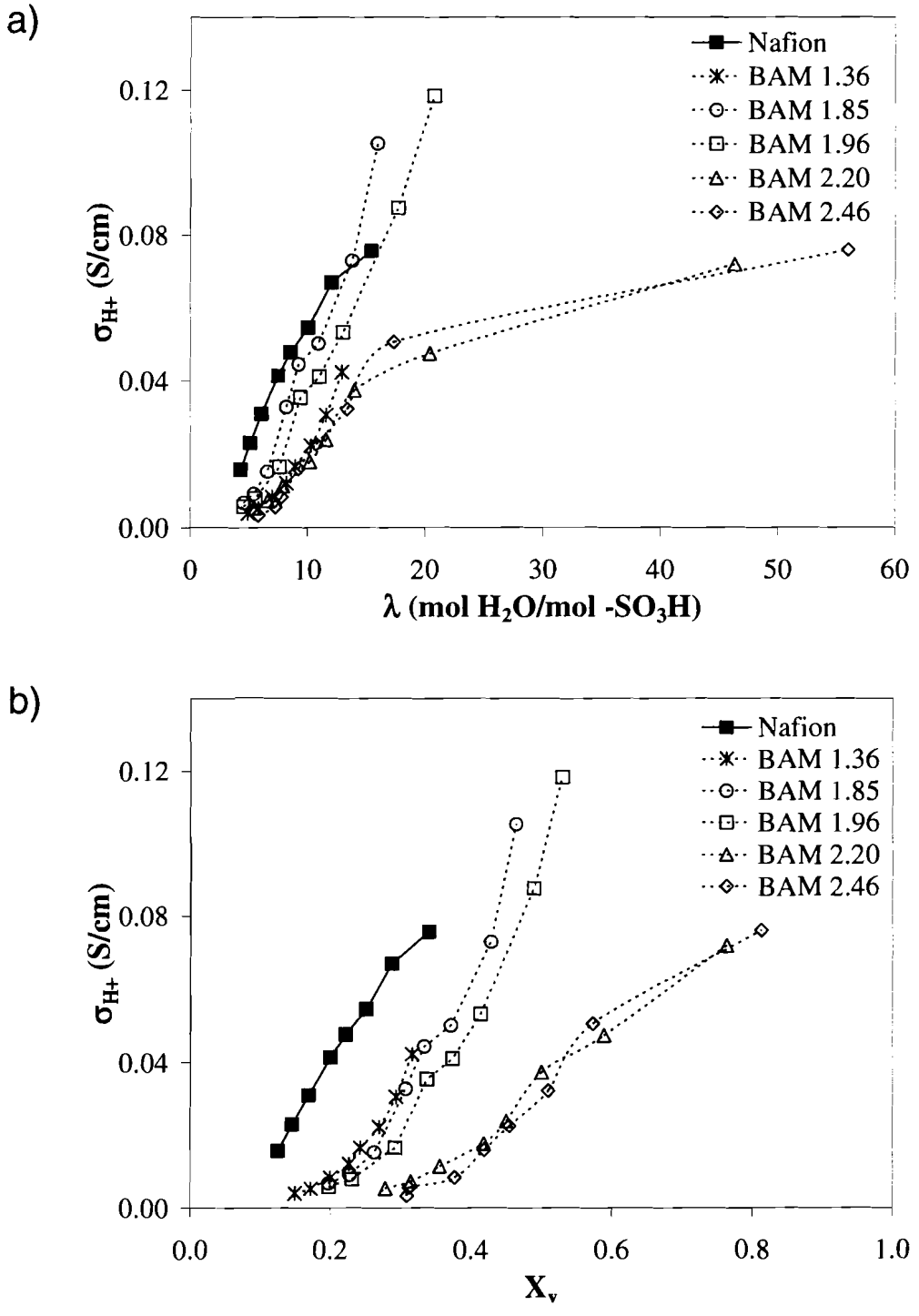

Within the series of BAM membranes, there are also interesting deviations from expected conductivity behaviour with increasing IEC. As was first reported in chapter 2, proton conductivity of the water-saturated BAM membranes reaches a maximum at IEC = 1.96 mmol/g, and then decreases with an effective increase in IEC. This behaviour is a result of the water uptake being proportionally greater, relative to the IEC, such that above IEC = 1.96 mmol/g, excessive amounts of water are incorporated, proton concentration is significantly lowered, and consequently, proton conductivity decreases. Interestingly, that trend is maintained across the 70 – 98% RH range, although it becomes less pronounced as RH decreases (Figure 3.13).

3.4.3 Effective Proton Mobility

As was discussed in chapter 2, the effects of proton concentration can be removed by examining the "effective" proton mobility. In general, an increase in proton mobility is observed as RH increases due to the absorption of water (Figure 3.14). With the exception of Nafion, all of the membranes exhibit negligible mobility between 50 - 60% RH. Between 70 – 95% RH, BAM 1.85 and 1.96 have consistently higher mobility than BAM 2.20 or 2.46. However, as 98% RH is approached the mobilities of BAM 2.20 and 2.46 increase twice as fast surpassing the mobility of BAM 1.85 and 1.96, and Nafion at 98% RH. On the other hand, BAM 1.36 and Nafion maintain a consistent mobility across the entire RH range, however, the mobility of Nafion is clearly higher.

Figure 3.13 **Proton conductivity of BAM as a function of IEC between 50-98% RH, relative humidity indicated beside plotted data points (conductivity of fully hydrated membranes are included for comparison).**

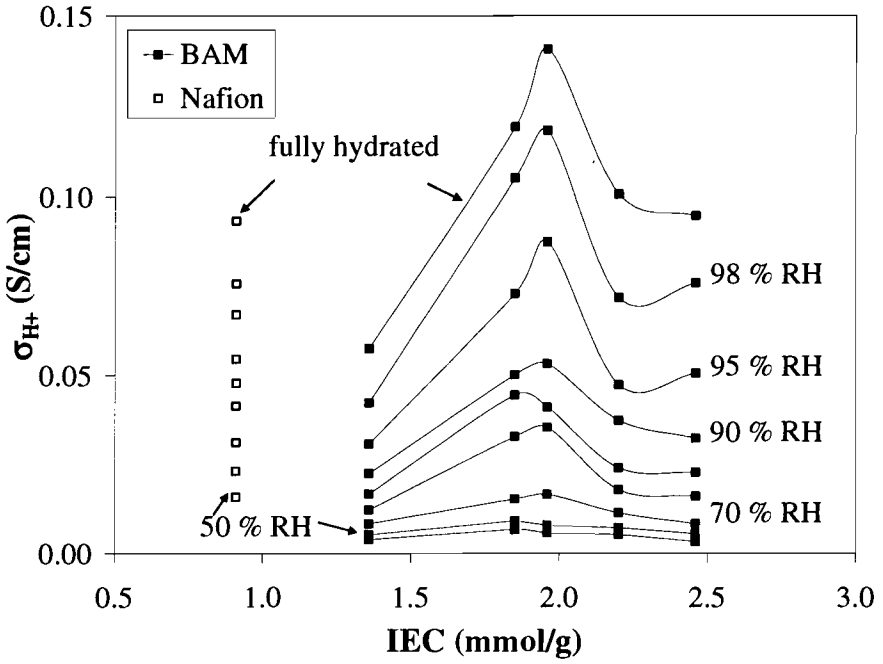

Figure 3.14 **Effective proton mobility of BAM as a function of relative humidity between 50 – 98% RH**

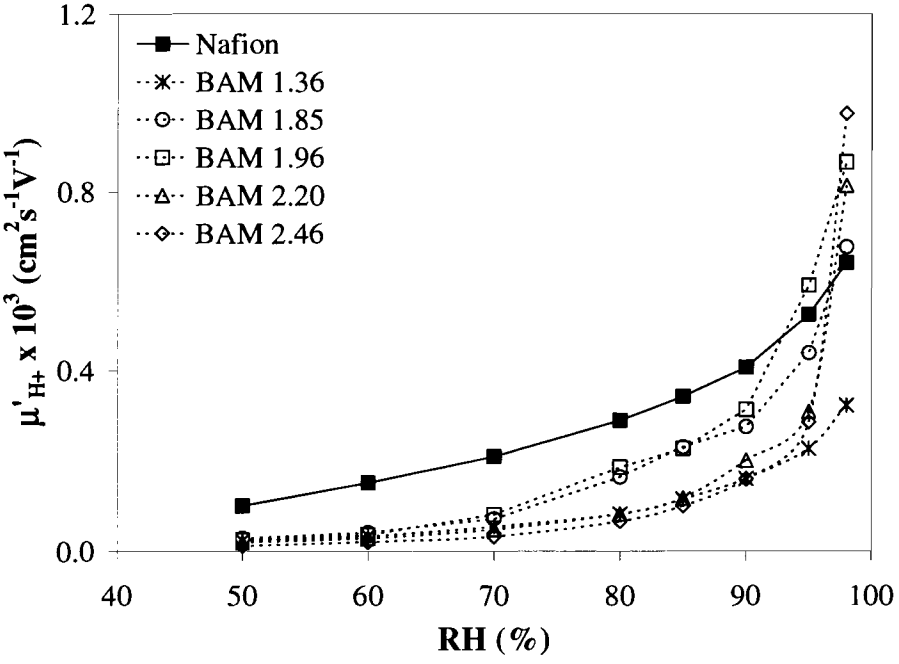

Because mobility is clearly influenced by water content, the relationship to λ was examined (Figure 3.15). In general, increasing λ for individual membranes by raising RH, results in increased mobility. At a first approximation it might have been expected that membranes with the same λ should exhibit the same mobility, however, this is clearly not the case. For example, Nafion exhibits a 5 – 8 times higher mobility than any of the BAM membranes across the 4 – 12 λ range. These results may be explained as a consequence of the difference in acid dissociation constants between a perfluorosulfonic acid-based system (Nafion, pKa ~ -6) and a benzensulfonic acid-based system (BAM, pKa ~ -2), i.e., given the same λ, the protons in Nafion are expected to be more dissociated than the corresponding protons in the BAM membrane, since Nafion is a stronger acid.[57] However, within the BAM series there are inconsistencies in mobility for membranes with the same λ that cannot be explained using this rationale. In the low λ regime, < 10 $H_2O/\text{-}SO_3H$, consistent mobility behaviour between the membranes is attributed to the fact that as λ increases, there are more water molecules between each proton and sulfonate group, leading to more effective screening of the proton from the negative charge, and thus proton transport becomes easier. In the high λ regime, the fact that the profiles diverge can be attributed to differences in X_v (Figure 3.16).

Because there are so many factors involved (variations in acid concentration, IEC; λ, X_v), the mobilities, λs, and proton concentrations at constant X_v were compared. Water contents $X_v = 0.30$ and $X_v = 0.40$ were chosen, as most of the membranes are able to achieve water contents near those values in the RH range studied. Since none of the measured X_v values fell exactly on 0.30 or 0.40, an interpolation of the data was necessary. A linear relationship was assumed between the points on either side of the X_v

of interest. A few exceptions were made for data that fell outside those ranges. Over the RH range studied, Nafion did not achieve $X_v = 0.4$, but the water content is very close to 0.4 in the wet state so a linear interpolation was performed between the $X_v = 0.34$ and $X_v = 0.41$ values. Because BAM 1.36 was not able to achieve $X_v = 0.4$, even in the fully hydrated state, no values are reported as an extrapolation seemed an unreasonable solution. BAM 2.46 does not achieve $X_v = 0.3$ in the RH range studied, so the values at $X_v = 0.31$ were used as a rough estimate. A summary of the interpolated values are included in Table 3.2 and Table 3.3.

Figure 3.15 Effective proton mobility of BAM as a function of λ

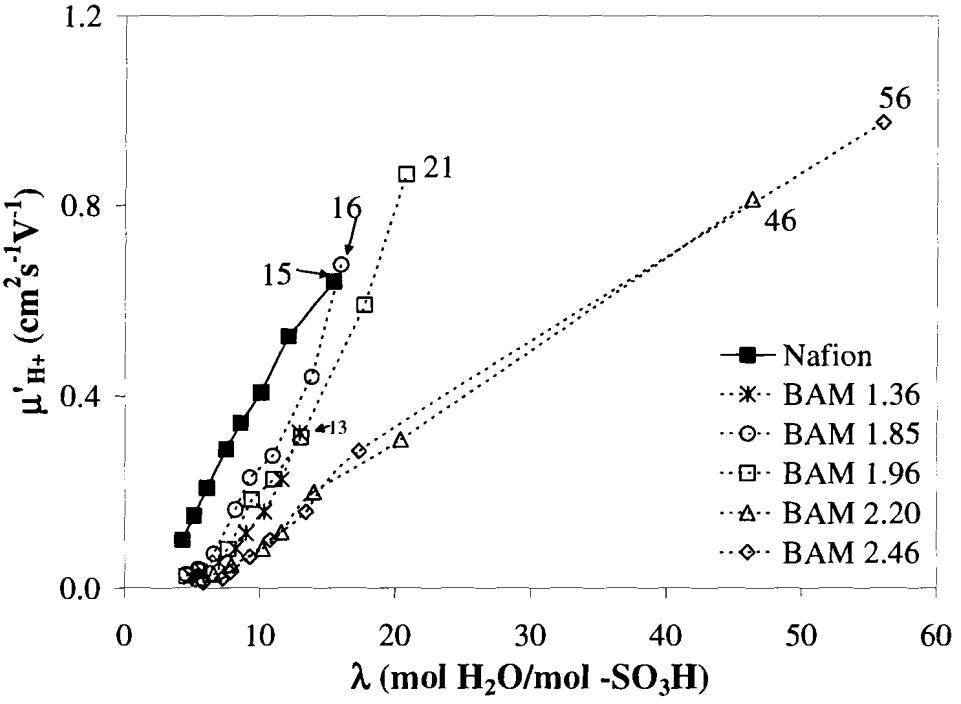

Figure 3.16 Effective proton mobility of BAM as a function of X_v

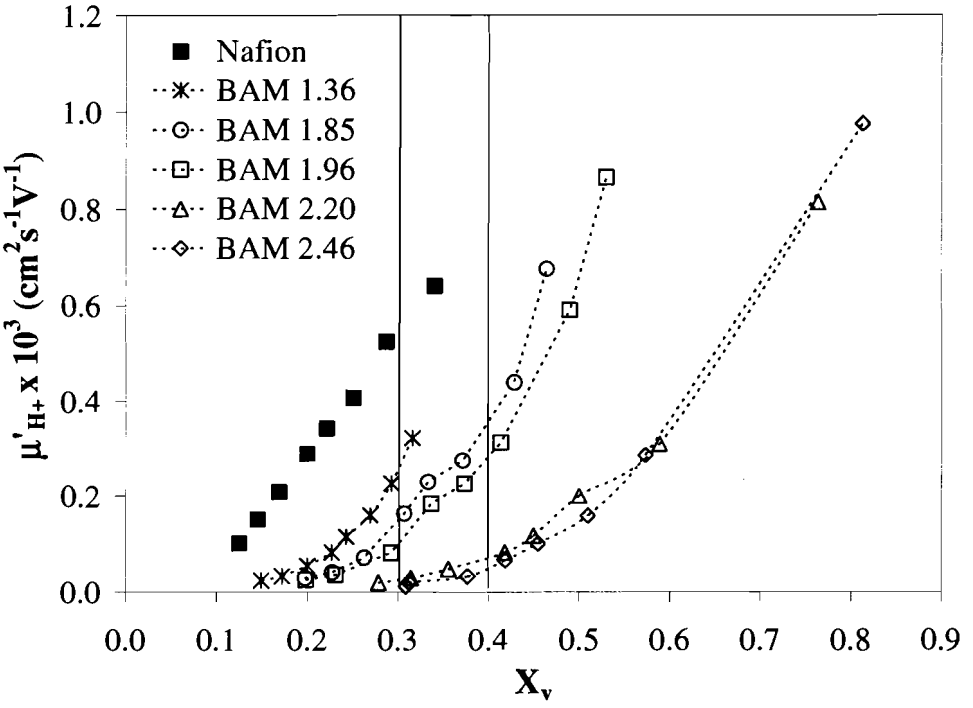

Figure 3.17 Effective proton mobility of BAM as a function of IEC interpolated to $X_v = 0.3$ and $X_v = 0.4$

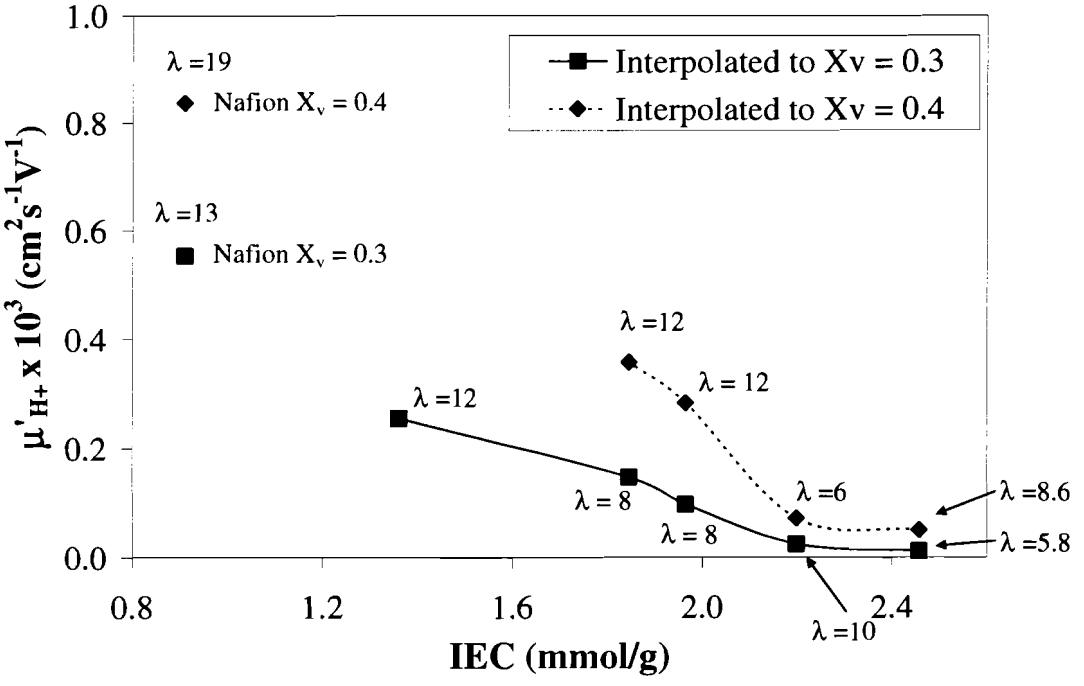

Table 3.2 Comparison of mobility, λ, and proton concentration at X_v = 0.3

Membrane	IEC (mmol/g)	$\mu'_{H+} \times 10^3$ ($cm^2s^{-1}V^{-1}$)	λ (mol H_2O/ mol $-SO_3H$)	[$-SO_3H$] (M)
Nafion	0.91	0.55	12.9	1.3
BAM 1.36	1.36	0.26	12.0	1.4
BAM 1.85	1.85	0.15	7.9	2.1
BAM 1.96	1.96	0.10	7.9	2.1
BAM 2.20	2.20	0.02	6.2	2.7
BAM 2.46	2.46	0.01	5.8	3.0

Table 3.3 Comparison of mobility, λ, and proton concentration at X_v = 0.4

Membrane	IEC (mmol/g)	$\mu'_{H+} \times 10^3$ ($cm^2s^{-1}V^{-1}$)	λ (mol H_2O/ mol $-SO_3H$)	[$-SO_3H$] (M)
Nafion	0.91	0.84	19.3	1.1
BAM 1.36	1.36	----	----	----
BAM 1.85	1.85	0.36	12.4	1.8
BAM 1.96	1.96	0.28	12.4	1.8
BAM 2.20	2.20	0.07	9.5	2.3
BAM 2.46	2.46	0.05	8.6	2.6

Examining the effect of water content on proton mobility behaviour can provide information regarding how "effectively" a PEM utilizes its available water molecules. When comparing two membranes with the same λ, the membrane with the higher mobility is surmised to utilize its waters more effectively in the proton transport process. Nafion is a good example of this, as it exhibits higher mobility than the BAM membranes, for similar λ (Figure 3.17). This suggests that Nafion has a higher "effective" use of water in comparison to the BAM series. These results are consistent with the findings of Kreuer, where he observed that the mobility of Nafion is higher than that of S-PEEKK for similar X_v.[54] Given that both S-PEEKK and BAM are main chain sulfonated hydrocarbon based membranes, and exhibit minimal microphase separation, it is not surprising that they would demonstrate similar behaviour. Kreuer attributed his findings to increased connectivity of the hydrophilic domains in Nafion, due to its more

pronounced hydrophobic/hydrophilic separation. Furthermore, it is possible that the BAM membranes do not swell homogenously. It has been suggested by Eikerling and coworkers that inelastic membranes tend to swell inhomogenously, resulting in a less connected network. On the other hand more elastic materials, such as Nafion, are expected to exhibit the opposite behaviour, resulting in a more connected network and hence better overall transport properties.[70]

A comparison between the BAM membranes within the series would suggest that BAM 2.20 and 2.46 membranes exhibit the least "effective" use of water, revealed by the fact that they exhibit the lowest mobility at both $X_v = 0.3$ and $X_v = 0.4$. However, it is more likely related to the condensed structure that results from the low IEC membranes losing up to 50 vol% water in going from the fully hydrated state to $X_v = 0.3$. This will likely result in much more tortuous and constricted channels, and consequently decreased proton mobility.

3.5 Conclusions

Dynamic vapour sorption analysis has been shown to be a useful method to control and measure water contents of milligram sized samples of membranes subjected to variable humidity environments at constant temperature.

Increasing the relative humidity of the membrane environment for a series of α, β, β-trifluorostyrene-co-substituted α, β, β-trifluorostyrene copolymers (BAM), results in an increase in water content and an improvement in proton transport properties. All 5 BAM membranes, and Nafion, exhibit behaviour that is consistent with "Schroeder's Paradox" taking up less water from the humidified state than that of liquid water.

In the high humidity regime, ~ 98% RH, the high IEC BAM membranes are able to maintain good proton conductivities and mobilities, even surpassing those of Nafion. However, below 98%RH the transport properties in BAM decrease drastically such that at 90% RH the proton conductivity and mobility is significantly less than that of Nafion. By comparison, Nafion exhibits a moderate variation in proton transport properties over the RH range studied yet has the best proton transport in the low humidity regime.

Within the BAM series, the most drastic increases in water contents and proton transport, were seen for the high sulfonic acid content membranes. However when compared to the other membranes in the series, at similar water contents, they exhibited the least effective use of their water molecules. This has been attributed to the fact that under low relative humidity conditions, high IEC BAM membranes have lost a significant portion of their water giving them a very compact tortuous structure. On the other hand Nafion exhibits a greater use of its water molecules and is less significantly effected by changes in relative humidity.

Table 3.4 Data summary for BAM 1.36 equilibrated with water vapours of 50-98% RH

Relative Humidity (%)	X_v (%)	λ (mol H_2O/mol – SO_3H)	[-SO_3H] (M)	σ_{H+} (S/cm)	μ'_{H+} x 10^3 ($cm^2s^{-1}V^{-1}$)
50	0.15	5	1.69	0.004	0.02
60	0.17	6	1.64	0.005	0.03
70	0.20	7	1.59	0.008	0.05
80	0.23	8	1.54	0.012	0.08
85	0.24	9	1.50	0.017	0.11
90	0.27	10	1.45	0.022	0.16
95	0.29	12	1.40	0.031	0.23
98	0.32	13	1.36	0.042	0.32
fully hydrated	0.33	14	1.34	0.057	0.45

Table 3.5 Data summary for BAM 1.85 equilibrated with water vapours of 50-98% RH

Relative Humidity (%)	X_v (%)	λ (mol H_2O/mol – SO_3H)	[-SO_3H] (M)	σ_{H+} (S/cm)	μ'_{H+} x 10^3 ($cm^2s^{-1}V^{-1}$)
50	0.20	5	2.41	0.007	0.03
60	0.23	5	2.32	0.009	0.04
70	0.26	7	2.22	0.015	0.07
80	0.31	8	2.08	0.033	0.16
85	0.33	9	2.00	0.044	0.23
90	0.37	11	1.89	0.050	0.28
95	0.43	14	1.72	0.073	0.44
98	0.46	16	1.61	0.105	0.68
fully hydrated	0.55	24	1.27	0.119	0.97

Table 3.6 Data summary for BAM 1.96 equilibrated with water vapours of 50-98% RH

Relative Humidity (%)	X_v (%)	λ (mol H_2O/mol – SO_3H)	[-SO_3H] (M)	σ_{H+} (S/cm)	μ'_{H+} x 10^3 ($cm^2s^{-1}V^{-1}$)
50	0.20	5	2.41	0.006	0.02
60	0.23	6	2.31	0.008	0.04
70	0.29	8	2.13	0.017	0.08
80	0.34	9	1.99	0.035	0.18
85	0.37	11	1.88	0.041	0.23
90	0.41	13	1.76	0.053	0.31
95	0.49	18	1.54	0.087	0.59
98	0.53	21	1.42	0.118	0.87
fully hydrated	0.62	31	1.12	0.141	1.29

Table 3.7 Data summary for BAM 2.20 equilibrated with water vapours of 50-98% RH

Relative Humidity (%)	X_v (%)	λ (mol H_2O/mol – SO_3H)	[-SO_3H] (M)	σ_{H+} (S/cm)	μ'_{H+} x 10^3 ($cm^2s^{-1}V^{-1}$)
50	0.28	6	2.8	0.005	0.02
60	0.31	7	2.7	0.007	0.03
70	0.36	8	2.5	0.011	0.05
80	0.42	10	2.3	0.018	0.08
85	0.45	12	2.1	0.024	0.12
90	0.50	14	1.9	0.037	0.20
95	0.59	20	1.6	0.047	0.31
98	0.76	46	0.9	0.072	0.81
fully hydrated	0.82	76	0.6	0.101	1.74

Table 3.8 Data summary for BAM 2.46 equilibrated with water vapours of 50-98% RH

Relative Humidity (%)	X_v (%)	λ (mol H_2O/mol – SO_3H)	[-SO_3H] (M)	σ_{H+} (S/cm)	μ'_{H+} x 10^3 ($cm^2s^{-1}V^{-1}$)
50	0.31	6	2.97	0.003	0.01
60	0.31	7	2.89	0.006	0.02
70	0.38	8	2.68	0.008	0.03
80	0.42	9	2.52	0.016	0.07
85	0.45	11	2.35	0.023	0.10
90	0.51	13	2.11	0.032	0.16
95	0.57	17	1.84	0.051	0.29
98	0.81	56	0.81	0.076	0.98
fully hydrated	0.85	84	0.56	0.095	1.74

Table 3.9 Data summary for Nafion equilibrated with water vapours of 50-98% RH

Relative Humidity (%)	X_v (%)	λ (mol H_2O/mol – SO_3H)	[-SO_3H] (M)	σ_{H+} (S/cm)	μ'_{H+} x 10^3 ($cm^2s^{-1}V^{-1}$)
50	0.13	4	1.62	0.016	0.10
60	0.15	5	1.59	0.023	0.15
70	0.17	6	1.54	0.031	0.21
80	0.20	8	1.48	0.041	0.29
85	0.22	9	1.44	0.048	0.34
90	0.25	10	1.39	0.055	0.41
95	0.29	12	1.32	0.067	0.52
98	0.34	15	1.22	0.076	0.64
fully hydrated	0.41	20	1.11	0.093	0.87

Chapter 4: Synthesis and Characterization of Photocured PEMs Bearing Weak and Strong Acid Groups

4.1 Introduction

The proton exchange membrane (PEM) is a key component of solid polymer electrolyte fuel cells. It acts as both a separator to prevent mixing of reactant gases, and as an electrolyte for transporting protons from anode to cathode.[1,89,90] Nafion® is the most widely studied PEM because it exhibits high conductivity, good mechanical strength, chemical stability, and is commercially available. Sulfonated poly(arylenes) such as sulfonated poly(ether ether ketone) (S-PEEK), are under intense investigation as possible low cost alternatives to Nafion.[91-93]

Conventionally, Nafion and sulfonated polyarylenes are employed as pre-cast or pre-molded membranes and compressed between two catalyzed gas diffusion electrodes, (i.e., the anode and cathode). Compression generally takes place at elevated temperatures and pressures to achieve good interfacial adhesion between the membrane and the electrodes. However, the requirement of using preformed membranes may restrict new fuel cell processing designs, in which high temperatures and high pressures must be avoided. For instance, novel fuel cell design concepts might require the PEM to be conformable by injection molding, formed as micro-channels and unique shapes, or

---

Sections of this work have been reproduced in part with permission from:
Chemistry of Materials Schmeisser, J.; Holdcroft, S.; Yu, J.; Ngo, T.; McLean, G., 17, 387, © 2005, American Chemical Society
Differential scanning calorimetry of the films was performed by Dr. Ana Siu.

strongly adhering to the catalyst layer without hot pressing. One conceptual route to enhance processability of PEMs is to prepare viscous liquids that can be cast, printed, or sprayed as films, or as microstructured designs, and subsequently photocured. A plausible demonstration of this concept is to dissolve a linear preformed proton conducting polymer in a vinyl monomer/cross-linking agent, and subsequently polymerize this composition to form a solid electrolyte. Organization of the resulting material is referred to as a semi-IPN (semi-interpenetrating network).

Interpenetrating polymerization is a method of blending two or more polymers to produce a mixture in which phase separation of the two systems is not as extensive as it would be with mechanical blending. An interpenetrating polymer network is defined as an intimate combination of two polymers both in network form, at least one of which is synthesized or cross-linked in the immediate presence of the other, Figure 4.1a. IPN-based systems are used extensively in commercial products such, as plastic dental fillings, epoxy adhesives, and optically smooth plastic surfaces.[94]

Polymers in IPNs are physically rather than chemically combined, i.e., there are no covalent bonds between the two network polymers. Ideally, monomers of polymer A react only with other monomers of polymer A, and likewise for polymer B. In semi-interpenetrating network systems, one polymer is cross-linked and the other polymer is linear. If the two systems are sufficiently miscible, the linear polymer becomes immobilized in the cross-linked polymer, Figure 4.1b. The physical properties of the combined polymers depend on both the properties of the polymers and the way they are combined.

In this work, a series of semi-interpenetrating networks of proton conducting membranes have been formed by the photocuring of polymerizable polyelectrolyte liquids, comprised of linear **S-PEEK** (Figure 4.2a), immersed in a solution of the following: acrylonitrile **ACN**; vinylphosphonic acid **VPA**; divinyl sulfone **DVS**; dimethylacetamide **DMA** (Figure 4.2b). Radical polymerization of the monomer mixtures was initiated by the bis(2,4,6-trimethylbenzoyl)-phosphineoxide photoinitiator shown in Figure 4.2c.

Figure 4.1 Schematic of (a) IPN and (b) semi-IPN.

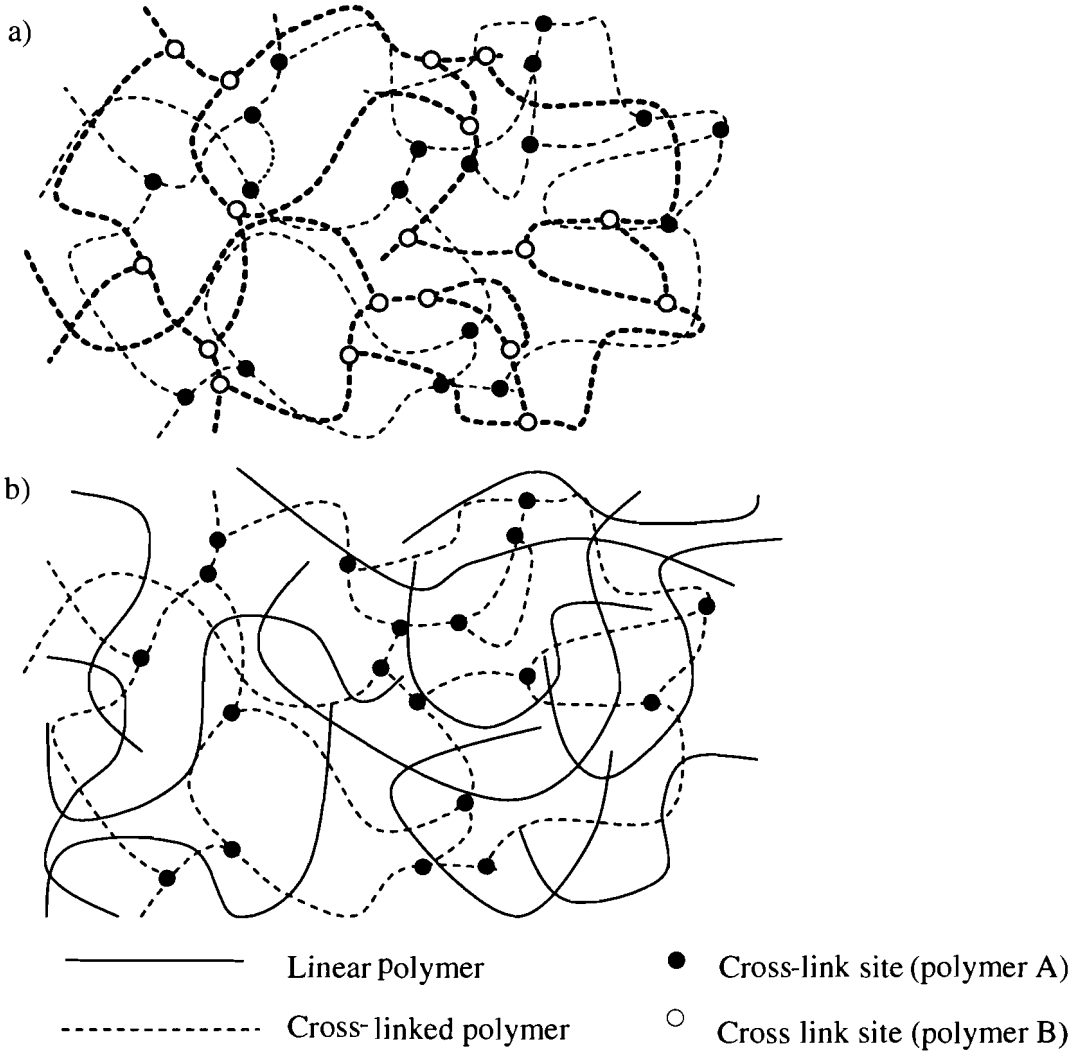

S-PEEK was chosen as the proton conductive medium because of its solubility in a variety of solvents. The photocurable monomers were chosen primarily because of their ability to solvate S-PEEK and because of their functionality: ACN provides flexibility and reduces brittleness of photocured films; VPA has been shown to enhance proton conductivity when polymerized into PEMs through weak acid dissociation;[95] DVS for its cross-linking ability; and DMA to reduce the viscosity of the liquid polyelectrolyte solution. The resulting films can be described as a host/guest type system, in which the crosslinked matrix comprising VPA, DVS, and ACN is considered the host polymer while S-PEEK is considered the guest.

Figure 4.2 Chemical structure of (a) S-PEEK, (b) host monomers, and (c) photoinitiator.

a)

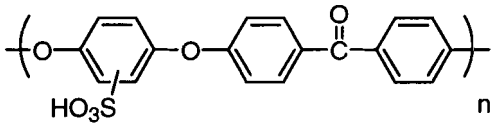

S-PEEK
sulfonated poly(ether ether ketone)

b)

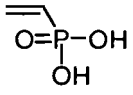

vinylphosphonic acid

acrylonitrile

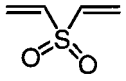

divinylsulfone

c)

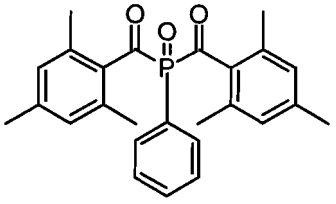

bis(2,4,6-trimethylbenzoyl)-phenylphosphineoxide

The goal of the work in this chapter was to systematically study the effect of photocurable polyelectrolyte composition on fuel cell pertinent properties such as sulfonic acid content, proton conductivity, water content, and thermal characteristics of the resultant solid polymer electrolytes. In an effort to achieve this goal, two series of photocurable materials were prepared: 1) a series to study the effect of varying the content of the linear strong acid proton conducting polymer, S-PEEK and 2) a series to study the effect of degree of cross-linking, by varying the content of the cross-linking agent.

Background

In the late 1980's, Petty-Weeks et al. investigated proton conducting IPNs for hydrogen sensor applications.[96-98] In their work, a three dimensional polymer network composed of methacrylic acid and methylenebisacrylamide was synthesized in the presence of a poly-vinyl alcohol/phosphoric acid blend. Although their study focused mostly on polymer physical properties such as bulk modulus, water insolubility, and incorporation into hydrogen sensors, a section discussing proton conductivity was also included. They found that mechanical properties and polymer insolubility in water improved with increasing amounts of the network polymer, but proton conductivity suffered due to the non-conducting nature of the cross-linked network. Although plans of further investigation were included in the conclusions of the last paper, no further studies can be found in the literature. In this work, a proton conducting component was incorporated into the cross-linked matrix to avoid a similar decrease in conductivity as network polymer content increases.

More recently, and following the publication of this work, DiSimone and coworkers presented a new strategy for synthesizing photocurable PEMs.[99] There are some differences between their work and what is discussed in this chapter. Firstly, whereas the S-PEEK materials reported here are hydrocarbon-based, who have prepared hydrocarbon-based materials and post-fluorinated them with elemental fluorine gas to produce highly fluorinated PEMs. They have observed that their fluorinated materials display a ~ 10% increase in decomposition temperature and improved mechanical stability, in comparison to the nonfluorinated analogues. Secondly, in an effort to synthesize PEMs with high acid loading, yet good mechanical strength, they prepared materials that are 100% curable, with the proton conductive sulfonic acid groups incorporated directly into the cross-linked structure. However, they found that with high acid loading (IEC = 1.82 mmol/g), they achieved high proton conductivity 0.250 S/cm, yet the materials absorbed 121 wt% water, and exhibited a loss of mechanical strength at high water contents. One of the properties that is similar between the S-PEEK PEMs and their fluorinated PEMs is the ability to pattern three-dimensional features using photolithographic techniques.

4.2 Experimental

4.2.1 Materials

S-PEEK was synthesized by direct sulfonation of poly [ether ether ketone] (PEEK) to a sulfonic acid content of 2.14 mmol sulfonic acid per gram of dry polymer according to the detailed procedure outlined in Section 2.3.1. Concentrated sulphuric acid (Anachemia), vinylphosphonic acid (Aldrich), dimethylesulfoxide (DMSO), and dimethylacetamide (Aldrich) were used as received. Divinyl sulfone (DVS) and

acrylonitrile (ACN) were obtained from Aldrich, and vacuum distilled prior to use. The photoinitiator, bis(2,4,6-trimethylbenzoyl)-phenylphosphineoxide (IRGACURE 819), was provided courtesy of Ciba Specialty Chemicals Canada Inc., and used as received.

4.2.2 S-PEEK Membranes

S-PEEK ionomer films were prepared by casting from (DMSO) solutions. The S-PEEK polymer was dissolved (~25 wt %) in DMSO at room temperature until a clear yellow solution formed. The solution was cast onto glass plates and heated under ambient atmosphere at 90°C overnight. Films, 70 - 150 μm thick, were released from the casting plate by immersing them in Milli-Q water for 2 - 10 minutes. Cast membranes were subsequently washed in deionized water to remove residual solvent and sulfuric acid.

4.2.3 Synthesis and Preparation of Photocured Polyelectrolytes

Photocurable polyelectrolytes were prepared according to the compositions shown in Table 4.1. The appropriate amounts of liquid monomer (VPA, DVS, ACN), solvent (DMA), and photoinitiator (PI) were mixed and sealed in the dark, at room temperature for 12 hours to ensure dissolution of the initiator. The appropriate amount of S-PEEK was added to another vial, and the corresponding solution of monomer/solvent/PI mixture added. Complete dissolution of the S-PEEK in the monomer mixture took ~2 days at room temperature. The viscosity of the resulting clear yellow solutions varied from free flowing to honey-like syrup as the S-PEEK content was increased.

Table 4.1 Relative compositions of liquid polyelectrolytes (wt%)

Sample	S-PEEK	VPA	DVS	AN	PI	DMA
			Series 1 - Varying S-PEEK Content			
S1	0	19	44	19	3	16
S2	4	17	43	17	3	15
S3	8	17	41	17	3	15
S4	17	15	37	15	3	13
S5	31	13	31	13	2	11
			Series 2 - Varying DVS Content			
S6	26	9	18	33	2	12
S7	26	9	25	25	2	12
S8	26	9	32	18	2	12
S9	26	9	41	9	3	12

Thin films of each polyelectrolyte solution were spread with a casting knife onto glass slides fitted with Cu wire (150 μm diameter) spacers, Figure 4.3. The liquids were cured with broad spectrum visible light, 410-520 nm using an ELC-500 (Electro-lite Corp., Connecticut USA) light exposure chamber fitted with four 9 W visible lamps. Films were situated inside the chamber at approximately 10 cm from the light source and cured for up to 4 hours, or until they were no longer tacky. Photocured films were released from the glass slides by soaking in Milli-Q water.

Figure 4.3 Schematic of photocuring apparatus

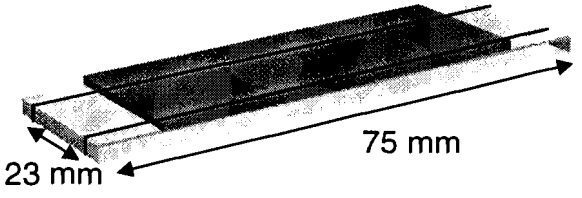

4.2.4 Water Content Analysis

Circular samples (~8.5 mm diameter) were cut from fully hydrated sheets and soaked in Milli-Q water for a minimum of 12 hours. Wet weights, W_{wet} (+/- 0.0001 g), were obtained after blotting with a Kimwipe to remove surface water. This was performed on as short a time scale as possible (< 10 s) to avoid water loss to the

atmosphere. Dry weights, W_{dry} (+/- 0.0001 g), were obtained after membranes were vacuum dried (1 mmHg) at 80°C for two hours and cooled in a desiccator.

Membrane volumes were obtained for both wet, V_{wet}, and dry, V_{dry}, samples by measuring diameter, d, with a calliper (+/ 0.1 mm), thickness, h, with a micrometer (+/ 0.001 mm), and applying the following relationship:

$$Volume = \frac{1}{4}\pi d^2 h \qquad [4.1]$$

Membrane water content was calculated as a weight percentage:

$$Water\ Content\ (wt\%) = \frac{W_{wet} - W_{dry}}{W_{dry}} \qquad [4.2]$$

as a volume percentage, X_v:

$$Water\ Content\ (vol\%) = Xv = \frac{V_{water}}{V_{wet}} \qquad [4.3]$$

and as the number of water molecules present per acid group, λ:

$$\lambda = \frac{moles\ H_2O}{moles\ \text{Acid}} \qquad [4.4]$$

Proton concentration was calculated as number of moles of acid present in a given sample volume:

$$[H^+] = \frac{\text{moles of acid}}{V_{wet}} \qquad [4.5]$$

4.2.5 Ion Exchange Capacity

Experimental ion exchange capacity IEC^{exp}, determined using a direct titration method, represents the number of millimoles of ion exchange sites per dry gram of polymer and was used to quantify total acid content in this work. Circular samples were cut and placed in ~2M HCl and stirred for 12 hours. The membranes were then

transferred to a new beaker containing Milli-Q water and stirred for 30 minutes, after which the water was decanted and replaced with fresh water and stirred for another 30 minutes. This process was repeated two more times. The acidified membranes were then immersed in 50 mL of ~2 M NaCl solution for 2 hours, with occasional agitation, and titrated with standardized NaOH to the phenolphthalein endpoint. Before obtaining a dry weight, the membranes were reprotonated with HCl, rinsed with Milli-Q water, dried under vacuum (1mmHg) at 80°C, and cooled in a desiccator. Ion exchange capacity was calculated as follows:

$$IEC(mmol\,SO_3H\,/\,g) = \frac{(vol.\,\mathrm{NaOH}, mL) \times (conc.\,\mathrm{NaOH}, M)}{(dry\ wt.\ of\ membrane, g)} \qquad [4.6]$$

4.2.6 Proton Conductivity

Proton conductivity was measured using electrochemical impedance spectroscopy with a Hewlett Packard 8753A Network Analyzer employing a transverse two-electrode configuration as described by Gardner and Anantaraman.[100] The network analyzer was calibrated using an open, short, load (50 Ω) procedure, as directed by the manufacturer.

Measurements were performed using a gold plated coaxial probe (ACME plating, Vancouver) as shown in Figure 4.4a. The probe was constructed in house, using a male-male BNC connector (Electrosonic, Canada), one side of which was cut down and polished flat to expose a central disc 2.18 mm diameter, surrounded by a ring of inner diameter of 6.44 mm. These rings were separated by a Teflon dielectric, which was recessed from the end of the probe by ~5 mm.

Circular samples of hydrated membranes were cut to 1cm diameter and soaked in Milli-Q water for a minimum of 12 hours prior to use. Samples were removed from

water, blotted with a Kimwipe to remove surface water, and laid across the surface of the coaxial probe. A spring-loaded Teflon plunger was used to ensure intimate contact between the end of the probe and the membrane of interest. Figure 4.4b shows a cross sectional diagram of the probe/membrane assembly. This whole assembly was housed in a cylindrical sheath made from an electrically inert plastic material, which had an opening in the side to allow the membrane to be inserted between the probe and plunger.

Figure 4.4 (a) End on view of probe tip (b) Cross section of probe/membrane assembly

a)

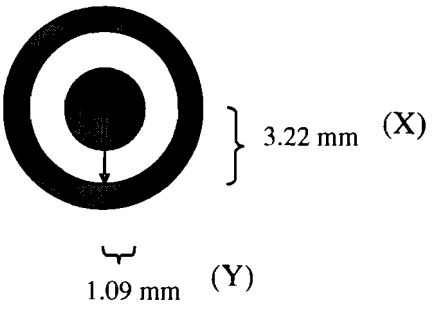

b)

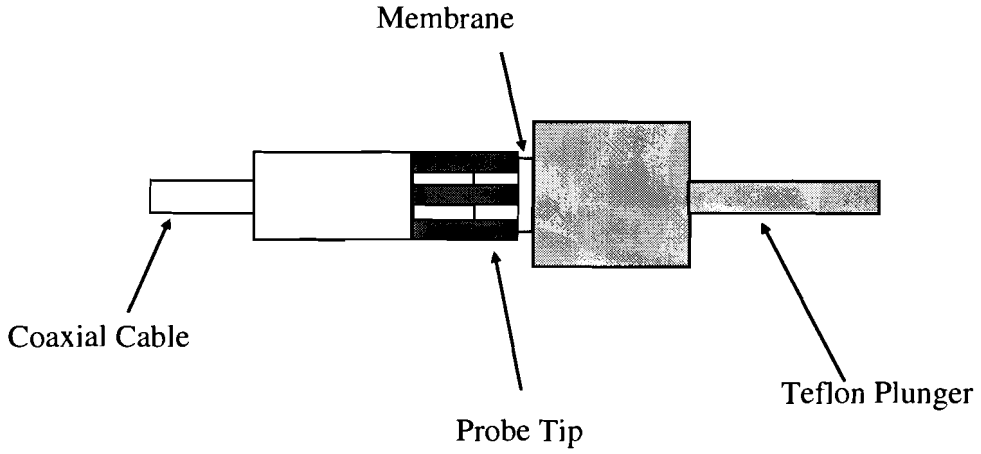

Once completely assembled, the gold probe was connected to the instrument with a coaxial cable, and impedance spectra were obtained over the frequency range from 300 kHz to 1 GHz. Probe assembly was carried out on as short a time scale as possible (< 20

s) to reduce water loss before completion of the impedance measurement. Data was analyzed using Zplot software (Scribner).

4.2.7 UV/IR Spectroscopy

Infrared Spectroscopy was performed on a Bomen BM-Series FT-IR spectrometer over the frequency range 4000 to 550 cm^{-1} at 16 scans. UV-visible absorption spectra were recorded on a Cary 3E spectrophotometer over the wavelength range 200 to 600 nm.

4.2.8 Thermal Analysis

Thermal decomposition temperatures for the homopolymers and semi-IPNs were determined using thermogravimetric analysis (TGA) on a Shimadzu TGA-50 thermogravimetric analyzer. Samples of dry films of ~ 2-5 mg were placed in platinum pans and heated from 25°C to 500°C at a rate of 10°C/min under ambient atmosphere.

Differential scanning calorimetry (DSC) using a DSC Q10 (TA Instruments) was used to determine the glass transition, T_g, of the pure host/guest polymers and photocured semi-IPNs. The instrument was first calibrated against indium. Samples of dry films (~ 2-10 mg) were placed in aluminium DSC pans and heated under a nitrogen atmosphere at a rate of 10°C/min from 20°C to 150°C and held at 150°C for 10 minutes to remove residual water. The samples were cooled from 150°C to -100°C, and melting thermograms were obtained at a constant heating rate of 10°C/min from -100°C to 250°C. The data was analyzed using Universal Analysis 2000 version 3.7A.

4.3 Results

4.3.1 Photocured Films

Relative compositions of the two series of photocured PEM's that were synthesized are summarized in Table 4.1. The assumption was made that all of the liquid monomers added to the polyelectrolyte mixture were incorporated into the cross-linked structure. Series 1 (Sample # S1-S5) was prepared to study the effect of varying the content of the linear proton conducting polymer, S-PEEK, and Series 2, (Sample # S6-S9) to study the effect of varying cross-linker content, DVS. Upon photocuring, all samples resulted in clear yellow solid films of varying thicknesses (70-150 μm) depending on both the diameter of the wire spacers and the viscosity of the polyelectrolyte solutions. No significant difference was apparent between the two series upon visual inspection.

4.3.2 Conductivity of Photocured Films

Ionic resistance was measured for three samples of each polyelectrolyte composition. Complex-plane impedance plots for representative membranes from both series are shown in Figure 4.5. A detailed explanation of the rationale for the data analysis was presented in detail in Section 2.3.2. Briefly, the semi-circles in the complex-plane impedance plots were fitted, using non-linear least squares, to a Randles equivalent circuit model. All samples fit near perfect semi-circles.

Figure 4.5 Complex plane impedance plots for Sample S4 (17 wt% S-PEEK) and Sample S6 (18 wt% DVS)

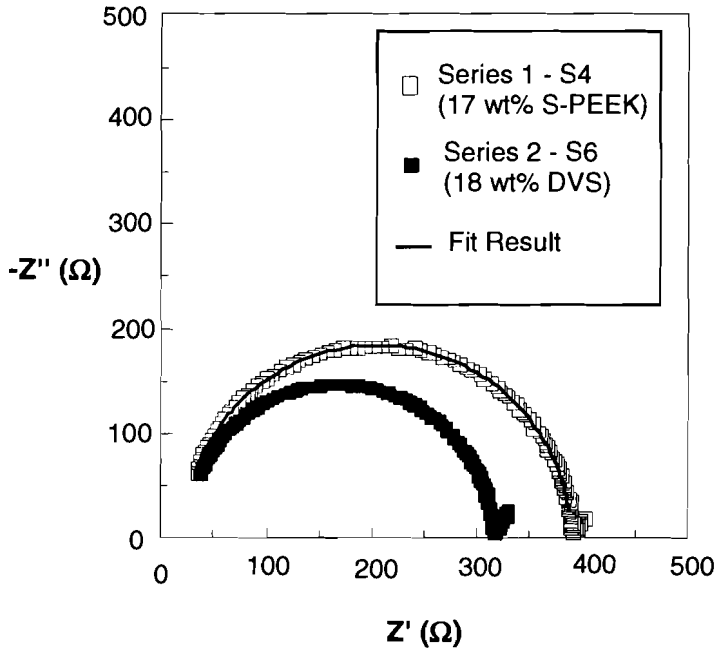

Ionic resistance, R_m, was used to calculate proton conductivity, σ_{H+}, according to the following relationship:

$$\sigma_{H^+} = \frac{1}{2\pi R_m h} \ln\left(\frac{X}{Y}\right); \qquad [4.7]$$

where h is the thickness of the film, X is the inner radius of the outer electrode, and Y is the radius of the inner electrode. The average of three conductivity measurements is reported in Table 4.3 and Table 4.4.

4.3.3 UV-Visible Spectroscopy

UV-Vis absorption by the photocurable solution extends from the UV to 450 nm, as illustrated in Figure 4.6 for a thin liquid film (70 μm) containing 17 wt% S-PEEK (Sample S4). Upon comparison with the UV-Vis spectrum of the pure photoinitiator, it

was concluded that the broad absorption peak that is seen as a shoulder between 385-415 nm is due to the absorption of the photoinitiator. The transmittance at λ_{max} of the initiator (400 nm) is 19%, and hence may be irradiated uniformly throughout the thickness of the liquid film. The incident light source, while having maximum power at 450 nm, emits a broad spectrum of light between 410 and 520 nm which is, sufficient to photodegrade the initiator. Also shown in Figure 4.6 is the evolution of the UV-Vis absorption spectrum as a function of photocure time. The loss of the 385-415 nm shoulder corresponds to photolysis of the photoinitiator.

Figure 4.6 UV absorption spectra of Sample S4, 17 wt% S-PEEK, liquid and photocured polyelectrolyte.

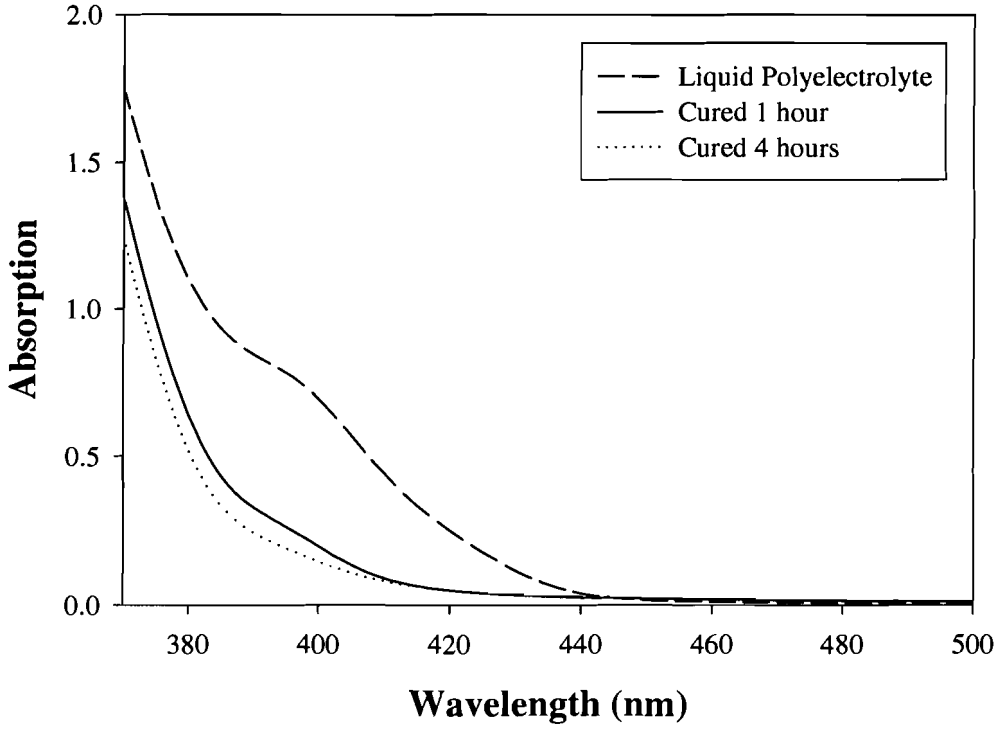

4.3.4 Infrared Spectroscopy

The resulting photocured polyelectrolytes are assumed to be semi-IPN's, with S-PEEK playing the role of the linear guest polymer residing in a cross-linked random

copolymer of VPA, ACN, and DVS host. In order to confirm that the polymerization proceeds as expected, changes in the FTIR spectrum of the photocurable solutions were monitored *in situ*. A small amount of the sample, < 1 mg, was sandwiched between two 6 mm NaCl plates (Aldrich) and the IR spectrum obtained periodically after 0, 15, 30, 60, 120, and 240 min. curing time. Figure 4.7a shows the evolution of the FTIR spectra for the 17 wt% S-PEEK sample (Sample S4), with an enlarged portion of the fingerprint region included in Figure 4.7b. For clarity, only data obtained at 0, 60, and 240 min. curing times are shown. IR spectra of S-PEEK and pure unreacted monomers were obtained and used as references in assigning peaks for the polymerizable mixture.

The number of components and similarity between the functional groups in the polymeric solution renders the IR spectrum complex, and hence, accurate identification of each peak difficult. Rather, groups of peaks in characteristic frequency ranges, corresponding to specific functional groups, were monitored with curing time. The broad peak centred at 3060 cm^{-1}, attributed to the hydrogen bonding between the phosphonic acid groups and present in the FTIR spectrum of pure VPA, diminishes rapidly. This is considered due to a decrease in hydrogen bonding as VPA is incorporated into the cross-linked structure. Although the characteristic vinyl (C=C) stretch expected at ~1610 cm^{-1} is masked by the large broad peak at 1598 cm^{-1} due to S-PEEK, there is a decrease in peak size attributed to the consumption of the vinyl groups. Further evidence of vinyl group consumption comes from the decrease in all peaks between 1000-550 cm^{-1}, characteristic of the out of plane bending modes ($-CH=CH_2$) for all mono-substituted monomers. This evidence indicates that the monomers are consumed and that cross-linking has taken place.

Figure 4.7 **(a) IR spectrum of Sample S4, 17 wt% S-PEEK, semi-IPN (b) fingerprint region.**

a)

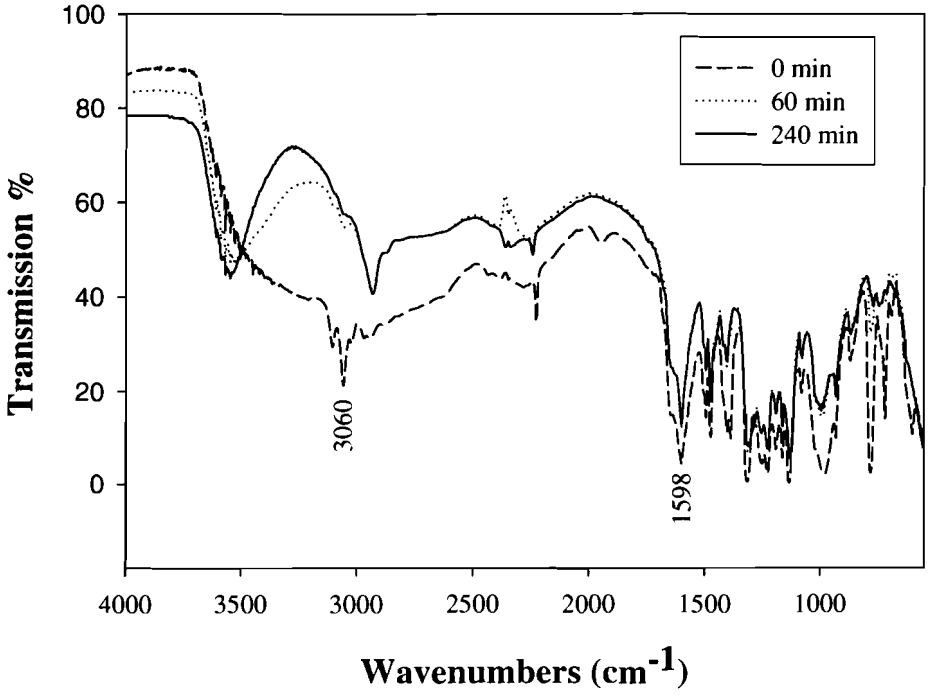

b)

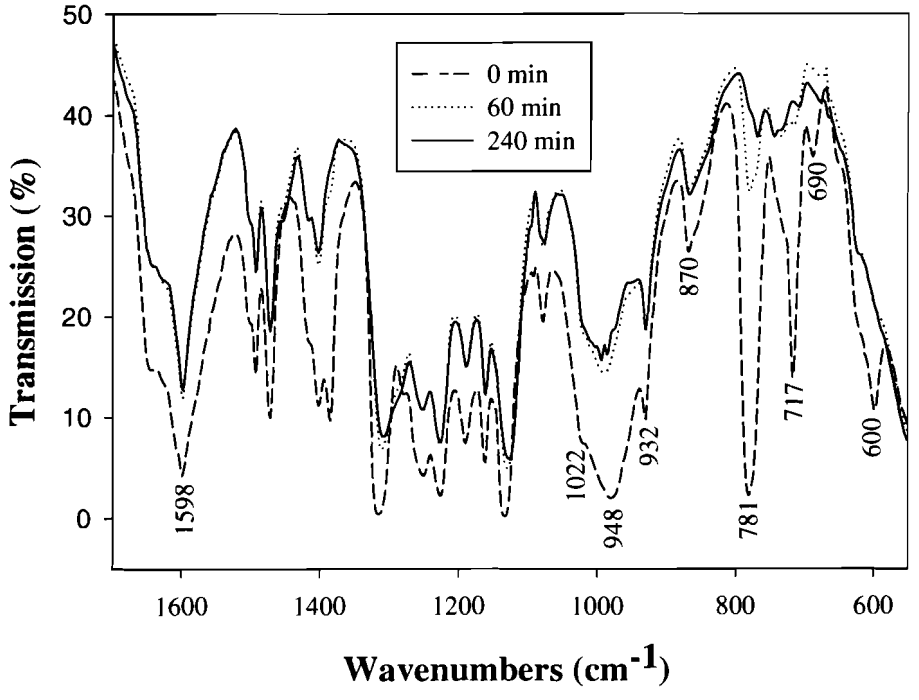

4.3.5 Effect of Curing Time on Conductivity

To determine the minimum time to achieve photocuring, a series of 17 wt% samples (Sample S4) were prepared and cured for 15, 60, 90, 120, 180, and 240 minutes. Each sample was immediately submersed in water after the allotted cure time to stop the photocuring reaction. Three samples representing each curing time were cut, and proton conductivity was measured at room temperature. As can be seen in Figure 4.8, there is improvement in conductivity (0.03 to 0.05 S/cm) when the cure time is increased from 15 to 90 minutes. Curing for longer than 90 minutes appears to have a negligible effect on proton conductivity.

Figure 4.8 Effect of curing time on proton conductivity of Sample S4, 17 wt% S-PEEK, photocured semi-IPN

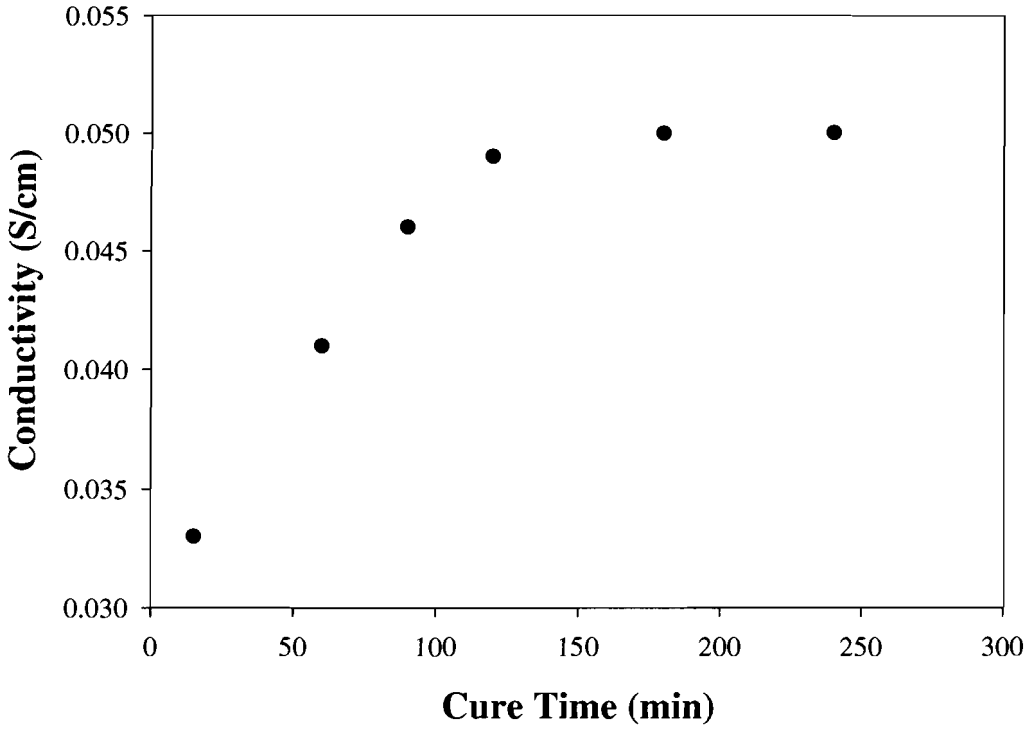

4.3.6 Thermogravimetric Analysis

TGA was used to determine the decomposition temperatures for pure S-PEEK and the photocured films. Figure 4.9 shows thermograms for 0, 31, and 100 wt% S-PEEK samples (S1, S5, and S-PEEK, respectively). All films show an ~10 wt% decrease between 50-200°C, due to loss of residual water.

Figure 4.9 TGA of Samples S1, S5, and pure S-PEEK (0, 31, and 100 wt% respectively)

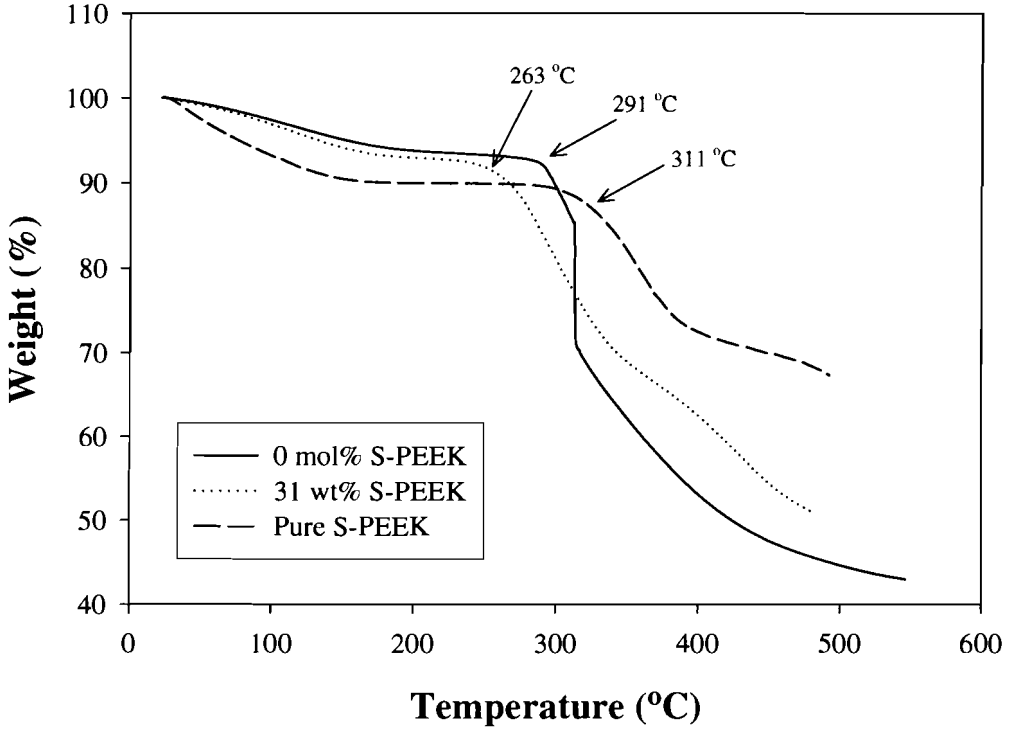

Desulfonation commences at 311 °C for pure S-PEEK, which is consistent with literature values for S-PEEK of similar IEC.[24,40] Decomposition of the pure host polymer and the 31 wt% S-PEEK semi-IPN begins at 291°C and 263°C, respectively. The combination of host and guest causes the semi-IPN to decompose at lower temperatures than each of the separate components. This phenomenon has also been observed by Chen *et al.* in composite materials, in which an interaction exists between functional groups on

the component polymers.[101] In the aforementioned work, it was speculated that a pseudo-hydrogen bond between the C-H groups on PVDF (polyvinylidene difluoride) and the C=O groups on PVP poly(vinylpyrrolidone) catalyzes the thermal decomposition of PVDF/PVP composites, leading to a decrease in observed decomposition temperature. A similar argument can be made here in regards to the decreased thermal stability observed for the semi-IPN materials, i.e., degradation is facilitated by hydrogen bonding between the carbonyl group on S-PEEK and the P-O-H group present on VPA, Figure 4.10.

Figure 4.10 Hydrogen bond between VPA and S-PEEK

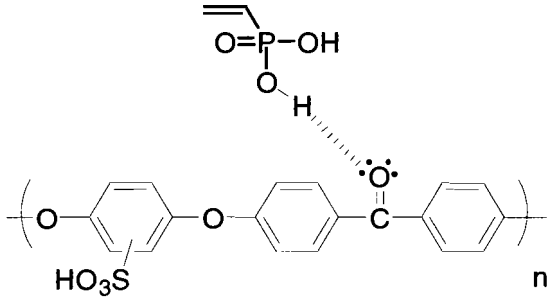

4.3.7 Differential Scanning Calorimetry

DSC measurements were used to determine glass transition temperatures for the 0, 31 wt% and pure S-PEEK samples, listed in Table 4.2. S-PEEK exhibits a clear Tg at 198°C, which is consistent with the literature.[40] For the 31 wt% S-PEEK semi-IPN, there appears to be a very subtle Tg at ~195°C. For the 0 wt% S-PEEK pure host polymer, no clear Tg can be seen. Two possible explanations exist: 1) either the Tg is broad, and the DSC method is not sensitive enough to detect it or 2) the Tg is located above the decomposition temperature, Td.

Table 4.2 Thermal properties of Samples S1, S5, and pure S-PEEK (0, 31, and 100 wt% respectively)

Sample	S-PEEK Content (wt%)	Td (°C)	Tg (°C)
S1	0	291	------
S5	31	263	195
S-PEEK	100	311	198

4.3.8 Ion Exchange Capacity

In an electrolyte that contains only strong acid groups that fully dissociate in water, such as hydrocarbon-based *p*-toluenesulfonic acid** (pKa ≈ -2), the theoretical IEC, IEC^{theo}, may be calculated simply from knowing the proportion of sulfonic acid sites within the polymer. This value, termed degree of sulfonation (DS), is defined in Equation 4.8, and can be determined by integrating the ^{1}H-NMR spectrum and comparing the characteristic peaks representing the unsulfonated polymer with those that represent the sulfonated polymer.[72] The DS of S-PEEK used in this study was found to be 74%, and the ion exchange capacity, IEC^{theo} ([mmol SO_3H units]/[g dry polymer]), determined using Equation 4.9, was calculated to be 2.04 mmol/g.

$$DS = \frac{(\text{molar \# of the } PEEK - SO_3H \text{ unit})}{(\text{molar \# of the } PEEK - SO_3H \text{ unit}) + (\text{molar number of the } PEEK \text{ unit})} \quad [4.8]$$

$$IEC_{S-PEEK} = \frac{1000 \cdot DS}{288 + 102 \cdot DS} \quad [4.9]$$

The IEC^{theo} and the IEC determined by titration, IEC^{exp}, usually agree when all the protons are accessible to titration. This is the case for S-PEEK, for which IEC^{exp} was found to be 2.14 mmol/g when compared to an IEC^{theo} of 2.04 mmol/g, as listed in Table 4.3.

** Used as a small molecule analogue for S-PEEK

In principle, for blends of S-PEEK, IEC^{theo} can be determined from the S-PEEK mass fraction in the blend. However, in the present case, a weak diprotic acid, methylphosphonic acid[***] ($pKa_1 \sim 1.70$, $pKa_2 \sim 7.10$), is introduced as a second proton source. According to acid-base equilibria theory, the fraction of weak acid that dissociates to release charge carrying protons is dependant on the acid concentration. In the presence of the strong sulfonic acid of S-PEEK, a large fraction of the weak acid is calculated to be undissociated, although still titrateable. Thus, since titration registers all protons, dissociated and undissociated, this method overestimates the number of protons available for conductivity.

A more appropriate estimation of the free protonic carrier concentration in these films is the effective, IEC (IEC^{eff}), i.e., mmol of dissociated H^+ in water swollen films per gram of dry polymer. In order to calculate these values, the assumption is made that sulfonic acid of S-PEEK is fully dissociated. Thus, the proton concentration due to the dissociation of S-PEEK can be estimated according to Eq.4.10.

$$[H^+] = \frac{W_{dry} \cdot W\%_{S-PEEK} \cdot IEC^{exp}_{S-PEEK}}{V_{wet} \cdot 1000} \qquad [4.10]$$

where W_{dry} is the sample dry weight (mg), $W\%_{S\text{-}PEEK}$ is the weight percent S-PEEK in the sample, IEC^{exp}_{S-PEEK} is the ion exchange capacity of S-PEEK (mmol/g) determined by titration, and V_{wet} is the wet sample volume (mL). Contribution from water to the $[H^+]$ for the 0 wt% S-PEEK was determined using the autodissociation of water at neutral pH. The corresponding fraction of undissociated VPA and dissociated VPA, due to both the first and second dissociation, are approximated using Eq.4.11, 4.12, and 4.13.

[***] Used as a small molecule analogue for poly (vinylphosphonic acid)

Degree of undissociated VPA: $$\alpha_{H_2(VPA)} = \frac{[H^+]^2}{[H^+]^2 + [H^+]\cdot Ka_1 + Ka_1 \cdot Ka_2}$$ [4.11]

Degree of first dissociation.: $$\alpha_{H(VPA)^-} = \frac{Ka_1 \cdot [H^+]}{[H^+]^2 + [H^+]\cdot Ka_1 + Ka_1 \cdot Ka_2}$$ [4.12]

Degree of second dissociation: $$\alpha_{(VPA)^{2-}} = \frac{Ka_1 \cdot Ka_2}{[H^+]^2 + [H^+]\cdot Ka_1 + Ka_1 \cdot Ka_2}$$ [4.13]

Except for films which contain no S-PEEK (Sample S1), $\alpha_{(VPA)}{}^{2-}$ was calculated to be negligible ($<10^{-7}$). IEC^{eff} values for cured polyelectrolyte films were calculated according to Equation 4.16, using the contributions from S-PEEK and VPA, calculated using Equation 4.14 and 4.15, respectively, and are included in Table 4.3. For comparison, IEC^{exp} values, determined by titration, are also included.

$$IEC^{eff}_{S-PEEK} = \left(W\%_{S-PEEK} \cdot IEC^{exp}_{S-PEEK}\right)$$ [4.14]

$$IEC^{eff}_{VPA} = \alpha_{H(VPA)^-}\left(\frac{W\%_{VPA} \cdot 1000}{MW_{VPA}}\right)$$ [4.15]

$$IEC^{eff} = IEC^{eff}_{VPA} + IEC^{eff}_{S-PEEK}$$ [4.16]

where $W\%_{S\text{-}PEEK}$ and $W\%_{VPA}$ are the weight percent of S-PEEK and VPA respectively, and MW_{VPA} is the molecular weight of VPA (g/mol).

IEC^{eff} values are observed to be much lower than the corresponding values obtained by titration, confirming that titration is an inappropriate technique for evaluating systems that incorporatt weak acids.

Once IEC^{eff} is calculated, the total proton concentration, $[H^+]_{Total}$, taking into account all dissociated protons, can be calculated using Equation 4.17.

$$[H^+]_{Total} = \frac{\left(IEC^{eff} \cdot W_{dry} / V_{wet} \right)}{1000} \qquad [4.17]$$

where W_{dry} and V_{wet} are the dry weight (mg) and the wet volume (cm^3) of the sample, respectively.

4.4 Discussion

4.4.1 Series 1: Effect of Varying S-PEEK Content on Photocured Semi-IPN Membranes

Samples S1-5 were prepared to determine the effect of varying the strong acid component, S-PEEK. The upper limit for S-PEEK content is 31 wt% S-PEEK, which is the limit of S-PEEK solubility in the mixture of monomers at this particular IEC.

The mechanical properties of the films vary greatly across the series and depend on both the S-PEEK content and hydration level of the semi-IPN. When wet, films with low S-PEEK content are very brittle and break easily, whereas high S-PEEK content films are much more flexible and robust. When dry, membranes containing a high content of S-PEEK are slightly more flexible than those containing low content, although generally all dry membranes crack easily.

IEC, proton conductivity, and water content data are shown in Table 4.3. For purposes of comparison, values of IEC^{eff}, λ, and $[H^+]$ are listed in Table 4.3. The experimental value of $[H^+]$ for Sample S1 could not be calculated because it was too brittle and its volume could not be measured.

Table 4.3 Effect of S-PEEK content on properties of photocured film Samples S1-5.

Sample	SPEEK (wt%)	VPA (wt%)	$(IEC^{eff}_{S\text{-}PEEK})^a$ (mmol/g)	$(\alpha_{H(VPA)-})^b$	$(IEC^{eff}_{VPA})^c$ (mmol/g)	$(IEC^{eff})^d$ (mmol/g)	$(IEC^{exp})^e$ (mmol/g)	Water Content (wt%)	λ (mol H_2O/ mol acid site)	$[H^+]^f$ M	σ^g (S/cm)
S1	0	19	-----	0.56	0.98	0.98	1.14	54	37	-----	0.015
S2	4	17	0.09	0.34	0.54	0.63	1.94	46	34	0.30	0.015
S3	8	17	0.17	0.19	0.28	0.45	1.98	44	29	0.23	0.023
S4	17	15	0.34	0.13	0.18	0.52	2.31	66	35	0.21	0.040
S5	31	13	0.61	0.06	0.08	0.69	2.12	58	37	0.36	0.070
S-PEEK	100	0	2.04^{a*}	-----	-----	2.14	2.14	36	15	1.52	0.066

a Contribution of S-PEEK to IEC^{eff}, calculated using Eq. 4.14

a* IEC^{theo}, calculated using Eq. 4.9

b Using Eq. 4.12

c Contribution of VPA to IEC^{eff}, calculated using Eq. 4.15

d IEC^{eff}, calculated using Eq. 4.16

e Determined by titration

f Based on free proton concentration, calculated using Eq. 4.17

g "Wet" films measured at 25°C

As the S-PEEK content is increased (from 0 to 17 wt%), IEC^{eff} drops. Upon a further increase (from 17 to 31 wt%), IEC^{eff} increases. This trend is explained by considering the separate contributions of S-PEEK and VPA. The contribution to IEC^{eff} from S-PEEK, calculated based on the degree of sulfonation and S-PEEK content in the semi-IPN, increases linearly from 0.00 to 0.61 mmol/g with S-PEEK content (see Figure 4.11); whereas the contribution to IEC^{eff} from VPA decreases non-linearly from 0.98 to 0.08 mmol/g over the same S-PEEK content increase. Due to these opposing trends, there is a non-linear relationship between total IEC^{eff} and S-PEEK content.

In addition to there being no clear relationship between IEC^{exp} and IEC^{theo}, Figure 4.12 shows that there is no clear relationship between S-PEEK content and water content. Of note however, is that the water contents are significantly higher for the semi-IPN materials (44-58 wt% H_2O, λ = 29-37) than for the pure S-PEEK materials (36.2 wt% H_2O, λ = 15), due to their having a larger percentage of hydrophilic groups when compared to pure S-PEEK.

Figure 4.11 Contribution of S-PEEK and VPA to IEC^{eff} as a function of S-PEEK content, Samples S1-5.

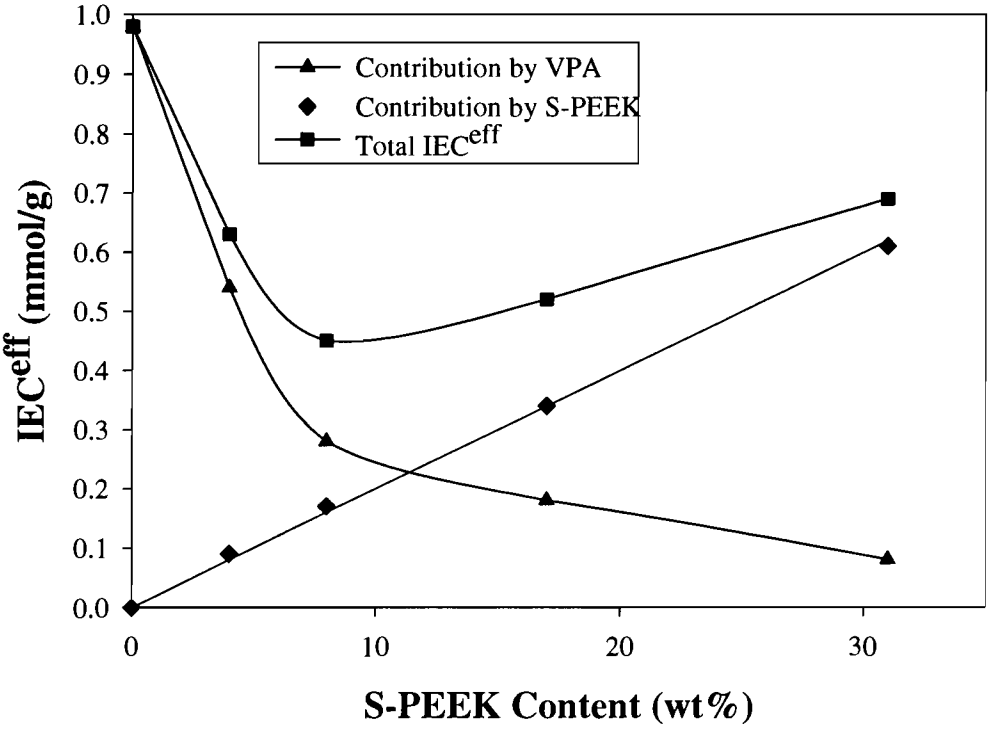

Figure 4.12 Effect of S-PEEK content on H_2O content and λ, Samples S1-5.

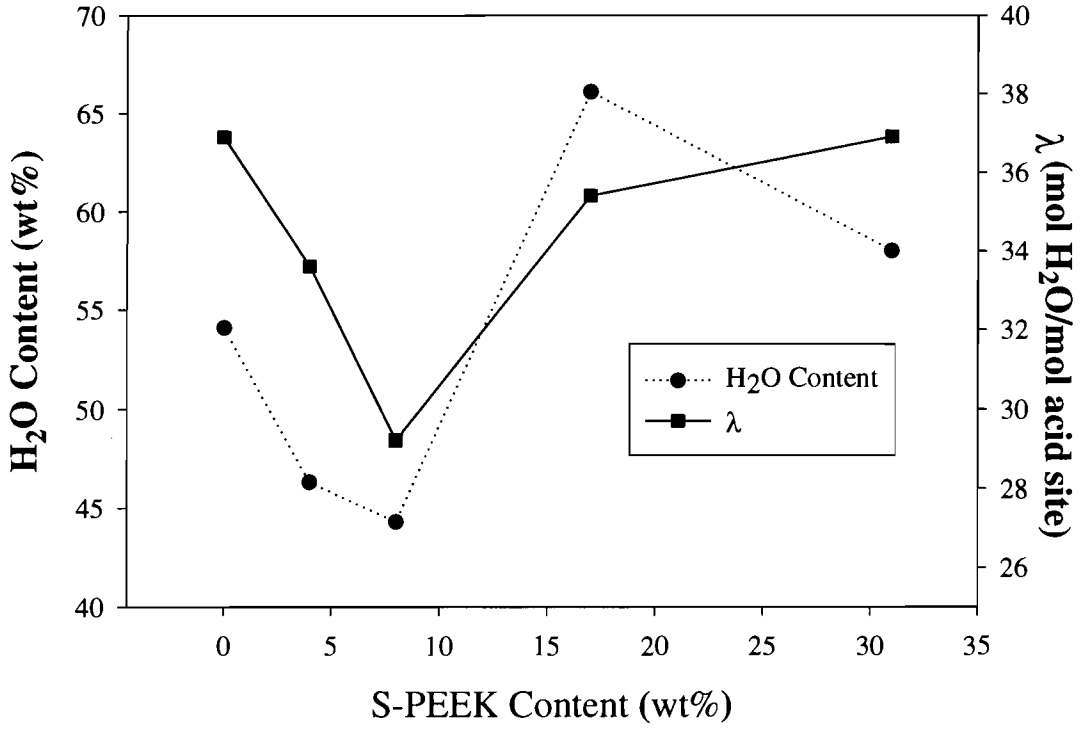

Even without S-PEEK present, the host polymer exhibits a measurable conductivity (0.015 S/cm) because of the presence of the secondary proton source, VPA. A minimum of at least 8 wt% S-PEEK is required for any further increase in conductivity, as shown in Figure 4.13. Above 8 wt%, conductivity increases linearly with S-PEEK content up to a value of 0.07 S/cm for the 31 wt% S-PEEK semi-IPN.

Figure 4.13 Effect of S-PEEK content on proton conductivity and H_2O content, Samples S1-5.

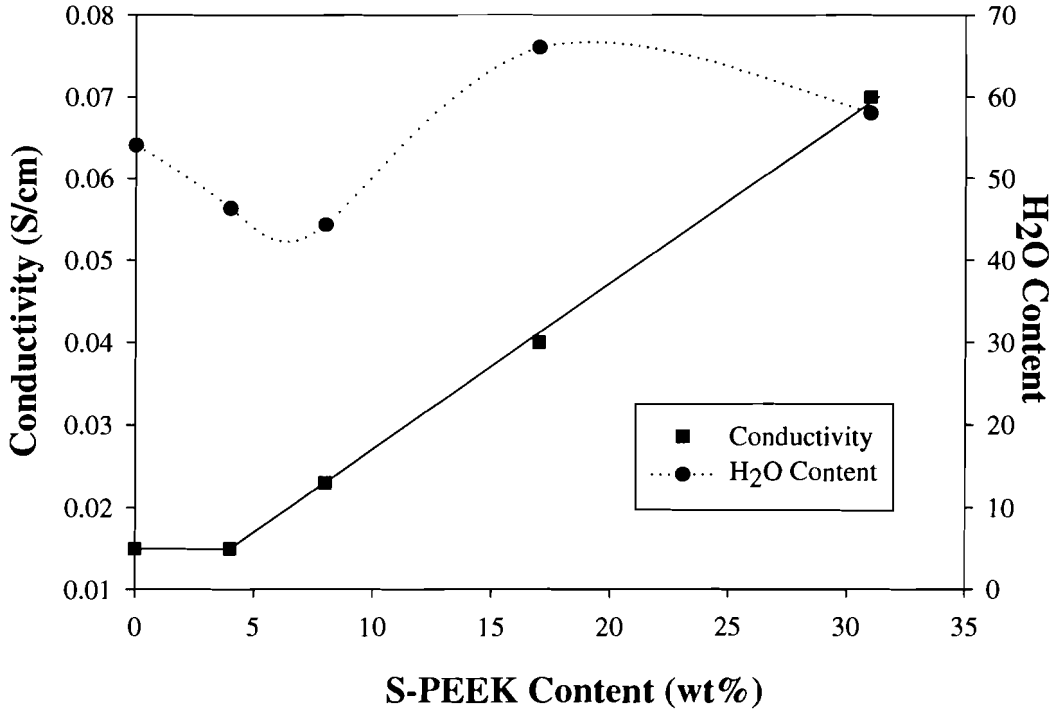

An interesting observation is that the proton conductivity of the 31 wt% S-PEEK semi-IPN is identical to the conductivity of the S-PEEK homopolymer, 0.07 S/cm, particularly since the $[H^+]$ within the samples is quite different, 0.36 M vs 1.52 M. Since the contribution of VPA to the free proton concentration is calculated to be negligible for this particular semi-IPN, 0.08 M, this observation is believed to be a direct result of the

higher λ value (37) and water content (58 wt%) in the semi-IPN film, compared to the pure S-PEEK (36.2 wt% H_2O, $\lambda = 15$).

4.4.2 Series 2: Effect of Cross-Linker Content on Photocured Semi-IPN Membranes

Semi-IPN films S6-S9, containing varying amounts of divinyl sulfone (DVS), were prepared in an effort to determine the effect of the cross linker content on the physical properties of the semi-IPN films. In order to maintain a similar ion content throughout the series, the acrylonitrile content was decreased proportionally, as the DVS content was increased. This provided a series of films possessing an S-PEEK content of 26 wt% and VPA content of 9 wt%. Results of IEC, proton conductivity, and water content measurements are shown in Table 4.4. For purposes of comparison, IEC^{eff}, λ, and $[H^+]$ have been calculated and are included in Table 4.4.

The mechanical properties of the photocured semi-IPNs are similar across this series for both wet and dry membranes. All membranes are fairly robust when hydrated, but are brittle when dry.

Table 4.4 Effect of cross linking/DVS content on photocured semi-IPN films.

	DVS[a] Content (wt%)	$(IEC^{eff}_{S\text{-}PEEK})^{b}$ (mmol/g)	$(\alpha_{H(VPA)\text{-}})^{c}$	$(IEC^{eff}_{VPA})^{d}$ (mmol/g)	$(IEC^{eff})^{e}$ (mmol/g)	$(IEC^{exp})^{f}$ (mmol/g)	Water Content (wt%)	λ (mol H_2O/ mol acid site)	$[H+]^{g}$ M	σ^{h} (S/cm)
S6	18	0.52	0.08	0.07	0.59	2.18	55	31	0.93	0.056
S7	25	0.52	0.07	0.06	0.58	1.99	49	27	1.00	0.048
S8	32	0.52	0.07	0.06	0.58	1.80	45	25	0.94	0.035
S9	41	0.52	0.06	0.05	0.56	1.47	35	20	0.94	0.025

a For full composition see Table 4.1

b Contribution of S-PEEK to IEC^{eff}, calculated using 4.14

c Using Eq. 4.12

d Contribution of VPA to IEC^{eff}, calculated using Eq. 4.15

e IEC^{eff}, calculated using Eq. 4.16

f Determined by titration

g Based on free proton concentration, calculated using Eq. 4.17

h "Wet" films measured at 25°C

Since the ion content is essentially the same across the series, the contribution to IEC^{eff} from S-PEEK and VPA, and hence overall IEC^{eff} total, is approximately the same for all semi-IPN membranes. Given this, it might be expected that IEC^{exp}, measured by titration, should be constant. However, as the DVS content is increased from 18 to 41 wt%, IEC^{exp} decreases from 2.18 to 1.47 mmol/g. The water content also decreases from 54.9 to 34.8 wt% as a result of increasing the DVS content, Figure 4.14. This decreased water content is perceived due to a more cross-linked compact structure, which has less pore volume to incorporate additional water molecules, and may render a fraction of the acidic sites inaccessible to titration. As a direct result of this more compact structure, the semi-IPN conductivity decreases from 0.06 to 0.03 S/cm as DVS content increases, also shown in Figure 4.14.

Figure 4.14 Effect of DVS content on proton conductivity and λ, Samples S6-9.

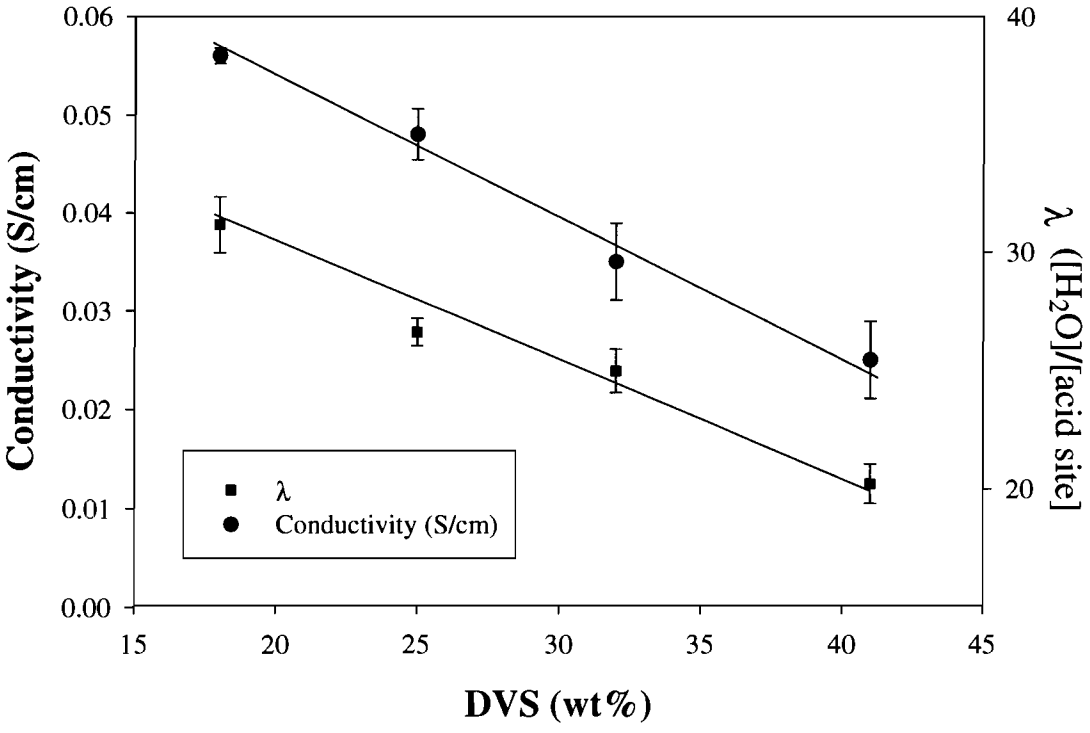

4.4.3 Conformability

Thin films of each composition, listed in Table 4.1, were readily photocured into solid materials by irradiation with 450 nm light. To illustrate that the polyelectrolyte solutions can be photocured into unique shapes, a sample was cured in a V-shaped mould (see Figure 4.15a) that was constructed from soft rubber. The liquid was poured into the mould, the excess overflow was removed with a casting knife, and the polyelectrolyte was cured in the UV chamber at 450 nm for 1 hour. A photograph of the cross section of the cured electrolyte in the mould is shown in Figure 4.15b. Although the electrolyte fills the gap entirely, there is noticeable shrinkage upon curing, as can be seen by the concavity on top of the sample. Little change in shape and/or concavity is observed after soaking the sample in water for several days.

To illustrate that the polyelectrolyte can be spatially cured, a sample was spread (~ 70 μm thickness) onto a glass slide, which had been rendered opaque by spray painting black on one side, and the copper mask, shown in Figure 4.15c, was placed overtop. The slide was then cured for 15 minutes, and the uncured monomers were washed away with methanol. The resulting imaged film is shown in Figure 4.15d.

Figure 4.15 **(a) Schematic of the rubber mould, (b) photograph of cross section of cured electrolyte in the mould, (c) copper mask, and (d) photolithographically cured film.**

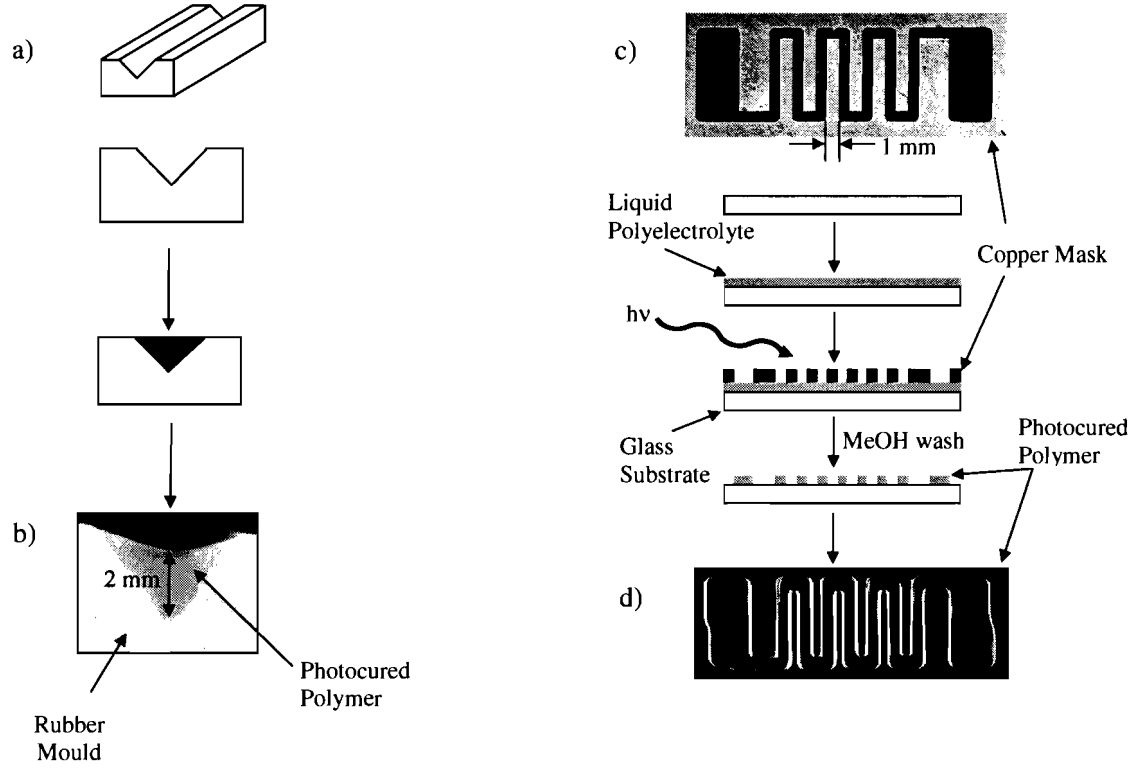

4.5 Conclusions

A series of novel photocurable liquid conformable polymer electrolytes have been prepared. The liquid polyelectrolytes are transformed into solid semi-IPN films by spreading the liquid onto glass substrates and UV-curing. Physicochemical properties of the films have been studied as a means to understand the role of composition on fuel cell pertinent properties.

Mechanical properties of these materials are directly related to the composition of the host polymer and the weight percent S-PEEK ionomer present. In general, materials containing low amounts of S-PEEK tend to be brittle and difficult to work with, whereas materials with high quantities of S-PEEK are more flexible and robust.

Although properties such as water content, λ, $[H^+]$, and IEC are not linearly related to S-PEEK content, conductivity is improved as S-PEEK content is increased. Conductivity values similar to that of pure S-PEEK and Nafion 117, 0.07 S/cm, have been achieved for a cured semi-IPN that contains as little as 31 wt% S-PEEK and 10 wt% VPA monomers. Increasing the cross-linker content results in decreased water content coupled with a lower conductivity. This is thought to be due to the more compact microstructure that results from increasing the degree of crosslinking in the network polymer host. Finally, the ability of these materials to be cured spatially and into unique shapes has made them promising candidates for novel fuel cell applications.

Chapter 5: Summary and Future Work

This research has shown that proton transport properties of proton exchange membranes are strongly linked to polymer structure, ion content, water content, and chemical composition. For this work, two distinct groups of proton exchange polymer systems were chosen, each group comprising several membrane series. Correlations between the series were drawn and compared to Nafion, a perfluorosulfonic acid polymer, and also the fuel cell industry benchmark.

Group One Main chain statistically sulfonated polymers:

a) sulfonated poly(ether ether ketone), **S-PEEK**

b) radiation-grafted ethylenetetrafluoroethylene-grafted-poly(styrene sulfonic) acid, **ETFE-*g*-PSSA**

c) sulfonated α, β, β-trifluorostyrene-co-substituted α, β, β-trifluorostyrene, **BAM**

d) sulfonated polystyrene-*b*-poly(ethylene-*r*-butylene)-*b*-polystyrene triblock copolymer **S-SEBS**

These materials were chosen because each series provided a minimum of 3 independent membranes that varied by IEC, yet had a common polymer backbone. Using these series, a method was developed, and employed, that enabled a systematic analysis of the effect of polymer structure on proton transport.

In this work, proton conductivities and water contents for each membrane were measured and the data combined to describe the effective proton mobility of the polymer systems. Proton conductivities were measured using AC impedance spectroscopy and water contents measured gravimetrically. Two methods were used to effectively control

the water content within the membranes during the investigation: 1) Indirect control of water content by altering the IEC of fully hydrated membranes 2) Direct control of water content by varying the RH of the environment surrounding the membrane.

In the first investigation, it was shown that IEC has a significant impact on the amount of water absorbed, and hence the proton conductivity of these systems. The typical increase in conductivity with an increase in IEC was observed in two of the four series studied, ETFE-*g*-PSSA and S-PEEK. However, while the conductivity in the BAM series initially increased, it reached a maximum at ~ 2.0 mmol/g, and subsequently decreased in the high IEC range. The conductivity of S-SEBS, on the other hand, was shown to be essentially independent of IEC, exhibiting only a minimal increase with IEC over the range studied. When the effect of IEC on water content was investigated, it was found that water uptake in these systems occurs at an disproportionate rate to IEC, resulting in a decreased proton concentration at high IEC.

In general, it was found that within each polymer system, maximum mobility was achieved for materials with high sulfonic acid content. However, high mobility comes at a cost of high water content, and decreased proton concentration. It appears that a balance between proton concentration and mobility is key to good overall conductivity, i.e., water content must be high enough to ensure good mobility of protons, yet not too high that the acid sites become diluted. Once the protons become significantly dilute, incorporation of additional water no longer serves to improve proton transport and a maximum value of mobility is reached. The results of this work suggest that membranes with good phase separation, close proximity of acid groups, and high acidity will exhibit higher maximum mobility values. In light of this information, it is proposed that further

increasing the IEC of BAM and S-SEBS will have little impact on proton mobility, and will likely have a negative impact on measured proton conductivity values. However, it appears possible to improve the proton transport properties of S-PEEK and ETFE-*g*-PSSA if membranes of higher IECs could be synthesized.

The second investigation was performed to explore the humidity dependant proton transport properties of the BAM materials. Measurements were made on membrane samples in equilibration with water vapours of known relative humidities between 50 – 98% RH. Proton conductivity was determined using AC impedance spectroscopy and water contents were measured using gravimetric dynamic vapour sorption analysis. In general, it was found that the proton transport properties of the BAM materials are highly susceptible to changes in relative humidity. Under conditions of high RH, BAM membranes are able to maintain reasonable proton transport properties yet for lower RH conditions their properties are very poor. Nafion exhibits a more modest variation in proton transport properties across the humidity range studied. Having a relatively consistent conductivity, even if not overly high, can be a desirable property of a PEM that is intended to operate in variable humidity environments. It is evident from these results that BAM would not be a good candidate for fuel cells operating under high temperature/low humidity conditions.

If one membrane in the BAM series had to be chosen for use in fuel cells, based on proton transport properties alone, it would be the intermediate IEC BAM 1.96 mmol/g. This membrane exhibits the highest proton conductivity under fully hydrated conditions, as it maintains the best balance between good proton mobility and sufficient proton concentration. Furthermore, BAM 1.96 exhibits the least susceptibility to changes

in RH conditions, and perhaps the best of the series to withstand small changes in relative humidity during fuel cell operation.

As polymer structure and morphology appear to be key to understanding proton transport properties of membrane systems, more work is needed to investigate the morphology of these membranes, specifically at various levels of hydration.

Group 2 – Photocured semi-interpenetrating network polymers

The third investigation showed that S-PEEK could be dissolved in a mixture of liquid monomers, to form polyelectrolyte solutions, and subsequently photo-cured into cross-linked matrices to prepare proton conducting semi-interpenetrating network films. Monomers were chosen based on their ability to solvate S-PEEK, and enhance physical properties of the photocured materials. These were acrylonitrile, vinylphosphonic acid, and divinyl sulfone. The effect of chemical composition was investigated by studying materials from two series that were prepared by systematically varying the composition of the S-PEEK and cross-linked matrix components while keeping the relative composition of all other components fixed:

a) Variable S-PEEK content
b) Variable divinyl sulfone content

Conductivity and mechanical properties of these materials are related to the chemical composition of the films. Higher S-PEEK content resulted in relatively flexible materials that exhibited good proton conductivity. However the materials exhibited very high water contents. The addition of divinyl sulfone reduced the amount of water absorbed, unfortunately at a cost of lower proton conductivity.

It was shown that the incorporation of vinyl phosphonic acid enhances the proton conductivity of these films as proton conductivities in the range of 0.07 S/cm were obtained for films that contained only ~31 wt% S-PEEK. Although the proton conducting, and mechanical properties of these materials appears sufficient, they have a significant disadvantage in that they absorb a lot of water and swell significantly. Future work with these materials should involve mechanical reinforcement, such as incorporation into fibreglass substrates.

Appendix: Sample Data

The following is sample data for the calculations that were performed in this work.

Water Content Analysis (fully hydrated samples)

$$Volume = \frac{1}{4}\pi d^2 h$$

$$Water\ Uptake\ (wt\%) = \frac{W_{wet} - W_{dry}}{W_{dry}}$$

$$Water\ Content\ (wt\%) = \frac{W_{wet} - W_{dry}}{W_{wet}}$$

$$Water\ Content\ (vol\%) = Xv = \frac{V_{water}}{V_{wet}}$$

$$\lambda = \frac{moles\ H_2O}{moles\ \text{Acid}} = \left(\frac{Water\ Uptake}{18g/mol}\right)\left(\frac{1000}{IEC}\right)$$

$$[-SO_3H] = \frac{\text{moles of } -SO_3H}{V_{wet}}$$

Table A 1 Sample data for fully hydrated water contnet analysis of S-PEEK with IEC = 2.14 mmol/g

Sample	Wet weight (mg) W_{wet}	Dry weight (mg) W_{dry}	Sample wet diameter (cm) d	Sample thickness wet (cm) h	Wet membrane volume (mL) V_{wet}
S-PEEK 2.14 #1	5.7	3.5	1.24	0.0042	0.0049
S-PEEK 2.14 #2	7.1	4.5	1.23	0.0055	0.0065
S-PEEK 2.14 #3	7.8	5.2	1.23	0.0061	0.0072

Sample	Water Content wt%	Water Uptake wt%	Water Content vol% X_v	[-SO_3H] (M)	λ (mol H_2O/SO_3H)
S-PEEK 2.14 #1	0.39	0.63	0.45	1.53	16.3
S-PEEK 2.14 #2	0.37	0.58	0.40	1.51	14.7
S-PEEK 2.14 #3	0.33	0.50	0.36	1.52	13.2
average	0.36	0.57	0.40	1.52	14.7
stdev	0.03	0.06	0.04	0.01	1.6

Water Content Analysis (partially hydrated samples)

Table A 2 Dry Nafion and BAM membrane densities (ρ_{dry})

Membrane	IEC (mmol/g)	Dry Density (g/cm)
Nafion	0.97	2.04 ± 0.03
BAM 1.36	1.36	1.46 ± 0.08
BAM 1.86	1.86	1.63 ± 0.09
BAM 1.96	1.96	1.53 ± 0.07
BAM 2.20	2.20	1.76 ± 0.07
BAM 2.46	2.46	1.76 ± 0.18

$$V_{hyd} = V_{dry} + V_{water}$$

$$V_{water} = \frac{W_{hyd} - W_{dry}}{\rho_{water}}$$

$$X_v = \frac{V_{water}}{V_{hyd}} = \frac{W_{hyd}}{W_{hyd} + \frac{W_{dry}}{\rho_{dry}}}$$

$$[-SO_3H] = \frac{\text{moles of } -SO_3H}{V_{hyd}} = \frac{IEC * W_{dry}}{V_{water} + \frac{W_{dry}}{\rho_{dry}}}$$

$$\lambda = \frac{moles\ H_2O}{moles\ \text{Acid}} = \left(\frac{Water\ Uptake}{18g/mol}\right)\left(\frac{1000}{IEC}\right) = \frac{\left(\frac{W_{hyd} - W_{dry}}{W_{dry}}\right)}{18g/mol} * \left(\frac{1000}{IEC}\right)$$

Table A 3 **Sample data for relative humidity dependent water content analysis of Nafion with a dry mass (W_{dry}) of 13.5264 mg**

Relative Humidity	Wet weight W_{hyd}	H_2O weight (mg)	H_2O volume V_{water} (μL)	X_v	[-SO_3H] (M)	λ (mol H_2O/SO_3H)
80	15.1884	1.6620	1.6620	0.2004	1.4843	7.5
85	15.4194	1.8930	1.8930	0.2221	1.4441	8.5
90	15.7559	2.2295	2.2295	0.2516	1.3893	10.0

Ion Exchange Capacity

Direct Titration

$$IEC^{\exp} = \frac{(vol.\,\mathrm{NaOH}, mL) \times (conc.\,\mathrm{NaOH}, M)}{(W_{dry})}$$

Table A 4 Sample data for determining IEC by titration for semi-IPN sample S1

Sample	Volume NaOH (mL) *vol.NaOH*	Dry weight (mg) W_{dry}	IEC^{exp} (mmol/g)
S1 #1	5.59	5.8	2.23
S1 #2	5.11	5.1	2.31
S1 #3	5.70	5.5	2.39
average			2.31
std dev			0.08

Calculated "effective IEC"

Table A 5 Physical constants for vinyl phosphonic acid (VPA)

pKa_1 (VPA)	1.7	Ka_1	2.0×10^{-2}
pKa_2 (VPA)	7.1	Ka_2	7.9×10^{-8}
MW (VPA)	108.03 g/mol		

The proton concentration due to the dissociation of S-PEEK in a composite made with S-PEEK of IEC = 2.14 mmol/g:

$$[H^+] = \frac{W_{dry} \cdot W\%_{S-PEEK} \cdot IEC^{exp}_{S-PEEK}}{V_{wet} \cdot 1000}$$

Degree of undissociated VPA:

$$\alpha_{H_2(VPA)} = \frac{[H^+]^2}{[H^+]^2 + [H^+] \cdot Ka_1 + Ka_1 \cdot Ka_2}$$

Degree of first dissociation:

$$\alpha_{H(VPA)^-} = \frac{Ka_1 \cdot [H^+]}{[H^+]^2 + [H^+] \cdot Ka_1 + Ka_1 \cdot Ka_2}$$

Degree of second dissociation:

$$\alpha_{(VPA)^{2-}} = \frac{Ka_1 \cdot Ka_2}{[H^+]^2 + [H^+] \cdot Ka_1 + Ka_1 \cdot Ka_2}$$

Contribution of S-PEEK to calculated IEC:

$$IEC^{eff}_{S-PEEK} = \left(W\%_{S-PEEK} \cdot IEC^{exp}_{S-PEEK}\right)$$

Contribution of VPA to calculated IEC:

$$IEC^{eff}_{VPA} = \alpha_{H(VPA)^-} \left(\frac{W\%_{VPA}}{MW_{VPA} \cdot 1000} \right)$$

Total calculated IEC:

$$IEC^{eff} = IEC^{eff}_{VPA} + IEC^{eff}_{S-PEEK}$$

Total proton concentration taking both S-PEEK and VPA into account considering incomplete dissociation of VPA

$$[H^+]_{Total} = \frac{\left(IEC^{eff} \cdot W_{dry} / V_{wet} \right)}{1000}$$

Table A 6 Sample data for the calculation of effective IEC, measured quantities

Sample	S-PEEK content (wt%) $W\%_{S\text{-}PEEK}$	VPA content (wt%) $W\%_{VPA}$	Dry weight (mg) W_{dry}	Wet sample length (cm)	Wet sample width (cm)	Wet sample thickness (cm)	Wet sample volume (cm^3) V_{wet}
S1 #1	16.6	15.2	5.8	1.23	1.23	0.0120	0.0143
S1 #2	16.6	15.2	5.1	1.23	1.23	0.0111	0.0131
S1 #3	16.6	15.2	5.5	1.23	1.23	0.0117	0.0139

Sample	$[H^+]$ (M)	$\alpha_{H_2(VPA)}$	$\alpha_{H(VPA)^-}$	$\alpha_{(VPA)^{-2}}$	IEC^{eff}_{S-PEEK} (mmol/g)	IEC^{eff}_{VPA} (mmol/g)	IEC^{eff} (mmol/g)	$[H^+]_{total}$ (M)
S1 #1	0.145	0.879	0.121	~0	0.344	0.171	0.515	0.209
S1 #2	0.138	0.874	0.126	~0	0.345	0.178	0.522	0.200
S1 #3	0.141	0.876	0.124	~0	0.344	0.175	0.519	0.203
average	0.141	0.876	0.124	---	0.344	0.175	0.519	0.204
std dev	0.003	0.002	0.002	---	0.0003	0.003	0.004	0.005

Proton Conductivity

Solartron Probe (Chapter 2, 3)

Sample data for BAM 2.20. L = 1.0 cm.

$$\sigma_{H^+} = \frac{L}{R_m A} = \frac{1.0cm}{R_m * W * h}$$

Table A 7 Sample data for the calculation of the proton conductivity of BAM 2.20 mmol/g using the Pt/Teflon probe connected to the Solartron frequency response analyzer

Sample	Membrane Thickness (cm) h	Membrane Width (cm) W	Membrane Resistance (Ω) R_m	σ_{H+} (S/cm)
BAM 2.20 #1	0.0079	0.92	1370	0.098
BAM 2.20 #2	0.0078	0.97	1216	0.106
BAM 2.20 #3	0.0078	0.93	1376	0.098
average				0.100
std dev				0.005

Coaxial Probe (Chapter 4)

Sample data for Semi-IPN sample S1. X = 3.22 mm, Y = 1.09 mm

$$\sigma_{H^+} = \frac{1}{2\pi R_m h} \ln\left(\frac{X}{Y}\right)$$

Table A 8 **Sample data for the calculation of proton conductivity of Semi-IPN sample S1 using the gold plated coaxial probe connected to the HP network analyzer**

Sample	Membrane Thickness (cm) h	Membrane Resistance (Ω) R_m	σ_{H+} (S/cm)
S1 #1	0.012	368.5	0.039
S1 #2	0.011	395.1	0.039
S1 #3	0.012	364.0	0.040
average			0.040
std dev			0.0008

Proton Mobility

Sample data for fully hydrated ETFE-*g*-PSSA samples.

$$\mu_{H^+} = \frac{\sigma_{H^+}}{[-SO_3H]F}$$

Table A 9 **Sample data for the calculation of proton mobility of the ETFE-*g*-PSSA membranes series**

Sample	$[-SO_3H]$ (M)	σ_{H+} (S/cm)	$\mu_{H+}*10^3$ ($cm^2s^{-1}V^{-1}$)
ETFE-*g*-PSSA 3540	1.78	0.150	0.85
ETFE-*g*-PSSA 2690	1.46	0.170	1.19
ETFE-*g*-PSSA 3551	1.28	0.200	1.59

References

1. Appleby, J.; Foulkes, R. L. *Fuel Cell Handbook*; Van Norstrand: NY 1989.
2. Roudgar, A.; Narasimachary, S. P.; Eikerling, M. *Journal of Physical Chemistry B* **2006**, *110*, 20469.
3. Yu, J. R.; Yi, B. L.; Xing, D. M.; Liu, F. Q.; Shao, Z. G.; Fu, Y. Z. *Physical Chemistry Chemical Physics* **2003**, *5*, 611.
4. Buchi, F. N.; Gupta, B.; Haas, O.; Scherer, G. *Electrochimica Acta* **1995**, *40*, 345.
5. Guo, Q. H.; Pintauro, P. N.; Tang, H.; O'Connor, S. *Journal of Membrane Science* **1999**, *154*, 175.
6. Savadogo, O.; Varela, F. J. R. *Journal of New Materials for Electrochemical Systems* **2001**, *4*, 93.
7. Mauritz, K. A.; Moore, R. B. *Chemical Reviews* **2004**, *104*, 4535.
8. Hickner, M. A.; Ghassemi, H.; Kim, Y. S.; Einsla, B. R.; McGrath, J. E. *Chemical Reviews* **2004**, *104*, 4587.
9. Ghielmi, A.; Vaccarono, P.; Troglia, C.; Arella, V. *Annals of the New York Academy of Sciences* **2003**, *984*, 226.
10. Rivard, L. M.; Pierpont, P.; Freemeye, H. T.; Thaler, A.; Hamrock, S. J., Development of a new electrolyte membrane for PEM fuel cells, Fuel Cell Seminar, Miami Beach, FL, 2003.,
11. Kreuer, K. D. *Journal of Membrane Science* **2001**, *185*, 29.
12. Eisenberg, A. *Macromolecules* **1970**, *3*, 147.
13. Gierke, T. D.; Hsu, W. Y. In *Perfluorinated Ionomer Membranes: The Cluster-Network Model of Ion Clustering in Perfluorosulfonated Membranes;* ACS Symposium Series 180; Eisenberg, A., Yeager, H. L., Eds.; American Chemical Society: Washington DC, 1982, p 283-310.
14. Yeager, H. L. In *Perfluorinated Ionomer Membranes: Cation Exchange Selectivity of a Perfluorsulfonate Polymer;* ACS Symposium Series 180; Eisenberg, A., Yeager, H. L., Eds.; American Chemical Society: Washington DC, 1982, p 25-40.
15. Gebel, G. *Polymer* **2000**, *41*, 5829.
16. Gebel, G.; Moore, R. B. *Macromolecules* **2000**, *33*, 4850.
17. Rollet, A. L.; Diat, O.; Gebel, G. *Journal of Physical Chemistry B* **2004**, *108*, 1130.

18. Rubatat, L.; Gebel, G.; Diat, O. *Macromolecules* **2004**, *37*, 7772.

19. Hickner, M. A.; Fujimoto, C. H.; Cornelius, C. J. *Polymer* **2006**, *47*, 4238.

20. Huang, H. S.; Chen, C. Y.; Lo, S. C.; Lin, C. J.; Chen, S. J.; Lin, L. J. *Applied Surface Science* **2006**, *253*, 2685.

21. Ramdutt, D.; Charles, C.; Hudspeth, J.; Ladewig, B.; Gengenbach, T.; Boswell, R.; Dicks, A.; Brault, P. *Journal of Power Sources* **2007**, *165*, 41.

22. James, P. J.; Elliott, J. A.; McMaster, T. J.; Newton, J. M.; Elliott, A. M. S.; Hanna, S.; Miles, M. J. *Journal of Materials Science* **2000**, *35*, 5111.

23. Savadogo, O. *Journal of Power Sources* **2004**, *127*, 135.

24. Rikukawa, M.; Sanui, K. *Progress in Polymer Science* **2000**, *25*, 1463.

25. Savadogo, O. *Journal of New Materials for Electrochemical Systems* **1998**, *1*, 47.

26. Steck, A. E., New Materials for Fuel Cell Systems I, Proceedings of the International Symposium on New Materials for Fuel Cell Systems, 1st, Montreal, July 9-13, **1995**

27. Wei, J., Stone, C., Steck, A.E.; Ballard Power Systems Inc.: US Patent Number 5,422,411, 1995.

28. Prober, M. *Journal of the American Chemical Society* **1952**, *75*, 968.

29. Gebel, G.; Diat, O. *Fuel Cells* **2005**, *5*, 261.

30. Steck, A. E.; Stone, C., New Materials for Fuel Cell and Modern Battery Systems II, Proceedings of the International Symposium on New Materials for Fuel Cell and Modern Battery Systems, 2nd, Montreal, July 6-10, **1997**

31. Beattie, P. D.; Orfino, F. P.; Basura, V. I.; Zychowska, K.; Ding, J.; Chuy, C.; Schmeisser, J.; Holdcroft, S. *Journal of Electroanalytical Chemistry* **2001**, *503*, 45.

32. Gebel, G.; Diat, O.; Stone, C. *Journal of New Materials for Electrochemical Systems* **2003**, *6*, 17.

33. Rouilly, M. V.; Koetz, E. R.; Haas, O.; Scherer, G. G.; Chapiro, A. *Journal of Membrane Science* **1993**, *81*, 89.

34. Buchi, F. N.; Gupta, B.; Haas, O.; Scherer, G. G. *Journal of the Electrochemical Society* **1995**, *142*, 3044.

35. Shen, M.; Roy, S.; Kuhlmann, J. W.; Scott, K.; Lovell, K.; Horsfall, J. A. *Journal of Membrane Science* **2005**, *251*, 121.

36. Horsfall, J.; Lovell, K. *Fuel Cells* **2001**, *1*, 186.

37. Horsfall, J. A.; Lovell, K. V. *Polymers for Advanced Technologies* **2002**, *13*, 381.

38. Jokela, K.; Serimaa, R.; Torkkeli, M.; Elomaa, M.; Sundholm, F.; Walsby, N.; Kallio, T.; Sundholm, G. *Journal of Applied Crystallography* **2000**, *33*, 723.

39. Kreuer, K. D. *Manuscript* **2001**.

40. Zaidi, S. M. J.; Mikhailenko, S. D.; Robertson, G. P.; Guiver, M. D.; Kaliaguine, S. *Journal of Membrane Science* **2000**, *173*, 17.

41. Inzelt, G.; Pineri, M.; Schultze, J. W.; Vorotyntsev, M. A. *Electrochimica Acta* **2000**, *45*, 2403.

42. Storey, R. F.; Baugh, D. W. *Polymer* **2000**, *41*, 3205.

43. Edmondson, C. A.; Fontanella, J. J.; Chung, S. H.; Greenbaum, S. G.; Wnek, G. E. *Electrochimica Acta* **2001**, *46*, 1623.

44. Brandon, N. P.; Skinner, S.; Steele, B. C. H. *Annual Review of Materials Research* **2003**, *33*, 183.

45. Slade, S.; Campbell, S. A.; Ralph, T. R.; Walsh, F. C. *Journal of the Electrochemical Society* **2002**, *149*, A1556.

46. Hsu, W. Y.; Barkley, J. R.; Meakin, P. *Macromolecules* **1980**, *13*, 198.

47. Hsu, W. Y.; Berzins, T. *Journal of Polymer Science, Polymer Physics Edition* **1985**, *23*, 933.

48. Wodzki, R.; Narebska, A.; Nioch, W. K. *Journal of Applied Polymer Science* **1985**, *30*, 769.

49. Edmondson, C. A.; Fontanella, J. J. *Solid State Ionics* **2002**, *152*, 355.

50. Pivovar, B. S. *Polymer* **2006**, *47*, 4194.

51. Agmon, N. *Chemical Physics Letters* **1995**, *244*, 456.

52. Martyna, G. J.; Tuckerman, M. E. *Journal of Chemical Physics* **1995**, *102*, 8071.

53. Tuckerman, M. E.; Marx, D.; Klein, M. L.; Parrinello, M. *Science* **1997**, *275*, 817.

54. Kreuer, K. D. *Solid State Ionics* **2000**, *136-137*, 149.

55. Marx, D.; Tuckerman, M. E.; Hutter, J.; Parrinello, M. *Nature* **1999**, *397*, 601.

56. Paddison, S. J.; Pratt, L. R.; Zawodzinski, T. A. *Journal of Physical Chemistry A* **2001**, *105*, 6266.

57. Eikerling, M.; Paddison, S. J.; Zawodzinski, T. A., Jr. *Journal of New Materials for Electrochemical Systems* **2002**, *5*, 15.

58. Eikerling, M.; Kornyshev, A. A. *Journal of Electroanalytical Chemistry* **2001**, *502*, 1.

59. Choi, P.; Jalani, N. H.; Thampan, T. M.; Datta, R. *Journal of Polymer Science Part B-Polymer Physics* **2006**, *44*, 2183.

60. Paddison, S. J.; Paul, R. *Physical Chemistry Chemical Physics* **2002**, *4*, 1158.

61. Zawodzinski, T. A. J.; Springer, T. E.; Uribe, F.; Gottesfeld, S. *Solid State Ionics* **1993**, *60*, 199.

62. Elliott, J. A.; Paddison, S. J. *Physical Chemistry Chemical Physics* **2007**, *9*, 2602.

63. Kreuer, K. D.; Paddison, S. J.; Spohr, E.; Schuster, M. *Chemical Reviews (Washington, DC, United States)* **2004**, *104*, 4637.

64. Peckham, T.; Schmeisser, J.; Rodgers, M.; Holdcroft, S. *Journal of Materials Chemistry* **2007**, *17*, 3255.

65. Schmeisser, J.; Holdcroft, S.; Yu, J.; Ngo, T.; McLean, G. *Chemistry of Materials* **2005**, *17*, 387.

66. Paddison, S. J. *Annual Review of Materials Research* **2003**, *33*, 289.

67. Hickner, M. A.; Wang, F.; Kim, Y. S.; Privovar, B.; Zawodzinski, T. A.; McGrath, J. E. *Abstracts of Papers of the American Chemical Society* **2001**, *222*, U467.

68. Rieger, P. H. *Electrochemistry*; Prentice-Hall: Englewood Cliffs, N.J, 1987.

69. Bozkurt, A.; Ise, M.; Kreuer, K. D.; Meyer, W. H.; Wegner, G. *Solid State Ionics* **1999**, *125*, 225.

70. Eikerling, M.; Kornyshev, A. A.; Kuznetsov, A. M.; Ulstrup, J.; Walbran, S. *Journal of Physical Chemistry B* **2001**, *105*, 3646.

71. Sumner, J. J.; Creager, S. E.; Ma, J. J. A.; DesMarteau, D. D. *Journal of the Electrochemical Society* **1998**, *145*, 107.

72. Huang, R. Y. M.; Shao, P.; Burns, C. M.; Feng, X. *Journal of Applied Polymer Science* **2001**, *82*, 2651.

73. Uosaki, K.; Okazaki, K.; Kita, H. *Journal of Electroanalytical Chemistry and Interfacial Electrochemistry* **1990**, *287*, 163.

74. Xue, S. N.; Yin, G. P. *Polymer* **2006**, *47*, 5044.

75. Doyle, M.; Lewittes, M. E.; Roelofs, M. G.; Perusich, S. A. *Journal of Physical Chemistry B* **2001**, *105*, 9387.

76. Petersen, M. K.; Voth, G. A. *Journal of Physical Chemistry B* **2006**, *110*, 18594.

77. Choi, P. H.; Datta, R. *Journal of the Electrochemical Society* **2003**, *150*, E601.

78. Choi, P.; Jalani, N. H.; Datta, R. *Journal of the Electrochemical Society* **2005**, *152*, A1548.

79. Mackin, L.; Sartnurak, S.; Thomas, I.; Moore, S. *International Journal of Pharmaceutics* **2002**, *231*, 213.

80. Maskavs, M.; Kalnins, M.; Laka, M.; Chernyavskaya, S. *Mechanics of Composite Materials* **2001**, *37*, 159.

81. Kim, S. J.; Park, S. J.; Chung, T. D.; An, K. H.; Kim, S. I. *Journal of Applied Polymer Science* **2003**, *89*, 2041.

82. Burnett, D. J.; Garcia, A. R.; Thielmann, F. *Journal of Power Sources* **2006**, *160*, 426.

83. Nyquvist, H. *International Journal of Pharmacy, Technology and Products Manufacturing* **1983**, *4*, 47.

84. Zawodzinski, T. A., Jr.; Derouin, C.; Radzinski, S.; Sherman, R. J.; Smith, V. T.; Springer, T. E.; Gottesfeld, S. *Journal of the Electrochemical Society* **1993**, *140*, 1041.

85. Morris, D. R.; Sun, X. *Journal of Applied Polymer Science* **1993**, *50*, 1445.

86. Pushpa, K. K.; Nandan, D.; Iyer, R. M. *Journal of the Chemical Society, Faraday Transactions 1: Physical Chemistry in Condensed Phases* **1988**, *84*, 2047.

87. Steininger, H.; Schuster, M.; Kreuer, K. D.; Kaltbeitzel, A.; Bingol, B.; Meyer, W. H.; Schauff, S.; Brunklaus, G.; Maier, J.; Spiess, H. W. *Physical Chemistry Chemical Physics* **2007**, *9*, 1764.

88. Bunce, M.; Sondheimer, S.; Fyfe, C. *Macromolecules* **1986**, *19*, 333.

89. Prater, K. *Journal of Power Sources* **1990**, *29*, 239.

90. Srinivasan, S. *Journal of the Electrochemical Society* **1989**, *136*, C41.

91. Wang, F.; Hickner, M.; Ji, Q.; Harrison, W.; Mecham, J.; Zawodzinski, T. A.; McGrath, J. E. *Macromolecular Symposia* **2001**, *175*, 387.

92. Wang, F.; Hickner, M.; Kim, Y. S.; Zawodzinski, T. A.; McGrath, J. E. *Journal of Membrane Science* **2002**, *197*, 231.

93. Hasiotis, C.; Li, Q. F.; Deimede, V.; Kallitsis, J. K.; Kontoyannis, C. G.; Bierrum, N. J. *Journal of the Electrochemical Society* **2001**, *148*, A513.

94. Klempner, D.; Berkowski, L.; Krochwitz, J. I., Mark, H. F., Bikales, N. M., Overberger, C. G., Menges, G., Eds.; Wiley Interscience: New York, 1987, p 279-341.

95. Florjanczyk, Z.; Wielgus-Barry, E.; Poltarzewski, Z. *Solid State Ionics* **2001**, *145*, 119.

96. Polak, A. J.; Petty-Weeks, S.; Beuhler, A. J. *Sensors and Actuators* **1986**, *9*, 1.

97. Petty-Weeks, S.; Polak, A. J. *Sensors and Actuators* **1987**, *11*, 377.

98. Petty-Weeks, S.; Zupancic, J. J.; Swedo, J. R. *Solid State Ionics* **1988**, *31*, 117.

99. Zhou, Z. L.; Dominey, R. N.; Rolland, J. P.; Maynor, B. W.; Pandya, A. A.; DeSimone, J. M. *Journal of the American Chemical Society* **2006**, *128*, 12963.

100. Gardner, C. L.; Anantaraman, A. V. *Journal of Electroanalytical Chemistry* **1995**, *395*, 67.

101. Chen, N.; Hong, L. *Solid State Ionics* **2002**, *146*, 377.